CRCLEME
Cooperative Research Centre for
Landscape Environments
and Mineral Exploration

action
Salinity & Water
AUSTRALIA

Government
of South Australia

OPEN FILE
REPORT
SERIES

Australian Government
Geoscience Australia

REGOLITH-LANDFORMS AND SALT STORES IN THE ANGAS-BREMER HILLS

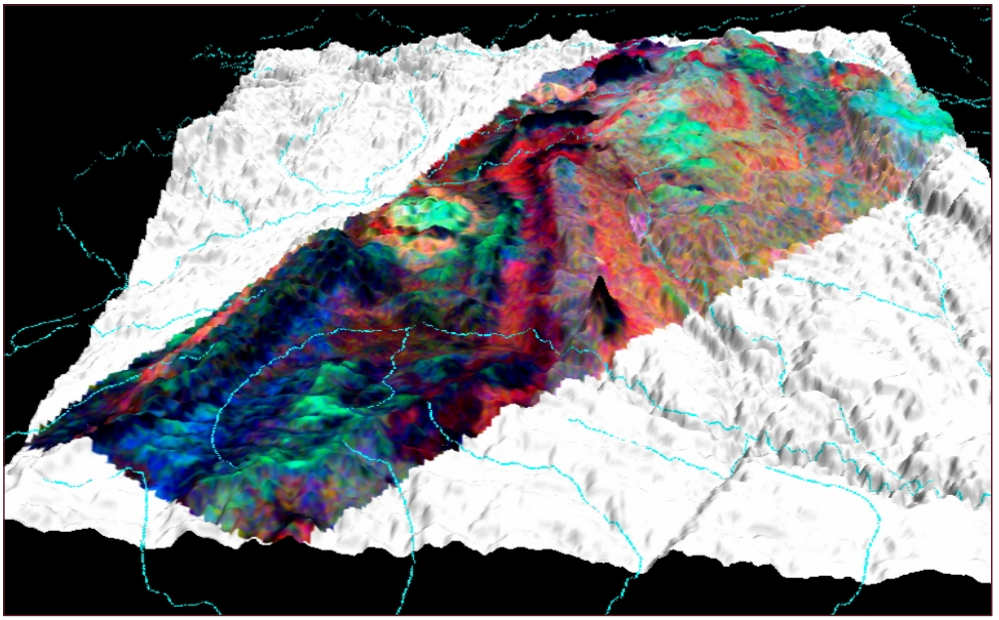

J. Wilford

CRC LEME OPEN FILE REPORT 177

September 2004

Australian Government
Geoscience Australia

CRCLEME
Cooperative Research Centre for
Landscape Environments
and Mineral Exploration

REGOLITH-LANDFORMS AND SALT STORES IN THE ANGAS-BREMER HILLS

J. Wilford

CRC LEME OPEN FILE REPORT 177

September 2004

Report prepared for the South Australia Salinity Mapping and Management Support Project.
This project is jointly funded by the South Australian and Commonwealth Governments under the National Action Plan for Salinity and Water Quality.

Copies of this Publication can be obtained from :
The publications Officer, CRCLEME, c/- CSIRO Exploration and Mining, PO Box 1130, Bentley WA 6120, Australia. Information on other publications in this series may be obtained from the above, or from http://crcleme.org.au
Cataloguing-in-Publication:
Name: Wilford, J., Title: Regolith-Landforms and salt stores in the Angas-Bremer Hills
ISBN 1 921039 15 9
1.Angas Bremer Hills, South Australia 2. Regolith-landforms 3. Salinity
I. Name II. Title
CRCLEME Open File Report 177
ISSN 1329-4768

Address and Affiliation of Authors

John Wilford
Cooperative Research Centre for Landscape
Environments and Mineral Exploration
Geoscience Australia
GPO Box 378,
Canberra, ACT 2601
Australia

SUMMARY……1

1. INTRODUCTION **2**
1.1 Background and rationale for the study 2
1.2 Objectives 2
1.2.1 Specific Objectives 3
1.3 Links to other projects 3

2. APPROACH **4**

3. STUDY AREA AND REGIONAL SETTING **5**
3.1 Location and geophysical survey areas. 5
3.2 Climate, vegetation and land use 5
3.3 Physiography 8
3.4 Geology and structure 14
3.5 Weathering and Landform history 18

4. SALINITY IN THE ADELAIDE HILLS **19**
4.1 Salinity – relationships with hydro-geology 19
4.1.1 Salinity and the Regolith 21
4.1.2 Soil landscape mapping and GIS modelling for generating salinity hazard maps. 24
4.2 Expression of salinity in the Adelaide Hills 28

5. STUDY METHODS **29**
5.1 Datasets and processing 29
5.1.1 Magnetics and gamma-ray spectrometry 29
5.1.2 Ground geophysics – EM31 31
5.2 Digital elevation model 35
5.3 Sample preparation and drilling 36
5.3.1 1:5 soil water extracts, conductivity and moisture content 36
5.3.2 Drilling 36
5.4 Residual modelling (separating bedrock and regolith responses) 36

6. RESULTS **37**
6.1 Gamma-ray response of bedrock and regolith 37
6.1.1 Precambrian rocks. 37
6.1.2 Cambrian bedrock 38
6.1.3 Weathering responses (regolith and soils) 42
6.1.4 Alluvial and colluvial sediments 45
6.2 Residual analysis – delineating highly weathered regolith 46
6.2.1 K-residuals compared with Tertiary weathering and Pleistocene-Holocene sediments 51
6.3 Correlations with soil-landscape mapping 51
6.4 K-residual compared with drill logs 56
6.5 Comparison of K-residuals and Smartem and NanoTEM TEM surveys. 58

6.6 Relationships between highly weathered regolith materials delineated by the K-residuals and landforms. 62
6.7 Surface hydrology characteristics 69
6.7.1 FLAG 69
6.7.2 Multi Resolution Valley Bottom Index (MRVBF) 70
6.8 Regolith salt storage 75
6.9 Salt stores and rainfall 79
6.10 Salt mobilisation 79

7. DISCUSSION AND CONCLUSIONS 81

8. RECOMMENDATIONS: 88

9. ACKNOWLEDGEMENTS 88

9. REFERENCES 89

LIST OF FIGURES

Figure 1. Location of study area and position of geophysical surveys…… 6

Figure 2. Study area and average annual rainfall…… 7

Figure 3. A – Landscape south of Mt Barker township. B – *Eucalytpus* woodland and native grasses and *Xanthorrhoea sp*…… 8

Figure 4. Elevation grid with added hillshade, main towns, geophysical survey areas and streams……9

Figure 5. Hillshaded DEM, main drainage divide and major fault scarps…… 10

Figure 6. Greyscale hillshaded digital elevation model with major rivers and drainage divide… 12

Figure 7. Slope class map derived from the digital elevation model…… 13

Figure 8. 3D perspective image with geology units draped over the digital elevation model. ……. 14

Figure 9. Geological units…….. 16

Figure 10. Major hydrological provinces for the Lofty Ranges…….20

Figure 11. Bore hole total dissolved solids…… 22

Figure 12. A – Gridded surface of bore hole salinity. B – Gridded surface of stream salinity…… 23

Figure 13. Areas of dry saline land (PIRSA Land Information 2001)…… 25

Figure 14. Areas of salinity induced by watertable…… 26

Figure 15. Areas of ranked salinity risk (PIRSA Land Information 2001)…… 17

Figure 16. Estimates of salinity for the Mt Torrens area compiled from modelling of soil dielectric, topographic index and geology…… 28

Figure 17. Magnetic intensity (left) and the first vertical derivative (FVD) of the magnetics for the Adelaide Hills survey…… 30

Figure 18. Magnetic intensity (left) and the first vertical derivative (FVD) of the magnetics for the PIMA survey. …… 31

Figure 19. Pseudo-coloured and three band false colour composite image of K, eTh and eU. Adelaide Hills survey…… 33

Figure 20. Pseudo-coloured and ternary image of K, eTh and eU. PIMA mining survey…… 34

Figure 21. Ternary gamma-ray image (Hills survey) with K in red, eTh in green and eU in blue. Geology units in light grey. …… 39

Figure 22. Ternary gamma-ray image (PIMA survey) with K in red, eTh in green and eU in blue…… 40

Figure 23. Geological unit names and location of the Hills and PIMA geophysical surveys. …… 41

Figure 24. Radioelement responses of bedrock and regolith materials from the selected regions in the study area……. 42

Figure 25. 3D perspective image of the three band gamma-ray data draped over the digital elevation model. The view shows the central-western part of the study area…… 44

Figure 26. Examples of highly weathered bedrock and ferruginous soil south of the Mt Barker Township. …… 44

Figure 27. 3D perspective view of the 3-band gamma-ray image draped over the digital elevation model. …… 45

Figure 28. Selected pictures of regolith materials…… 47

Figure 29. Selected pictures of regolith materials…… 48

Figure 30. Selected pictures of regolith materials……. 49

Figure 31. K-residual image (both surveys combined)……..... 50

Figure 32. K-residual image and soil landscape units…… 52

Figure 33. Soil profile descriptions and soil site locations on the ternary gamma-ray spectrometry image…….53

Figure 34. Thematic map showing degrees of rockiness derived from the soil-landscape GIS. …… 54

Figure 35. K-residual image and soil-landform units…… 55

Figure 36. Landscape pictures showing residual soil with little outcrop and bedrock (schist) dominated landscape…… 55
.
Figure 37. Scatter plot showing the relationship between K-residual response and maximum depth drilled into the bedrock. …… 56

Figure 38. Relationship between K-residual values and only drill holes that intersect saprock. …… 57

Figure 39. Relationship between K-residual values and only drill holes that intersect saprock and also excluding holes with transported regolith. …… 57

Figure 40. Stitched conductivity depth sections from a smooth Occams inversion of Smartem data for lines - HARSE1, MB1 and MT1…… 59

Figure 41. Stitched conductivity depth sections from a smooth Occams inversion of Smartem data for lines - HAR1, and MB2…… 60

Figure 42. Locations of geophysical survey lines over the K-residual image…… 61

Figure 43. A – hillshaded DEM, B- relief (low grey – high red hues), C - K-residual image (highly weathered regolith in blue – less weathered in reddish hues) and D - slope…… 63

Figure 44. 3D perspective view of the K-residual draped over the DEM. …… 64

Figure 45. Location of topographic x-sections over the K-residual image…… 65

Figure 46. Topographic x-section 1…… 66

Figure 47. Topographic x-section 2…… 66

Figure 48. Topographic x-section 3…… 67

Figure 49. Topographic x-section 4…….. 67

Figure 50. Distribution of erosional scarps over the K-residual image. …… 68

Figure 51. Series of photographs showing decreasing degrees of bedrock (metasiltstone) weathering from the top of the erosional scarp (A) to the base (D). …… 69

Figure 52. A - Flag index LOW over hillshaded DEM. B - K-residual image highlighting weathered landscapes in blue and less weathered in red……. 71

Figure 53. High and low MRVBF values compared to valley profiles. …… 71

Figure 54. MRVBF over the Mt Barker area. …… 72

Figure 55. K-residual (A) and MRVBF (B) for the northern part of the study area ……..... 73

Figure 56. Stream profiles. …… 74

Figure 57. Correlation between EC and chloride from the Keynes catchment…… 76

Figure 58. Relationship between salt store (t ha $^{-1}$) and K-residuals…… 76

Figure 59. Salt stores (t ha $^{-1}$) in the upper 5m of regolith over average annual rainfall grid…… 78

Figure 60. Correlation between salt storage (t ha $^{-1}$) and annual rainfall……. 79

Figure 61. Streams ECs and K-residual image. …… 80

Figure 62. Location of 3D hydrogeomorphic conceptual models…… 82

Figure 63. 3D hydrogeomorphic model based on the integration of information on the regolith, hydrological processes, salt stores, rainfall, stream EC and landforms. …… 84

Figure 64. 3D hydrogeomorphic model based on the integration of information on regolith, hydrological processes, salt stores, rainfall, stream EC and landforms……. 85

Figure 65. 3D hydrogeomorphic model based on the integration of information on regolith, hydrological processes, salt stores, rainfall, stream EC and landforms. …… 86

LIST OF TABLES

Table 1. Mineralogy of selected regolith materials……. 43

Table 2. Salt storage within the regolith…….. 77

APPENDIX. Regolith EC profiles.

SUMMARY

The combined interpretation of airborne gamma-ray spectrometry and terrain indices derived from a digital elevation model along with ground data has provided new insights into the distribution of regolith materials and related salinity in the Angas Bremer Hills of South Australia.

Modeling of the gamma-ray data has been able to separate highly weathered landforms from areas characterised by thin soil and slightly weathered bedrock. Highly weathered materials include leached ferruginous soils, mottled colluvial and alluvial sediments and highly weathered kaolinised bedrock. Weathered bedrock or saprolite is typically mottled with iron fragments and nodules common in the upper part of the profile. Iron induration is mostly associated with segregations of iron in the mottled zone of the weathering profile. In places these weathering profiles are covered by alluvial and colluvial sediments that in places are also highly weathered (mottled and ferruginised).

The gamma-ray data has the potential to improve existing soil-landscape and geological mapping. Variations in the concentration of the radioelements can be used to modify soil-landscape and geological unit boundaries and assist in describing variations of specific attributes within individual units. As similar gamma-ray responses can relate to different materials at the surface it is recommended that the imagery be interpreted within different geological formations and landform units (e.g. erosional vs depositional landscapes).

In the Angas Bremer Hills, a long weathering history, dating back to the Middle Mesozoic, combined with more recent tectonic activity resulting in faulting, uplift and associated erosion has led to complex landscapes where highly weathered landforms are juxtaposed with youthful landforms with little regolith development. Analysis of the gamma-ray imagery and digital elevation model has provided improved clarity on the weathering and geomorphological evolution of the region.

Regolith thickness and composition governs the capacity of the landscape to store cyclic salts (e.g. those salts derived from rainfall). Weathering is important when considering salts derived from bedrock minerals. In both cases (e.g. salt derived from rainfall and bedrock) delineating areas of deep weathering is important in predicting likely salt stores. For a local region the highest salt stores are associated with catchments that have thick soils and deeply weathered bedrock. The stores are associated with valley alluvium, colluvial fans and highly weathered bedrock. Stream ECs tend to be higher from these catchments compared to those catchments with relatively shallow regolith.

Across the whole region the main driver for controlling the amount of salt in the landscape is rainfall. The thickness and composition of the regolith might determine the capacity of the landscape to store salts, but rainfall largely determines the relative abundance of salts in the profile. When comparing similar regolith profiles across the study area, those profiles in the high rainfall zone (western side of the Hills) store considerably less salt than those profiles on the drier eastern side.

The highest salt fluxes are associated with Western Flat Creek in the Mt Barker catchment. The average annual rainfall is the highest in the study area. Modelling of the gamma-ray imagery indicates that a high proportion of this catchment is deeply weathered, suggesting that the highest salt exports are associated with deeply weathered landscapes in high rainfall areas. Conversely, fresh water runoff is commonly associated with less weathered catchments in areas of high rainfall.

These relationships are summarised in a series of 3Dconceptual models which detail relationships between the distribution and thickness of regolith materials, salinity and hydrogeomorphic processes. These models provide a basis for understanding processes controlling the distribution of soil and river salinity across the Hills region.

1. INTRODUCTION

1.1 Background and rationale for the study

Salinisation of land and rivers is a major environmental concern throughout agricultural regions in Australia. To help resolve environmental issues arising from these concerns there is a need to better understand where the salt is stored, and to determine how these stores interact with ground and surface water.

The Bremer Hills region, located between Mt Barker and Mt Torrens in the Eastern Mt Lofty Ranges, supports a wide range of farming activity. Widespread land clearing in the late 1800's significantly altered the hydrology, with soil and stream salinity the direct consequence. These effects are of increasing concern to farming communities, local townships and larger urban centres including Adelaide. They relate specifically to local areas of salt induced soil erosion, salt scalds, saline seeps and salinisation of irrigation groundwater, streams and water on farm dams. Revised 1993 estimates of land effected by salinity from the state Dryland Salinity Committee (1990) are over 2 800 ha. Increases in stream salinity in the Hills region has the potential to directly affect the quality of Adelaide's drinking water, since 60% of the drinking water supply comes from reservoirs in the Lofty Ranges (Oh, et al. 2000). Clearing of native vegetation has caused increased rates of recharge into the groundwater and increased discharge into springs and rivers. Salt outputs into streams exceeded salt input from rainfall by an average of 4.5 times compared to pre-clearing where salt input and output ratios were thought to be closer to 1:1 (Williamson, 1990). In 1992 the Bremer Barker Catchment Group was established in response to increasing concerns about soil and stream salinity in the Adelaide Hills.

To better manage this region using a mix of salinity abatement practices, there is a need to better understand the variability of regolith and soil materials across the landscape at scales appropriate to land management at the paddock level. There is also a need to link this information to geology, geomorphology, groundwater and stream salinity. Of particular importance is the need to understand whether the regolith (all weathered materials including soils between the land surface and fresh bedrock) contain significant quantities of salt that are now being mobilised to the land surface and into streams. This information would assist in targeting and managing areas of higher salt store and salt input into streams.

The application of airborne geophysics, in particular gamma-ray spectrometry, together with other datasets (eg. terrain derived indices from a digital elevation model, ground geophysics, geology, drill hole information and climatic surfaces) are assessed to evaluate whether integration and interpretation of these datasets can provide key information for use in targeting and managing areas of dry salinity.

1.2 Objectives

The principal aim of this study was to better understand the relationships between geology, landform, regolith materials and associated weathering and geomorphic processes (including both present and palaeo-landscape processes), that are likely to constrain the distribution of salt in the Bremer Hills. This was achieved through the analysis and interpretation of high resolution airborne gamma-ray spectrometry imagery and terrain attributes derived from a high resolution (25 metre) digital elevation model over the Bremer Hills region.

1.2.1 Specific Objectives

Specific Objectives include:

1. To map regolith materials using gamma-ray spectrometry data and terrain attributes.

2. To determine the relationship between salts and regolith materials through the interpretation of stream and soil electrical conductivity (EC), drilling, existing water bores and ground geophysical surveys (NanoTEM). Particular emphasis was placed on old and highly weathered saprolites, as these materials were believed to hold most of the stored salt in the landscape. Drilling was used to assess the relationships between salt content and regolith materials over a range of the landscapes, bedrock and rainfall zones.

3. To investigate the relationships between regolith materials and geology (including bedrock structure) derived from the interpretation of airborne geophysics, geological maps and terrain analysis (digital elevation model).

4. To develop an improved understanding of the origin and distribution of regolith materials in the context of regional landscape evolution model for the area.

5. To integrate the results and develop, in conjunction with the State based project '*Salt transport in the Angus Bremer Hills*', a more robust hydrological model of the Bremer Hills.

6. To develop a methodology that will have application elsewhere in the state with similar regolith-landform characteristics.

Key outputs for the project are thematic maps of regolith material and predicted salt store, and an improved understanding of the relationships between landforms, geomorphic processes and regolith materials. This information will be assessed within an integrated catchment-based approach to manage salinity in the Bremer Hills and will link to other investigations currently underway.

1.3 Links to other projects

A complementary, parallel, investigation called the '*Salt transport in the Angus Bremer Hills*' has as its objectives, the:

1 - collation and summary of existing salinity work in the area;

2 - determination of the origin of the salts using isotope techniques (e.g. analysis of Br/Cl ratios)

3 - understanding of factors controlling the mobilisation of saline groundwater.

Groundwater behaviour will be modelled using flow tube to show the processes whereby salts are mobilised into streams. It is envisaged that these activities together with work described in this report, will lead to more holistic and robust hydrological model(s) for the Bremer Hills region to address dryland salinity management issues.

2. APPROACH

The approach adopted here will incorporate geomorphology, hydrogeology and geophysics to understand the character and distribution of regolith materials, landscape processes and salt stores in the study area. The mapping of regolith (including soils) involves the interpretation and integration of recently flown airborne gamma-ray spectrometry imagery and terrain attributes derived from existing high resolution digital elevation models. Airborne magnetics acquired simultaneous with the gamma-ray data has been processed to enhance major magnetic bedrock domains and structural features. However, particular emphasis is placed on the interpretation of gamma-ray data for delineating soil/regolith types. A previously flown gamma/magnetic survey by PIMA mining over the eastern side of Lofty Ranges has also been examined as part of this investigation. This additional dataset extended the project into the drier eastern part of the ranges and allowed comparisons of gamma-ray data for understanding regolith salt stores in differing rainfall zones.

Gamma-ray spectrometry has been widely used in geophysical exploration and, more recently, in soil and regolith mapping. Radioelements measured in airborne surveys vary according to geochemistry of the bedrock and the style of weathering and as a result can provide a considerable amount of information on regolith/soil characteristics (Wilford *et al*. 1992; 1997, Bierwirth 1996 Dauth 1997 and Cook 1996). Gamma-rays are emitted from the top 15-20cm of dry soil and have sufficient energy to pass through most vegetation to the receiver on the aircraft. The ability of gamma-rays to 'see through' vegetation is an advantage in agricultural regions like the Bremer Hills region where other remote sensing techniques such as Landsat TM are difficult to interpret due to the masking of soils by ground cover (eg. crops, native vegetation and pastures). Where the vegetation is thick (eg. pine plantation, native woodland) attenuation of gamma radiation can occur and therefore should be considered when interpreting radiometric patterns in the imagery.

An important component of the study was the interpretation, modelling and integration of terrain indices to map regolith materials and predict hydro/geomorphic processes. Digital elevation models (DEMs) are used widely in terrain classification and modelling. Primary surfaces (e.g. slope, aspect, elevation) and secondary or compound surfaces (e.g. wetness index, stream-power indices) are derived from DEMs. Secondary attributes, that involve combinations of primary attributes and incorporate physically based or empirically derived indices, are used to characterise the spatial variability of specific processes occurring in the landscape (Moore el al., 1991 and 1993; in Wilson and Gallant, 2000). Primary and secondary attributes are used in hydrological modelling (Wilson and Gallant, 2000, Roberts, et al., 1997, Dowling, el at., 2001), soil mapping (Mckenzie, et al. 1999, Gessler, et al., 1995) and in modelling erosional and depositional processes (Mitasova, et al., 1996). A list of primary and secondary terrain indices and uses are described in Wilson and Gallant (2000).

The work described here involves combining attributes from airborne gamma-ray spectrometry imagery and terrain analysis to map and describe the distribution of the regolith, landforms and salts within catchments of the Bremer Hills. Wilford et al., (2001) has demonstrated the combined used of gamma-ray spectrometry and DEMs to map regolith materials and potential salt stores in the Cootamundra region of central NSW. A similar approach is applied here, although a customised approach for the Hills region might be needed due to differing climate, geology, regolith and landscape histories.

In selected catchments, ground electromagnetic (EM) transects calibrated with drilling, are used to build 3-D regolith and salt distribution models. Drilling is also used to determine the depth, weathering characteristics and salt content of the regolith. Catchments based studies form the basis for understanding the relationships between geology, slope processes and regolith materials. Existing work on salt distribution in regolith/bedrock materials (Henschke, 1997, Henschke, 2002, Oh et al., 2000; Cox and Reynolds, 1995; Thompson et al, 1994, Fitzpatrick et al., 1994, 1996 and 2002) over the Lofty Ranges is incorporated into the models.

Rules and relationships between the thematic datasets (e.g. gamma-ray spectrometry, terrain attributes, geology), calibrated by drilling and field measurements, are integrated to produce a series of hydrological and regolith attributed thematic maps and conceptual models over the study area. These maps/models are intended to predict the location of likely salt stores and likely saline groundwater flow paths in the region.

3. STUDY AREA AND REGIONAL SETTING

3.1 Location and geophysical survey areas.

The study area is part of the Mt Lofty Ranges that extends from Angaston in the north to Cape Jervis, the southern point of the Fleurieu Peninsula in the south. It lies within the central and northern part of the Lofty Ranges and includes the townships of Mt Barker, Mt Torrens and Callington (Figure 1). Two airborne geophysical surveys (gamma-ray spectrometry and magnetic) were used in the study. The first was a 100m flight-line survey acquired as part of the SA Salinity Mapping and Management Support Project (SA-SMMSP) that covers the western side of the study area including the townships of Mt Barker and Mt Torrens. The second survey was an existing survey flown at 200m flight-line spacing by PIMA mining. This covers the eastern part of the study area and partly overlaps the western survey. These geophysical datasets delineate the extent of the study area (Figure 1).

3.2 Climate, vegetation and land use

The area has a Mediterranean climate with cool winters and generally warm to hot dry summers. Most rainfall occurs during the winter months. Temperatures are generally 3-5 degrees cooler than Adelaide due to the higher elevations. Average mean temperatures for winter and summer are around 14 (deg C) and 27 (deg C), respectively. There is a strong orographic influence on rainfall distribution with higher elevations and exposed hills along the western side of the ranges receiving between 800 to 1100 millimetres per year. Rainfall diminishes rapidly eastwards across the hills to between 350-500 mm per year along the eastern boundary of the study area (Figure 2). Mt Barker has annual average rainfall of 766 mm compared with Callington 17km east of Mt Barker with a annual average rainfall of 380 mm (source Bureau of Meteorology climate stations. Callington average based on average rainfall grid, therefore approximate value only).

Most of the original native vegetation was cleared for grazing (sheep and cattle) and cropping during European settlement. Crops are grown where rainfall exceeds 300mm. Horticulture (vineyards and fruit trees), piggeries, dairies and forestry are important locally.

Prior to clearing, the landscape was largely covered by *Eucalyptus* woodland. Where remnant vegetation is preserved, its distribution and type is strongly influenced by soil fertility and rainfall. These remnant woodlands have been described by Lange (1976). They consist of blue gums, pink gum and manna gum (*Eucalyptus viminalis; Eucalyptus huberana*), and brown stringybarks (*Eucalyptus obliqua and Eucalyptus axteri*). Tall candlebarks are locally common in the wettest gullies and river gums grow adjacent to water courses. Acacia species (*A. pycnantha, A. melanoxylon*) provide tall undergrowth vegetation. Beneath this layer, shrubs and grasses are found, including for example *Olearia axillaris, Stylidium vexiliferum, Hibbertia spp. Lepidosperma Spp* (tussock) and Themeda australis (Kangaroo grass). *Xanthorrhoea* are locally common on low nutrient soils (Figure 3). In many places the occurrence of *Xanthorrhoea* can be used to indicate ferruginous and highly leached soils (see section 3.5).

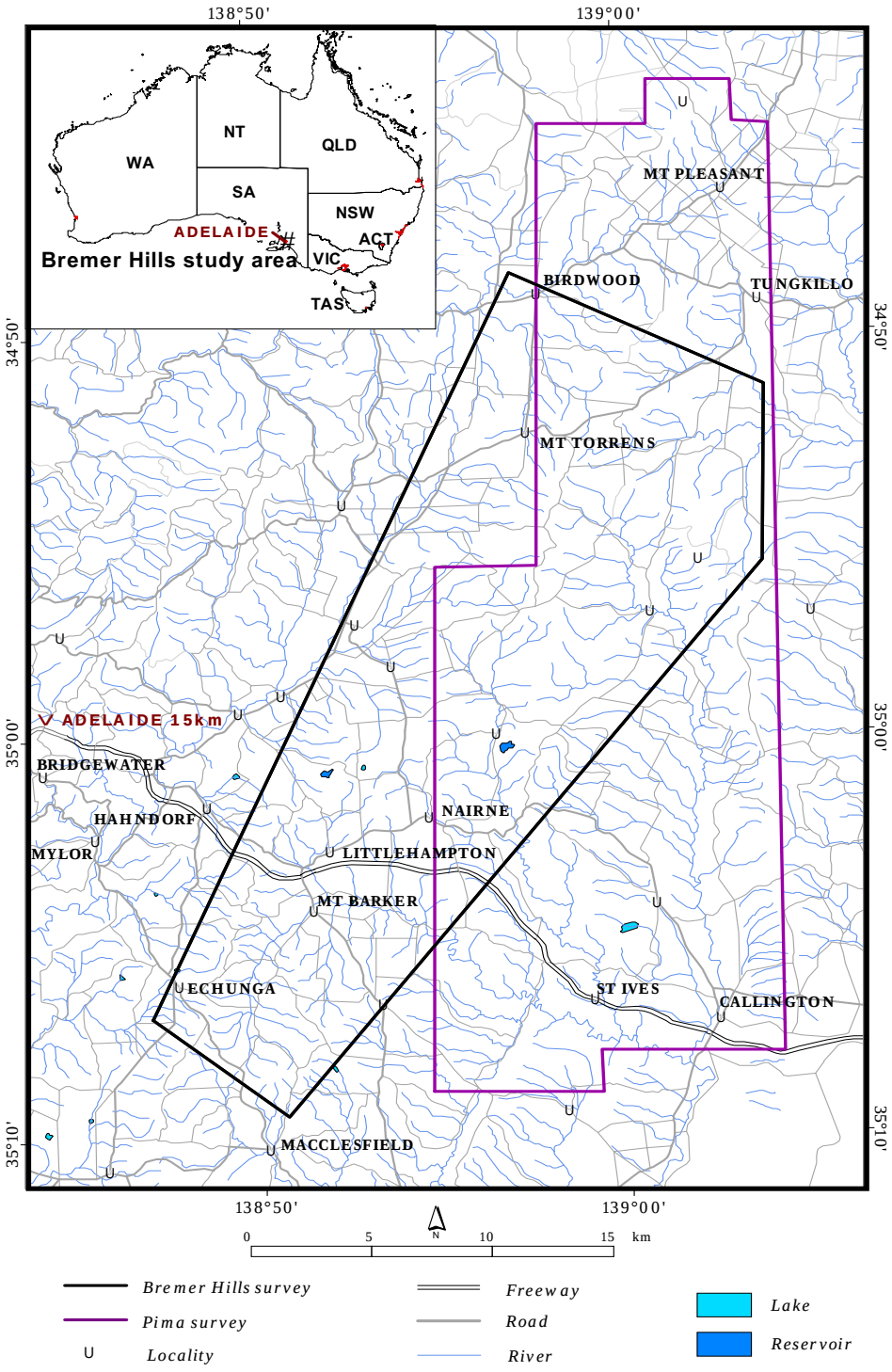

Figure 1. Location of study area and position of geophysical surveys.

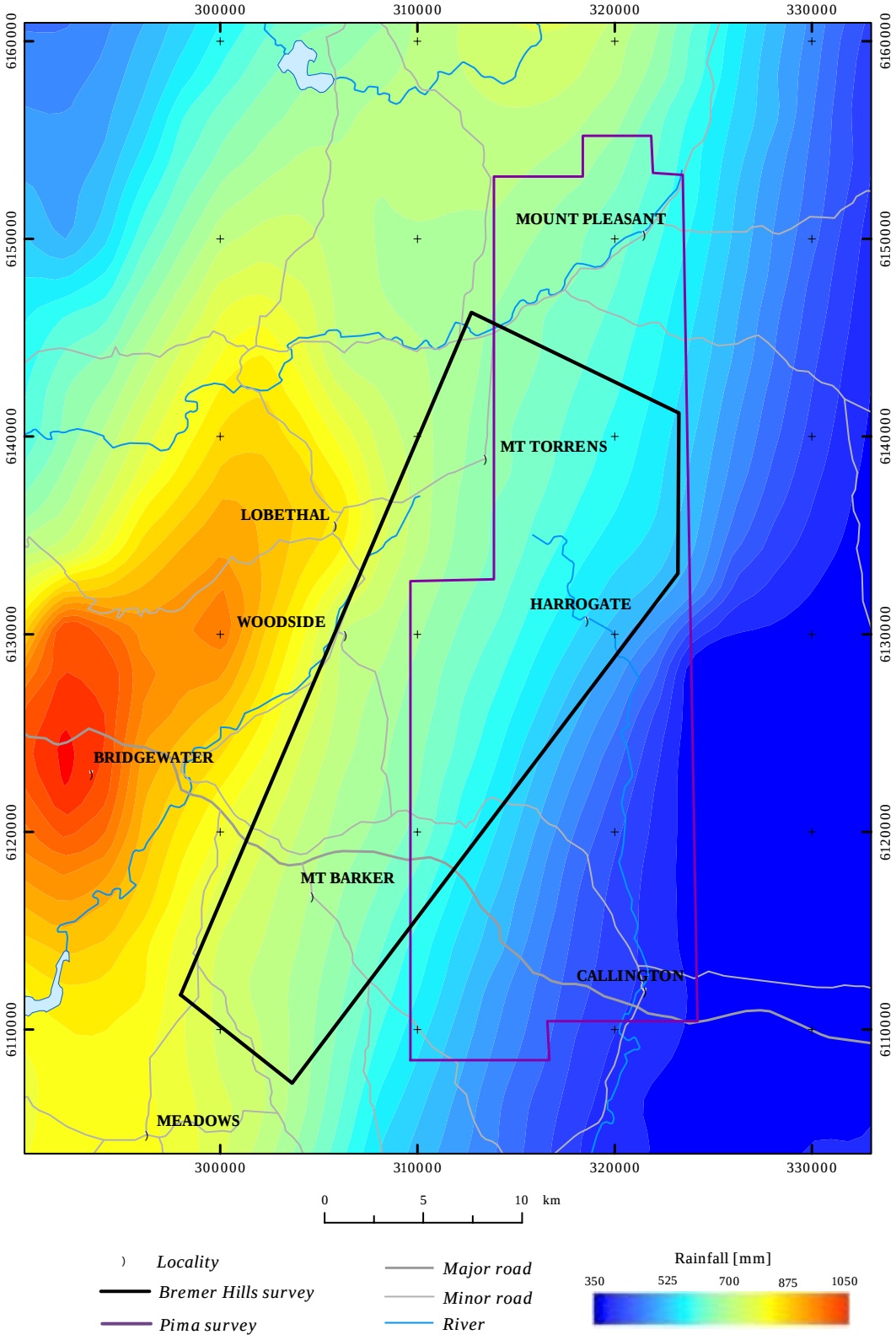

Figure 2. Study area and average annual rainfall.

3.3 Physiography

The 25m digital elevation model is used to highlight the main morphological and drainage characteristics of the study area (Figure 4). The study area lies for the most part, in erosional landscapes of the central and northern parts of the Lofty Ranges. The landscape is dominated by rises (9-30m relief), low hills (30-90m) and hills (90-300m). Low relief is associated with floodplains adjacent to major rivers and colluvial fans particularly along parts of the Bremer Fault Scarp on the

A B

Figure 3. A – Typical cleared landscape south of Mt Barker township. B – *Eucalytpus* woodland with an understory of native grasses and *Xanthorrhoea sp*.

eastern side of the study area. The central and western part of the region have the highest elevations (Bluff Range 610m) and lowest elevations are associated with the drainage channel of the Bremer River over the eastern part of the study area (Figure 4). The drainage divide that separates streams flowing into the Bremer River from stream flowing west into the Gulf of St Vincent occurs along the central western part of the study area (Figure 4). Tokarey et al. (1998) noted that the maximum elevations along the western margin of the Lofty Ranges are offset from the main drainage divide that separates west and east flowing rivers. This offset is evident in the hillshaded elevation model (Figure 4).

One of the most striking landform features in the region are a series of curve-linear fault scarps oriented mainly north-south across the study area. These include the Bremer, Meadows, Stoneyfell and the Kitchener fault scarps (Figure 5). The Bremer is the most distinctive with a local offset of approximately 150 m (east of Harrogate). In places, colluvial fans form aprons down-slope from the scarp edge with slopes between 1 - 2.2 degrees. These bounding fault scarps are formed by relatively

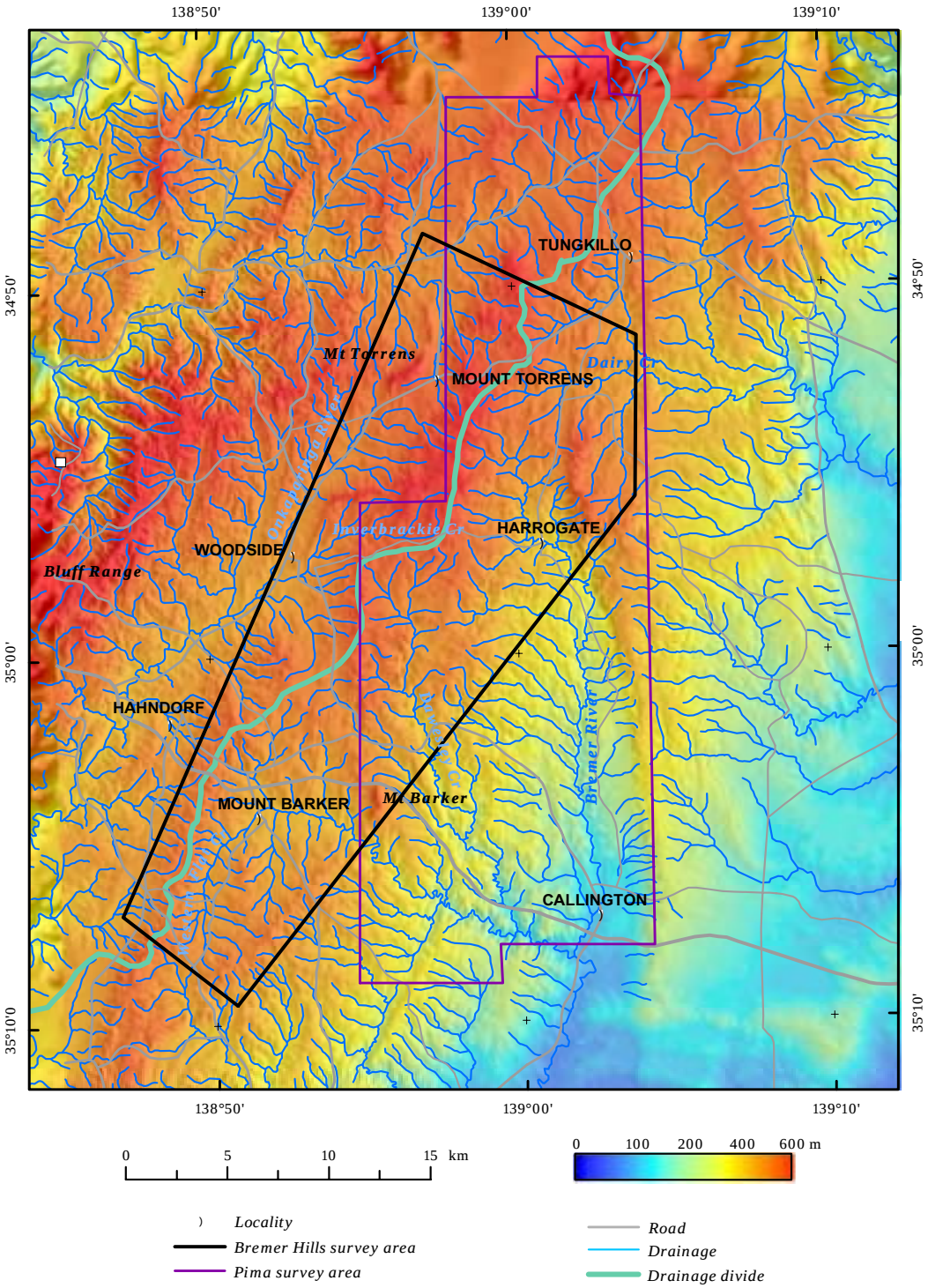

Figure 4. Elevation grid with added hillshade (artificially illuminated from the NE), main towns, geophysical survey areas and streams.

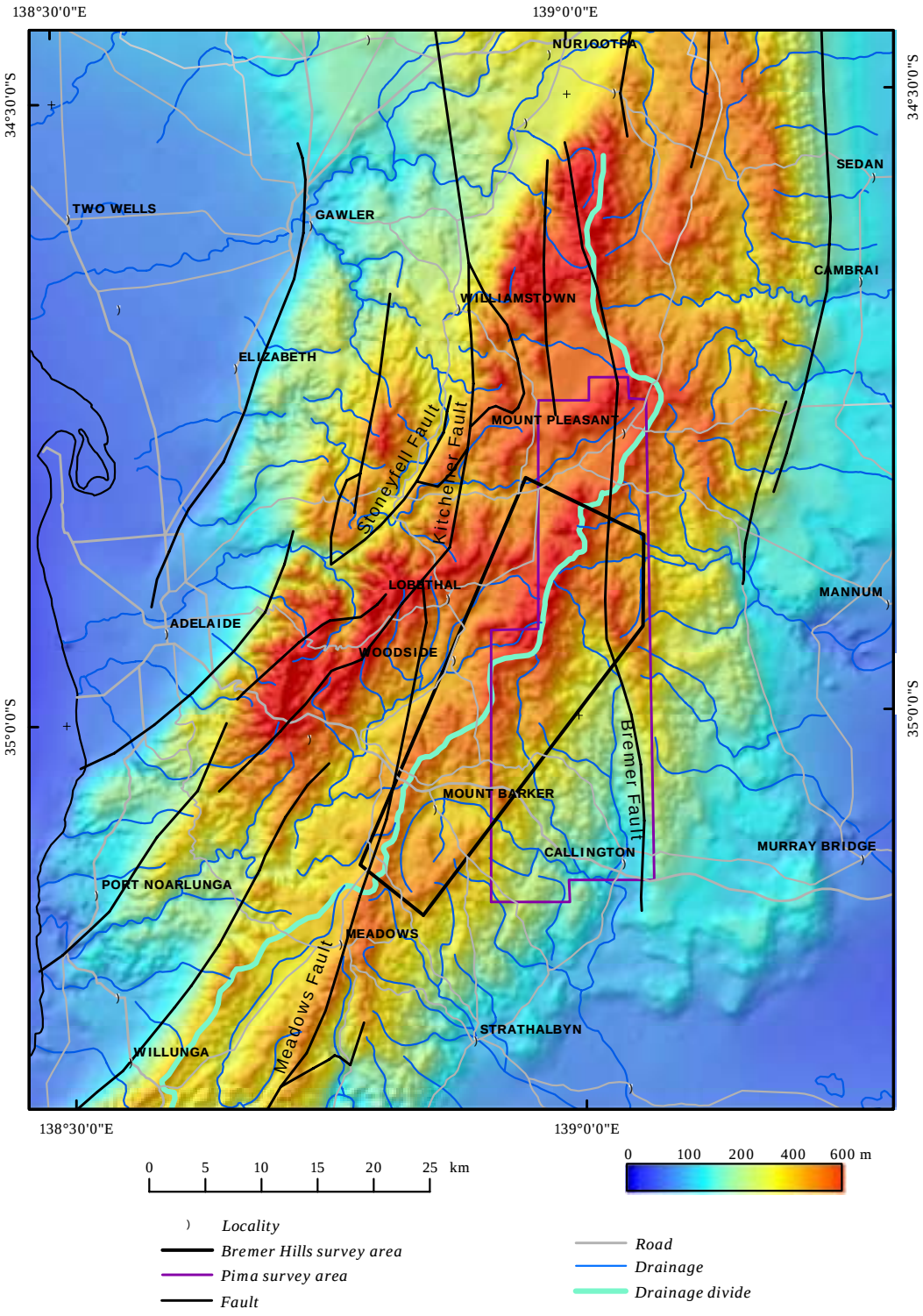

Figure 5. Hillshaded DEM, main drainage divide and major fault scarps. The location of the geophysical surveys are shown.

recent tectonic movement (Middle Eocene to Early Miocene and Early Pliocene) and provide a first order control on landscape morphology in the Lofty Ranges (Tokarev, et al. 1998). On the steeply incised western margin of the Lofty Ranges, nick points remain close to their generative scarps suggesting a youthful erosional system (Tokarev, et al. 1998). The fault scarps are associated with a series of major tilt blocks across the area. The fault scarps have been modified by stream incision and local erosional scarp retreat (see section 3.5).

The fault scarps and tilt blocks have disrupted an older, highly weathered and low amplitude surface commonly referred to as the 'summit surface'. The origin and characteristics of the older surface is discussed in more detail later in the report. The palaeo-surface is recognised on the hillshaded DEM as a smoother textural tone with relatively low relief (Figure 6). These low relief palaeo-landforms are best preserved on either side of the main drainage divide where they are associated with upper tributaries of Dawesley Creek, Western Flat Creek, Inverbrackie Creek, Williams Creek, Torrens River, Onkaparinga River and the western branch of the Onkaparinga River (Figure 6). The drainage divide crosses a variety of lithologies (eg. quartzites, schists) and faults suggesting that it is not inherited by the underlying geology and structure. Furthermore, the association of the divide with palaeo-landforms suggest that it developed before the regional uplift that formed the ranges. Drainage patterns over the palaeo-surface tend to be more widely spaced, compared with the steeply incised landforms over the western flank of the Lofty Ranges (western edge of the study area). Slopes on these palaeo-landscapes vary between 0-1 degree along river floodplains and between 2-5 degrees on adjacent rises.

The steepest slopes with greatest relief are associated with incised landscapes (20-30 degree slope common) on the western side of the study area in the vicinity of Cherryville. Other areas of high relief are associated protruding hills within the central uplands belt (eg. Mt Torrens, Mt Barker, Mt Charles), incised landscapes associated Mt Barker Creek and Dawesley Creek and erosional scarps, particularly the Bremer Fault Scarp near Mt Beevor (East of Harrogate) (Figure 7).

Relationships between geology and topography are revealed in a 3D perspective image where geological units are draped over a digital elevation model (Figure 8). More readily weathered lithologies have a more subdued topographic expression compared with more resistant rock types which have a greater relief. Resistant rocks including quartzites, siliceous siltstones and sandstones typically form the main hills and ranges (Mt Barker, Mt Torrens and Mt Charles).

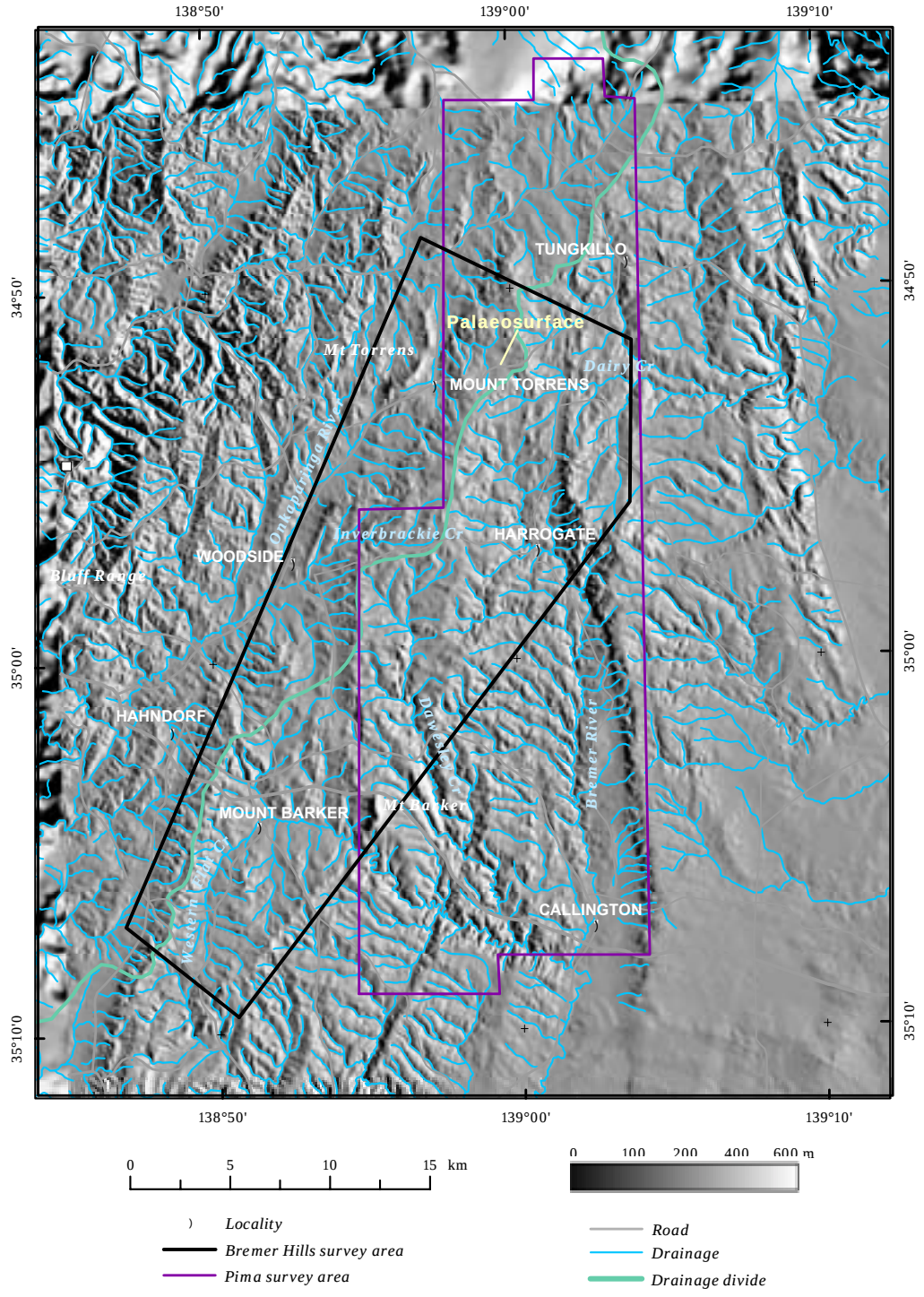

Figure 6. Greyscale hillshaded digital elevation model with major rivers and drainage divide. The 'palaeo-surface' partly preserved over the Lofty Ranges is identified by a smooth low amplitude landform pattern.

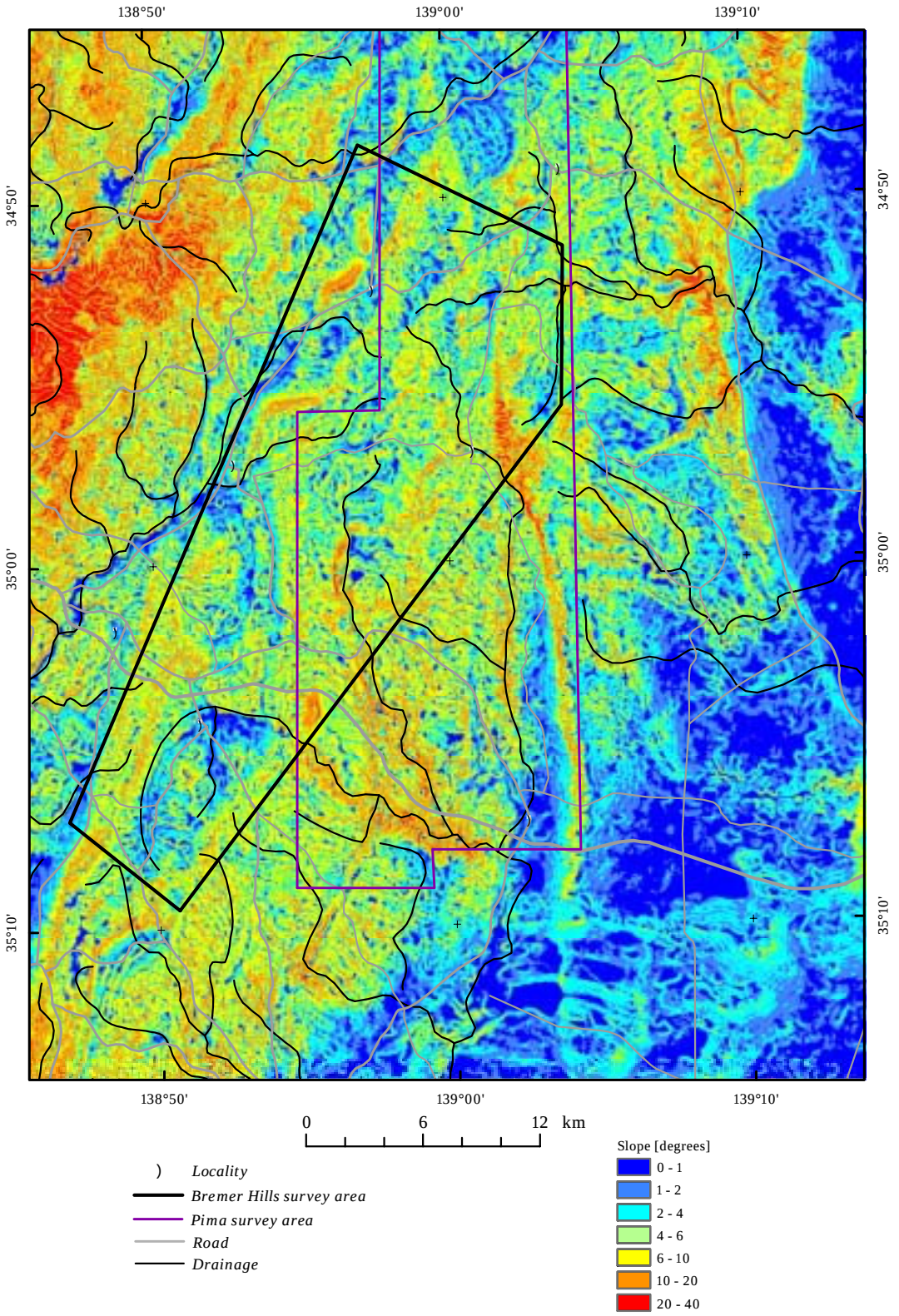

Figure 7. Slope class map derived from the digital elevation model.

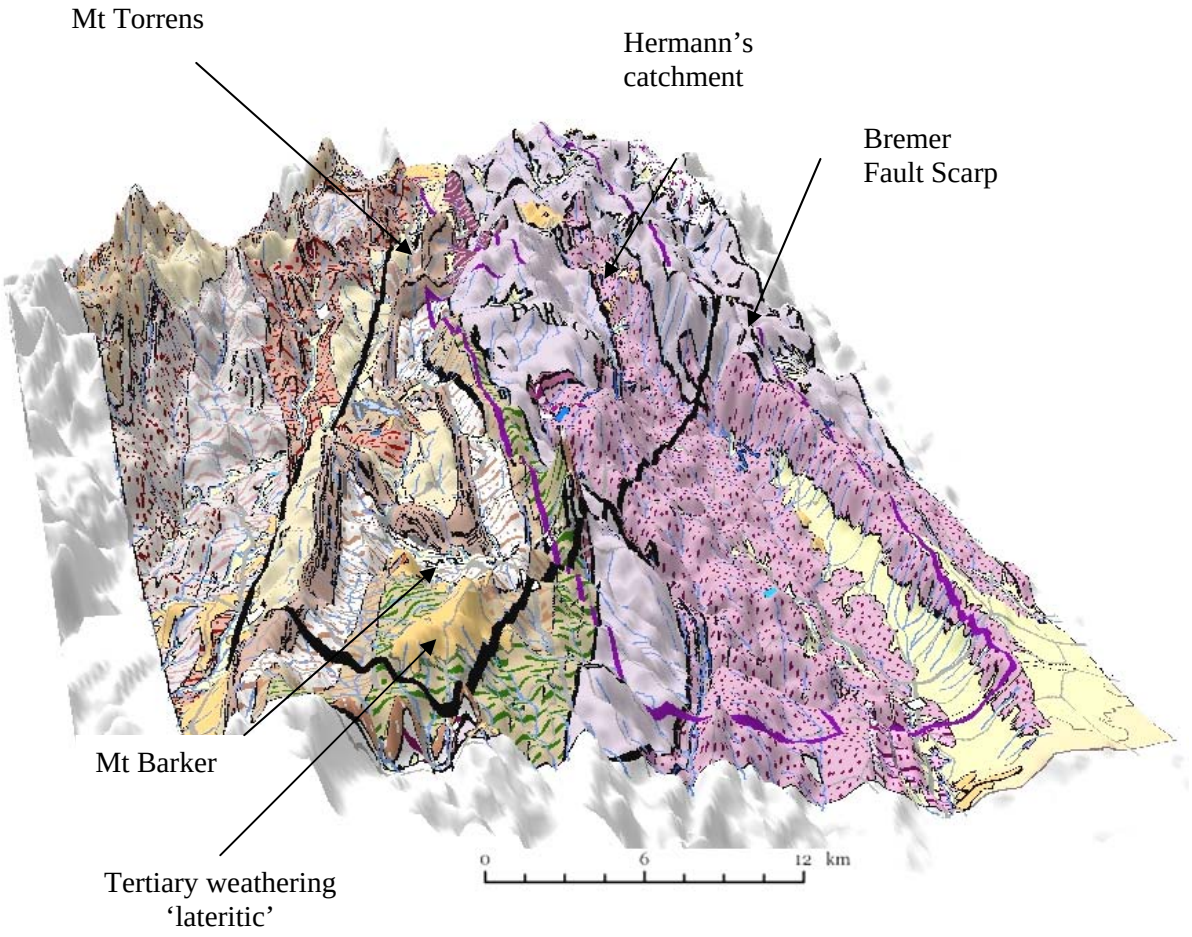

Figure 8. 3D perspective image with geology units draped over the digital elevation model. More resistant lithological units have a more pronounced topographic expression. Lateritic weathering shown in light brown.

3.4 Geology and structure

Bedrock in the study area can be broadly divided into rocks of Proterozoic, Cambrian and Tertiary age. Proterozoic rocks include metamorphosed gneiss and schist associated with the Barossa crystalline basement complex (> 900ma years old) and more recent Precambrian Adelaidean sediments (Thomson, 1969). The Adelaidean sediments include gravels, sands, clay, silt and carbonate. They occur mainly on the western side of the study area (Figure 9) and are dominated by feldspathic sandstones, siltstones, quartzites and dolomites (Figure 9). These sediments were uplifted and partly eroded prior to flooding by the sea and burial by marine sedimentation during the Cambrian (Daily et al, 1976). The Cambrian and underlying Proterozoic sediments are separated by a low angle unconformity.

Cambrian lithologies are mainly associated with the Kanmantoo Group sediments. These sediments include sandstones, siltstone and shales. Both the Proterozoic and Cambrian sediments have been folded, baked and fractured during the Late Cambrian Delamerian Orogeny. As a result most of the rocks in the area show varying degrees of metamorphism. Metamorphic textures range from low grade phyllite and slate to higher grade schist and gneiss bedrocks. The most common rocks associated with the Kanmantoo Group consist mostly of feldspathic meta-sandstones and meta-siltstones. These rocks

are typically highly micaceous (biotite and muscovite) and contain fine grained quartz, feldspar and plagioclase. Less common lithologies include quartzites, pegmatites, limestones, calc-silicates and pyritic shales (Nairne Pyrite Member). The pyritic shales are inter-bedded within the Kanmantoo Group sediments and have been mapped as narrow discontinuous units between Mt Pleasant in the North to the Fleurieu Peninsula in the South (Figure 9). Folding associated with the metamorphism has caused tight asymmetrical folds. Final crustal movements associated with the Delamerian Orogeny resulted in major upward thrusting that was accommodated along steeply dipping reverse faults (Sprigg, 1946.). Lineated and schistose granites were emplaced either prior to folding and were metamorphosed during structural deformation or were crystallised in the stress field created at the time of folding (Daily et al, 1976). Granite and high grade metamorphic rocks occur at Tungkillo, Springton, Eden Valley and Palmer.

Although no Permian sediments are recorded in the study area, rocks of Permian age occur south on the Fleurieu Peninsula. They include bedded claystones and crossbedded sandstones with pebbles and boulder erratics.

During most of the Cainozoic, the area was uplifted, exposed and underwent erosion and weathering Two main periods of tectonic activity are thought to have caused faulting, reactivation along faults and uplift that formed the Lofty Ranges. The first tectonics phase occurred in the middle Eocene to early Miocene (approx 43 to 14 Ma) as evidenced by dated sediments in basins flanking the Lofty ranges (Twidale, 1976). Tectonic movements were thought to be associated with reactivation of old established major crustal faults that were initiated during the early Palaeozoic Orogeny (Preiss, 1987). Movements along these faults during this time are thought to be related to an extensional stress regime associated with basin formation across the southern Australian margin (Tokarev, et al., 1998). The second tectonic phase associated with reactivation and displacement along faults occurred post Miocene and probably after 5 Ma (Tokarev, et al., 1998). Bourman and Lindsay, (1989) describes displacement of Pleistocene fanglomerates and Miocene limestones by tectonic uplift of 60-90m on the eastern margin of the Lofty Ranges since the Miocene. Movements that related to the younger tectonic phase were associated with reverse faulting and the east-west orientated compressional stress field that occurs to the present today (Tokarev, et al., 1998).

Weathering continued during uplift between the Palaeocene to Eocene. Deep weathering and subsequent dissection of the Lofty Ranges is discussed in more detail in section 3.5. Eocene clastic sediments sourced from Proterozoic and Cambrian lithologies were deposited in local basins and in river valleys draining from the surrounding highlands. In some low lying areas shallow marine limestone was deposited in association with several transgressive and regressive sea level cycles (Daily et al., 1976). Quaternary sediments consist of undifferentiated alluvial and colluvial clays, sands and gravels formed alluvial channel and footslope deposits, respectively. In places these sediments contain highly ferruginous lithic fragments derived from erosion of ferricretes and mottled ferruginous saprolite.

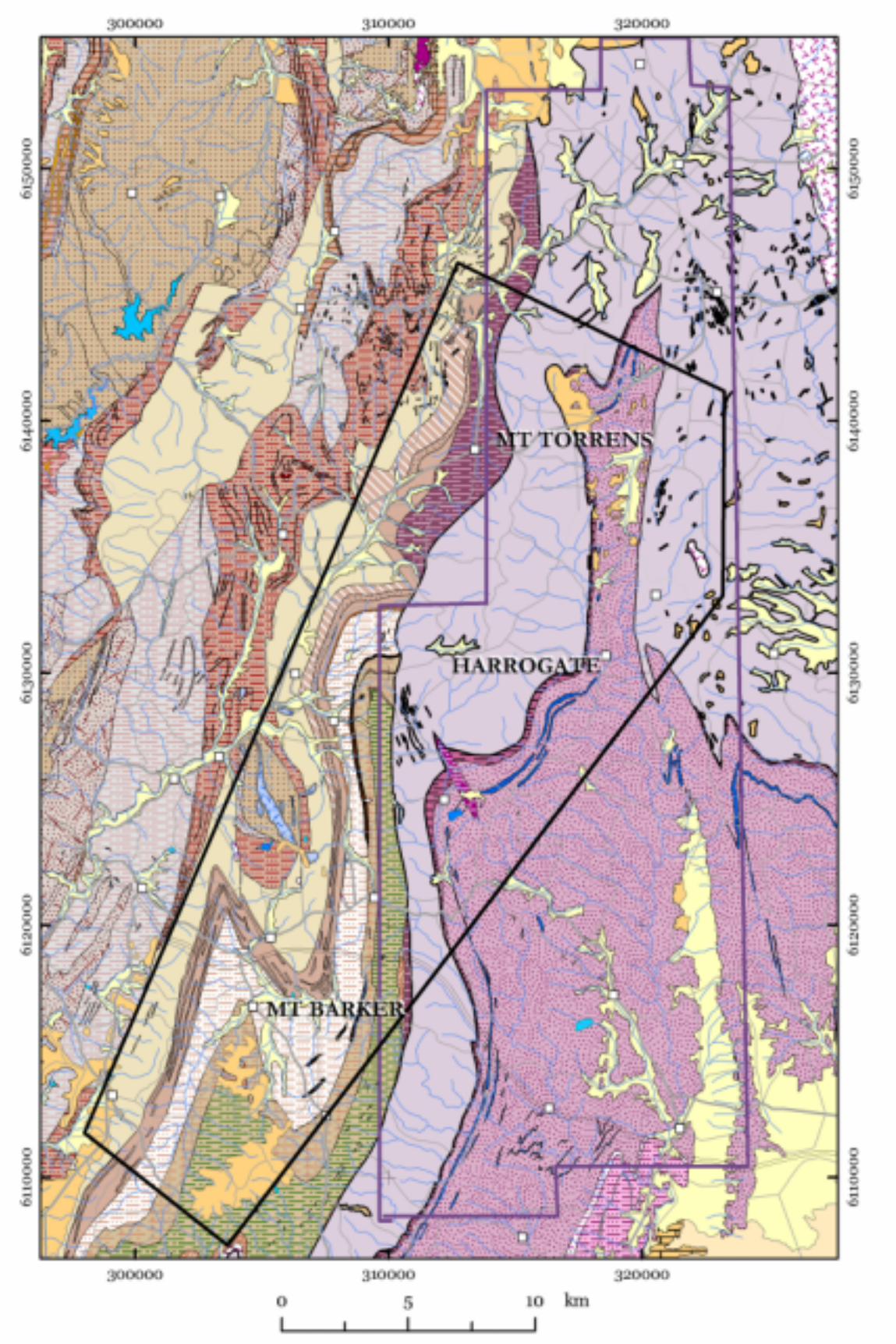

Figure 9. Geology. Legend is shown on following page.


Bremer Hills survey
PIMA survey area
Water
Pleistocene-Holocene
Undifferentiated Quaternary rocks
Pleistocene
Undifferentiated calcrete
Oligocene-Miocene
Limestone, echinoidal, bryzoal, crinoidal; sandstone, calcareous, minor carbonaceous clay and silt
Tertiary
Undifferentiated Tertiary rocks
Cambrian-Ordovician
Granitic, strongly foliated with lineation parallel to the country rock. Quartz, plagioclase(Oligiclase), and biotite, minor microcline.
Undifferentiated acid intrusives
Undifferentiated basic igneous rocks
Cambrian
Limestone; sandstone; shale; volcanics
Marble, white medium-grained crystals; Calc-silicate, grey,nodular
Siltstone, blue-black, laminated, sulphidic, partly limonitic, upper and lower horizons; Sandstone, medium to coarse-grained, dark grey, siltstone and phyllite interbeds. Pebble Conglomerate at base. Worm casts, bioturbation, very rare trilobites.
Sandstone and siltstone, laminated, graded bedding, flame structures and ripple drift crossbedding. Channelling.
Sandstone to greywacke, fine to coarse-grained, dark grey, thick-bedded to laminated; interbedded with laminated siltstone and thin, sulphidic siltstone and lenticular grit to conglomerate beds. Scour-and fill channels, rare cross-bedding.
Sandstone, grey, thick bedded, with thinly bedded, muddy, siltstone interbeds. Minor cross-bedding, ripples, rare trace fossils.
Sandstone, laminated, thick bedded, slumped, crossbedded, with minor siltstone interbeds. Widespread siltstone unit at base.
Sandstone; siltstone, occasionally sulphidic; metamorphosed.
Siltstone, laminated calcareous, light and dark grey (lighter bands being more calcareous), massive or laminated, local lenticular sandstone interbeds; sulphidic siltstone bands.
Neoproterozoic
Basal quartzite unit
Dolomite, cherty, magnesitic.
Dolomite; marble, with magnesite mud-pellet conglomerates.
Limestone, massive, oolitic, stromatolitic, ripple marks, overlain by dolomite with teepee structures. Colour from blue-grey at base to reddish-grey at top.
Limestone; dolomite; sandstone.
Middle quartzite member
Mudstone; siltstone; shale, partly carbonaceous.
Quartzite, feldspathic, with shale interbeds; silty sandstone in part schistose and calcareous.
Quartzite, sandstone, dolomite, conglomerate.
Quartzite, slightly feldspathic, fine to medium grained, pale pinkish grey, clay intraclasts, flaggy to medium bedded, heavy mineral lamination, minor siltstone.
Sandstone, massive, gritty, highly feldspathic; quartzite with pebbles.
Shale, black; dolomitic siltstone; dolomite; grey laminated siltstone.
Siltstone, dark grey, laminated with minor sandstone, dolomite interbeds; quartzite, fine to coarse, feldspathic, cross bedded, minor siltstone interbeds; slate
Siltstone, fine, sandy, cross bedding, minor thin dolomite lenses, local slumped siltstone beds.
Siltstone, grey to black, dolomitic and pyritic grading upwards to calcareous, thinly laminated, locally cross-bedded; dolomite, grey, flaggy to massive; limestone conglomerate, intraformational; greywacke.
Siltstone, sandy, flaser bedded.
Siltstone, shale, red-brown and olive green, laminated, flaggy to medium bedded; alternating with sandstone, fine grained, occasionally coarse grained. All lithologies calcitic in part.
Siltstone; shale, green-grey and purple.
Tillite; diamictite; shale; siltstone.
Tillite; quartzite; siltstone. Massive, grey.
Topmost quartzite unit
Palaeoproterozoic
Metamorphic rocks with retrograde metamorphism; metasediments, strongly banded parallel to gneissic foliation; minor intrusive granitic, pegmatitic and amphibolitic dykes.
Undifferentiated
Amphibolite, undifferentiated.
Breccia, undifferentiated.
Dolerite, undifferentiated.
Pegmatite, undifferentiated.
Pyrite, undifferentiated.
Quartz veins/bodies, undifferentiated

3.5 Weathering and Landform history

The weathering and geomorphic evolution of the Mt Lofty Ranges has been studied by numerous researchers (Woolnough, 1927; Fenner, 1930; Sprigg, 1945; Ward, 1966: Alley, 1977, Twidale and Bourne, 1975, Twidale, 1976; Milnes et al., 1985, Daily et al., 1974; Bourman, 1989, 1993b). Several landscape models have been proposed to explain the present distribution of regolith materials and landforms that form the Lofty Ranges. An overview of the main regolith-landscape models is presented here.

Two prominent regolith-landform features are recognised in the region. They comprise the highly weathered palaeo-surface, or what has been describe by many workers as the 'summit' surface, and a series of major north south trending fault line scarps. The palaeosurface is best developed or preserved on Kangaroo Island and the Fleurieu Peninsular to the south of the study area. The palaeosurface is generally characterised by highly weathered bedrock with iron induration and mottling common in the upper part of the weathering profile. Iron induration appears in several different forms including; Fe mottling in saprolite, Fe impregnated saprolites and alluvial/colluvial sediments, and as ferruginous lags. The soils are commonly described as gravely duplex types (Northcote, et al., 1975). In the study area (northern and central part of the Lofty Ranges), the 'summit' surface is less well defined and appears as scattered, typically ferruginised landscapes of relatively low relief. As mentioned earlier the surface is recognised on the hillshaded DEM by its generally smooth textural tone (Figure 6). Highly weathered regolith profiles have developed across a variety of different rock types and structures (Figure 8 - 3D drape of geology).

Twidale (1976) refers to these ferruginous materials as a laterisied peneplain that was subsequently disrupted due to faulting and uplift that form the Lofty Ranges. The laterite is thought to date back to the early Mesozoic with later faulting, uplift and erosion resulting in partial stripping of the ferruginous summit surface as rivers began to incise into fresh bedrock. Active drainage incision caused headward erosion, breached divides and river capture (Twidale, 1976). Similar ferruginous materials in the Lofty Ranges have been described by Mines et al. (1985) as ferricretes. The term ferricrete over laterite is the favoured terminology used in this report because of the broad genetic implications that are often applied when using the latter. In the past, the term "Laterite" has been used as a morphostratigraphic marker and typically implies discrete profile zonation at depth including mottled and bleached zones. Milnes el al. (1985) suggests that the ferricretes in the Lofty Ranges have evolved through a history of complex reworking involving erosion, transport and sedimentation and continuous weathering from the early Mesozoic to the present day. At Blackwood, Milnes et al. (1985) describe weathered alluvial sediments of early Tertiary age over mottled and pallid kaolinite saprolitic clays. Most of the ferricretes are thought to be remnants of iron-impregnated sediments of ancient valleys or depressions. A continuous weathering and erosional model rather than a major weathering event and subsequent uplift and stripping of the ferruginous summit surface is also favoured by Bourman (1993b). Bourman (1973) suggested that weathering profiles continued to develop in post-Early Miocene after the initial phase of faulting and uplift of the Adelaide Hills. A variety of ferricretes described by Bourman (1993b) including ferruginous saprolites and sediments, iron indurated lags and ferricretes with slabby and vesicular fabrics were best explained through multiple and multi-cyclic models of landscape development. Within this multi-cyclic model, ferruginous materials were recycled to form detrital ferricretes. Milnes et al, (1985) argues that the local variability seen in these weathered materials removes the need to explain their origin as a complete monogenetic weathering profile or peneplain surface that has been dissected or stripped to varying degrees.

Fault movements during the middle Eocene to early Miocene (approx 43 to 14 Ma) and Pleistocene (5 Ma) have created a series of major curvilinear fault line scarps broadly orientated north-south across the region. These scarps form the edge of a series of major tilt blocks. The tilt blocks have gently dipping east facing slopes and steeply faulted west facing edges that delineate the scarp face. Faulting and tilting gave rise to a series of host and graben type structures as the area was uplifted. Faulting was accompanied by renewed stream incision, dissection and stripping of raised blocks, and, typically lower rates of erosion and accumulation of depositional materials on the lower blocks. Down faulted blocks were inundated by the sea and shallow-marine Miocene sediments were deposited. In places

alluvial and colluvial fans have developed down slope and adjacent to the major fault scarps (e.g. Bremer Fault Scarp).

4. SALINITY IN THE ADELAIDE HILLS

4.1 Salinity – relationships with hydro-geology

Henschke (1997) divided the hills area into four principal hydrological provinces. These provinces were defined as areas having similar hydrological and groundwater characteristics. Although the provinces are largely based on geology they also take into account of soils and landforms. At a broad scale each province is inferred to have similar salinity processes and can be used to provide a first pass division of the major hydrological characteristics and associated salinity attributes over the region. Although the contact between these provinces is depicted as sharp boundaries on the map (Figure 10) in reality the groundwater boundaries are likely to be gradational between the major provinces (Henschke, 1997).

Of the four major provinces describe by Henschke (1997), three occur in the study area. These include landscapes and bedrock associated with the Adelaide geosyncline basement (Precambrian rocks), the Kanmantoo Group (Cambrian rocks) and sedimentary basins of Tertiary and Quaternary age.

Adelaide geosyncline basement province covers the western part of the study area and includes the townships of Mt Barker in the south and Mt Torrens in the North. Adelaidian rocks associated with this province include folded and faulted meta-sandstones, meta-siltstones, quartzites, limestones and tillites. The expression of dryland salinity is mainly confined to poorly drained valley systems. Deep weathering profiles scattered throughout this province are thought to store large quantities of soluble salts (Henschke, 1997). The fractured and weathered bedrock aquifers have total dissolved solids (TDS) ranging between 1500 to 3000 mg/L. Overall groundwater salinities are generally low compared with the other provinces particularly in areas of high rainfall where TDS values may be less than 200mg/L (Henschke, 1997).

The hydro-geological province associated with Kanmantoo Group rocks occurs over the central and eastern part of the study area. Lithologies include folded and faulted feldspathic sandstones and siltstones, shales, pyritic shales, limestones and calc-silicates. Most of the rocks have been regionally metamorphosed to produce phylitic, schistose and gneissic fabrics. Salinity is thought to be associated with the Nairne Pyrite Member and more regionally where geological controls constrain groundwater flow (eg. resistant bands of hard rock, quartz veining, faults, lineaments, shear zones). For example, moderately saline, shallow water tables in the Karrawirra catchment (northern part of the study area) appear to be related major geological barriers (Henschke, 2002). Conversely, fractured bedrock can facilitate rapid infiltration of fresh water into the deeper groundwater system. Oh, et al. (2000) showed that the groundwater associated with many of the major fractures and faults have lower salinities.

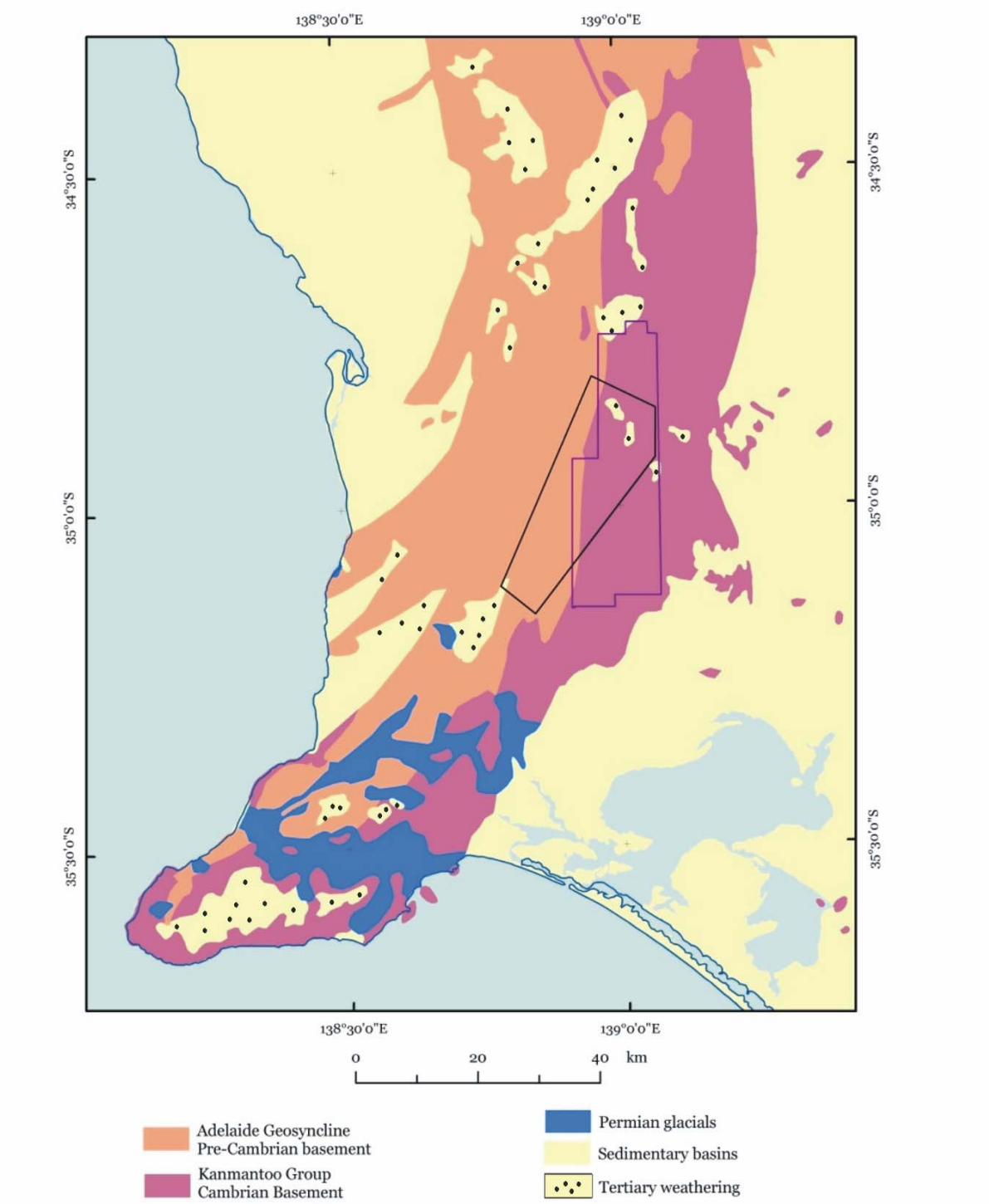

Figure 10. Major hydrological provinces for the Lofty Ranges (modified from Henschke, 1997). Tertiary weathering pattern refers to ferruginous weathering on either residual or transported materials.

Groundwater salinities in the Kanmantoo Group are higher than the Adelaidian lithologies to the west, ranging from 3000 – 10 000 mg/ L TDS. High TDS values are thought to be associated with highly weathered landscapes with generally lower hydraulic conductivity due the high clay content of the

regolith (Henschke, 1997). Lower TDS values are associated with bedrock dominated landscapes with fresh water recharge occurring on rocky ridges and hills (Figure 11).

The third hydrological province is associated with Quaternary and Tertiary sediments. Quaternary sediments include sands, silts, clays and gravels associated with modern river channels, colluvial fans down slope from major erosional scarps and aeolian sands that have been deflated from local rivers. Saline seeps are associated with perched water tables within these sediments and where creeks have incised into the valley alluvium. Tertiary sediments occur as locally scattered ferruginous sand, gravel and clay deposits. The Quaternary and Tertiary sediments are not well resolved on the generalised hydrological province map (Henschke, 1997) but are delineated from geological maps of the area (Thomson and Horwitz, 1962). Correlations between geology and salinity based on intersecting TDS measurements from bore holes with geological units over the Lofty Ranges indicate that the Quaternary and Tertiary sediments have the highest salinities compared with Cambrian and Pre-Cambrian lithologies (Oh, et al. 2000).

Trends in salinity observed across these major hydrological provinces compare favourably with salinity surfaces generated from kriging of stream EC and bore hole data points (Figure 12A and B). The surfaces were generated from points using the inverse distance weighted methodology (IDW) (Cox, et al., 2002). The stream EC surface was based on grab samples and doesn't include any salt load measurements. The bore hole derived interpolated surface used average bore hole values in situations where there was more than one measurement taken. Both surfaces (Figure 12a and B) show a general increase in salinity from west to east across the study area. The lowest salinities are centred around the township of Mt Barker with higher values east of Callington and Harrogate. In the bore hole derived surface several hot spots are noted to occur between Mt Barker and Callington, around Brukunga, east of Harrogate and around the Callington area. However, as several of these areas are only based on one or two data points, ascribing local scale significance to the results is not advisable.

4.1.1 Salinity and the Regolith

The regolith has been recognised as an important source of salt in the Adelaide Hills area. As mentioned earlier, Henschke (1997) noted that deep weathering associated with the partly dissected 'lateritic' was a potential source of stored salts. Henschke (1997) went on to say that the lack of extensive salinisation associated with the laterite maybe due to the high rainfall in the region that prevents an accumulation of salts in the upper part of the regolith profile. A comparison between a bedrock and regolith dominant catchments (Karrawirra and Cameron catchments eastern part of the Adelaide Hills) demonstrated that there was considerably more salt being discharged in the latter. This was attributed to the regolith storing substantial quantities of salt in the weathered zone (Henschke, 2002) Fitzpatick et al., (1996, 2002) showed a correlation between high salt fluxes from the Herrmann's catchment (in the northern part of the study area) and the intense weathering of scapolite bedrock minerals containing Na and Cl ions. Perched water trends in the Herrmann's catchment (Cox and Davies, 1997) showed a correlation between breached groundwater tables, water logging and salinity. The relationship between regolith materials and salt stores will be investigated in some detail later in this report (see section 6.8).

Studies of the weathered and bedrock materials in the Keynes catchment (Cox and Reynolds, 1995, Thompson et al, 1994) outside and to the north of the study area showed a negative relationship between salt storage in the aquifer and elevation. The lower salt content of weathered materials (> 27m deep - Thompson et al, 1994) in the upper part of the catchment compared with higher salt loads in the lower parts of the catchments suggested groundwater recharge and a preferential accession of salts in the lower parts of the catchment.

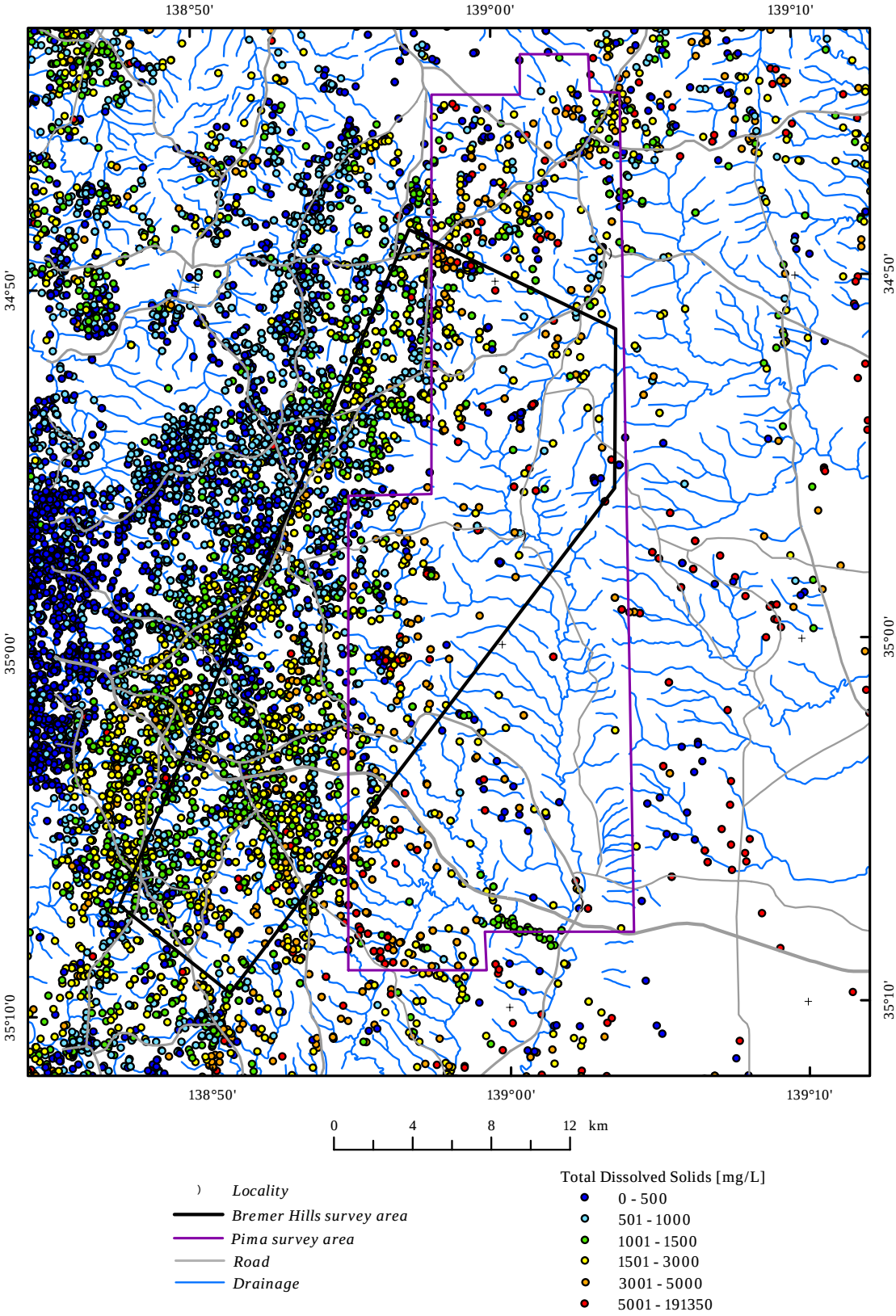

Figure 11. Bore hole total dissolved solids.

A

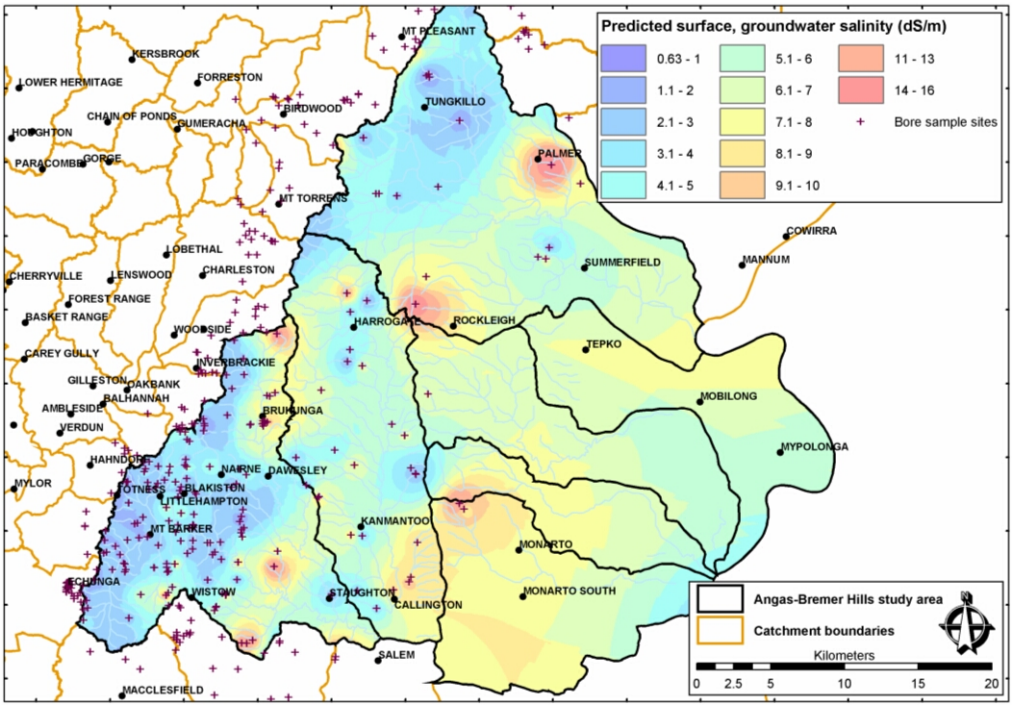

B

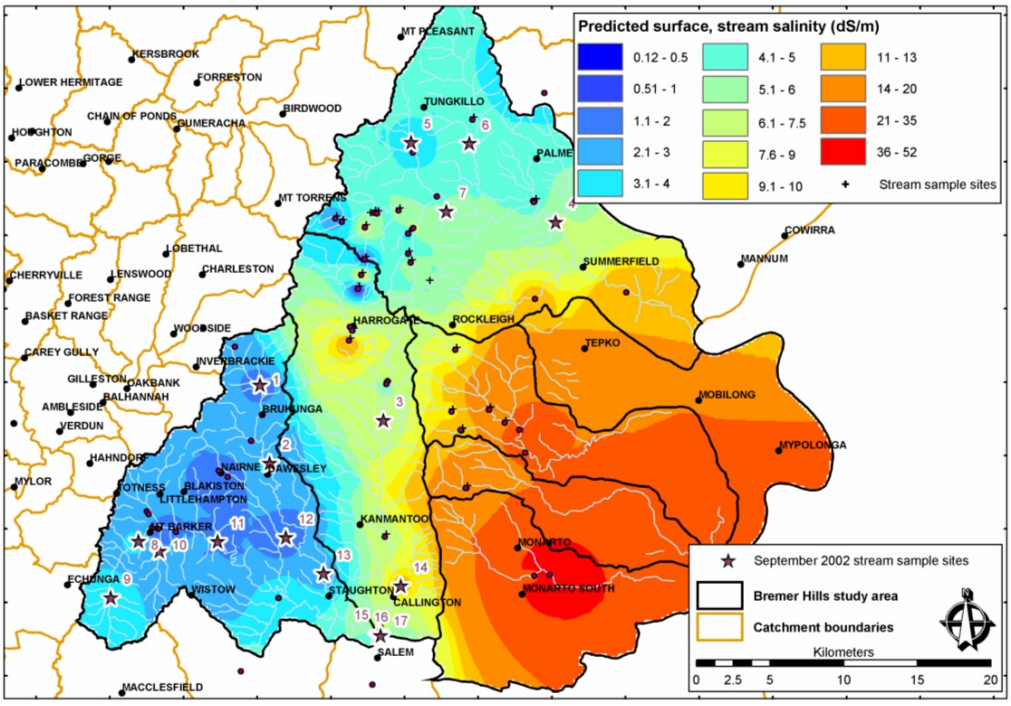

Figure 12. A – Gridded surface of bore hole salinity. B – Gridded surface of stream salinity. (from Cox et al., 2002)

4.1.2 Soil landscape mapping and GIS modelling for generating salinity hazard maps.

Soil landscape units have been mapped over the Lofty Ranges at 1:50 000 scale (Maschmedt, 1993, PIRSA Land Information 2001). Soil landscape units are based on landforms defined from aerial photography, geology and field site observation. Landforms are used as a surrogate to map soil because of the close genetic and spatial relationships between soils and landforms. Soil landscape units in the study area are divided into soils formed on basement rocks and those developed on unconsolidated sediments (Tertiary and Quaternary – sands clays and gravels). Landforms such as valley floors, rises, rocky hills, hill slopes are then used to further divide the different soil types. Physical and chemical properties of different soil types are based on field site and laboratory measurements. Attributes associated with each soil-landscape unit are used to generate customised thematic maps for specific applications. Thematic maps relevant to this study include dry saline land (Figure 13), ground water induced salinity (Figure 14) and salinity risk maps (Figure 15). The salinity categories are largely based on vegetation type, soil characteristics including soil test results and the occurrence of salt scalds or other physical indicators of salt toxicity. Areas of dry saline land show soils with elevated levels of salt that are not associated with the water table. Salts have accumulated through cyclic accession, saline groundwater and to a lesser extent through bedrock weathering. Salinity classes are based on the most saline part of the upper metre of soil. Groundwater salinity maps show soil-landscape units that are affected by saline groundwater discharge. Classes in groundwater salinity maps are based on soil tests and observation of vegetation type and condition. Salinity risk maps rank each soil landscape unit against a potential salinity risk value. The classification takes into account the ranking of adjacent units and topographic position in the landscape (PIRSA Land Information 2001 – Digital CD).

Fitzpatrick et al. (1999) developed an up-scaling approach that takes detailed soil attributes based on site measurements and toposequence relationships to enable broader scale extrapolations using remotely sensed and other regional datasets. Thematic attributes generated using this approach include drainage/waterlogging, salinity and soil acidity/alkalinity. The up-scaling procedure uses GIS integration and modelling techniques. Salinity classes were determined from field studies from the Herrmann's catchment, geology (geological maps), soil landscape maps and DEM derived topographic attributes (Figure 16). Soil dielectric properties (e.g. used to indicate waterlogging) were determined using airborne Synthetic Aperture Radar (SAR) data. Fitzpatrick et al., (1999) recognised Quaternary sediments as a likely source of stored cyclic salts and demonstrated that a significant amount of salt was being generated through bedrock weathering. Bedrock derived salts are thought to be associated with pyrites (iron sulphide) within the Tapanappa and Talisker Formation (FM). These sulphides cause aggressive acid weathering of the surrounding rock, in particular the weathering of salt bearing minerals such as scapolites (Fitzpatrick, et al., 2002).

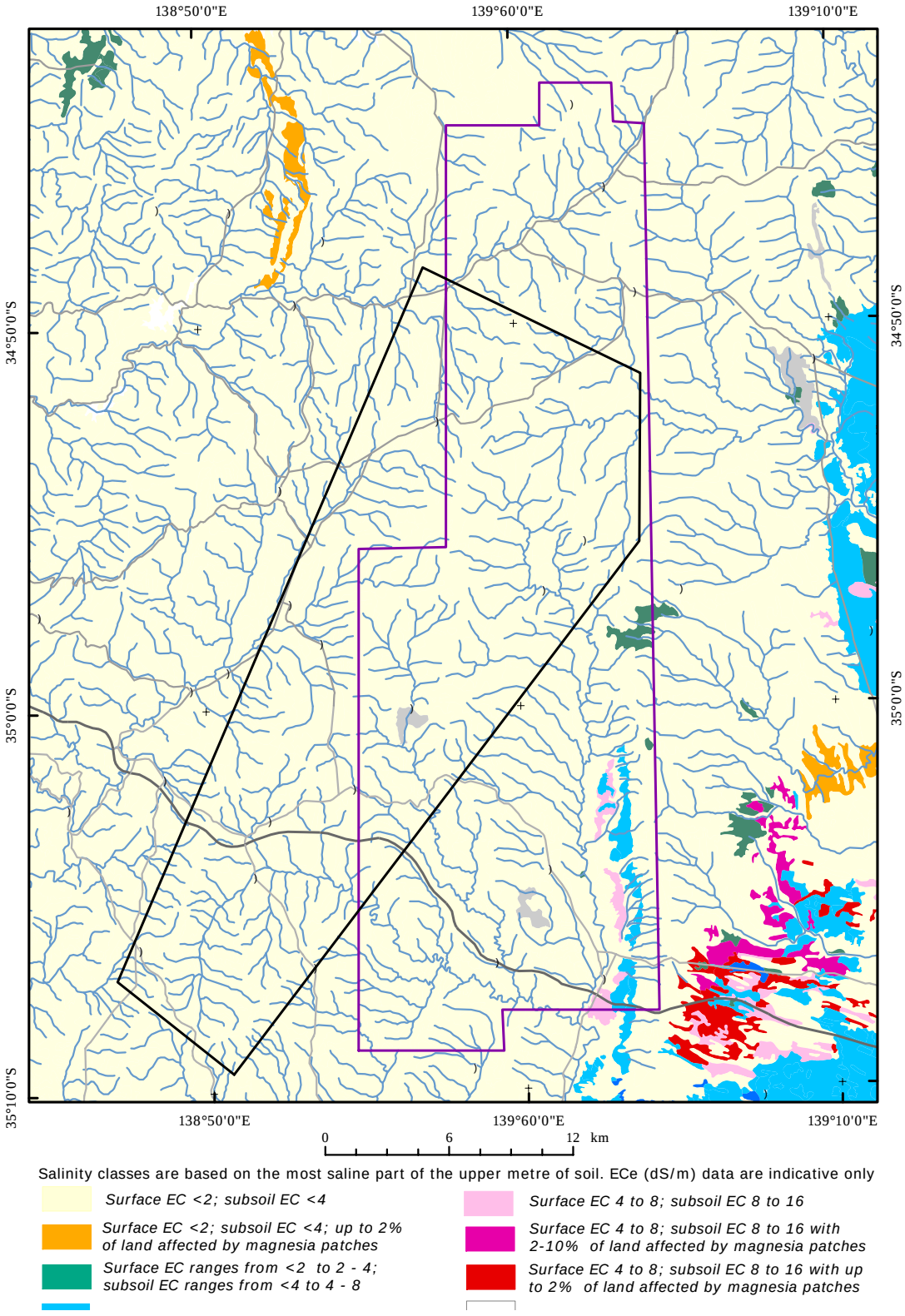

Figure 13. Areas of dry saline land (PIRSA Land Information 2001).

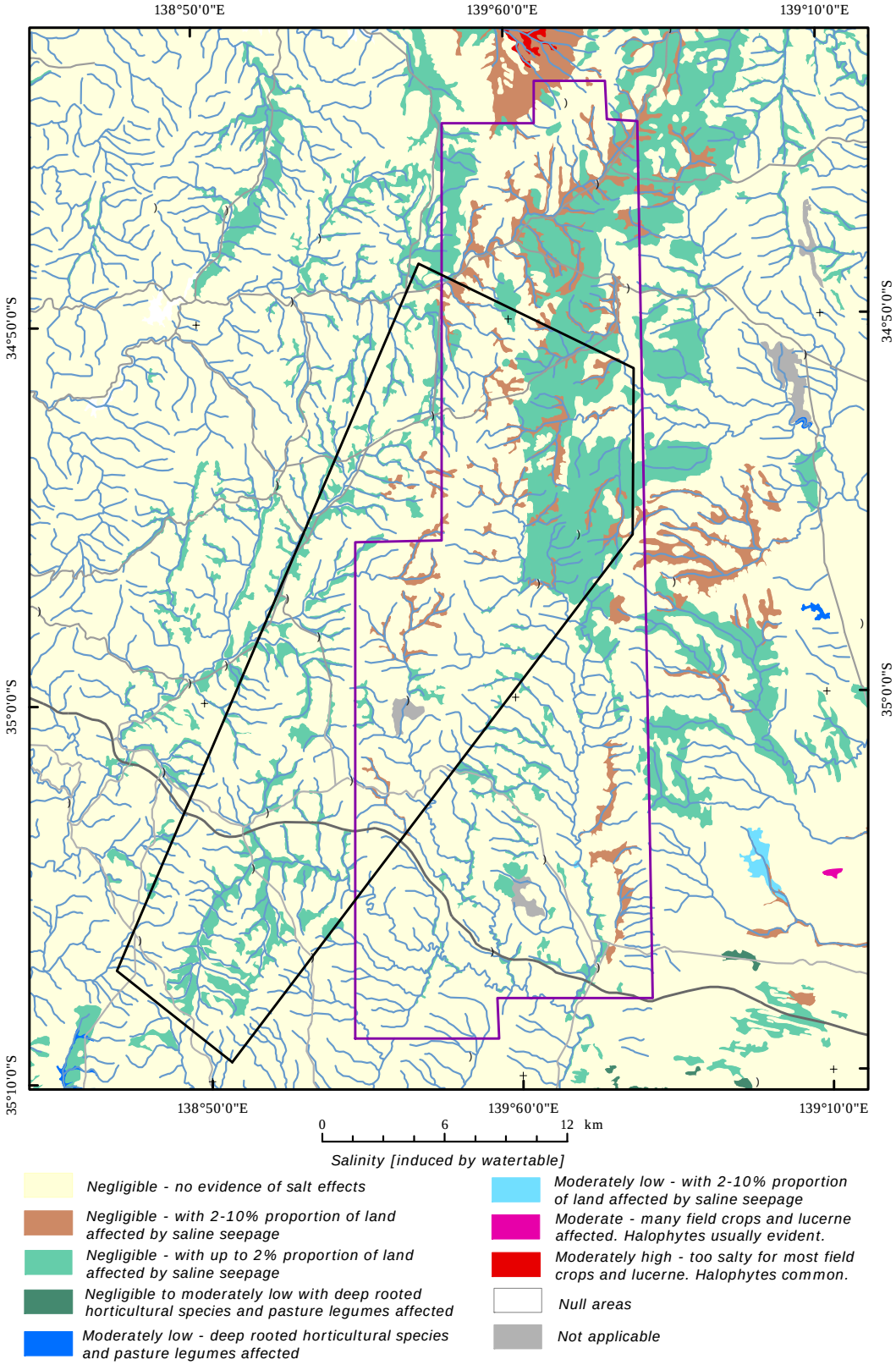

Figure 14. Areas of salinity induced by watertable (PIRSA Land Information 2001).

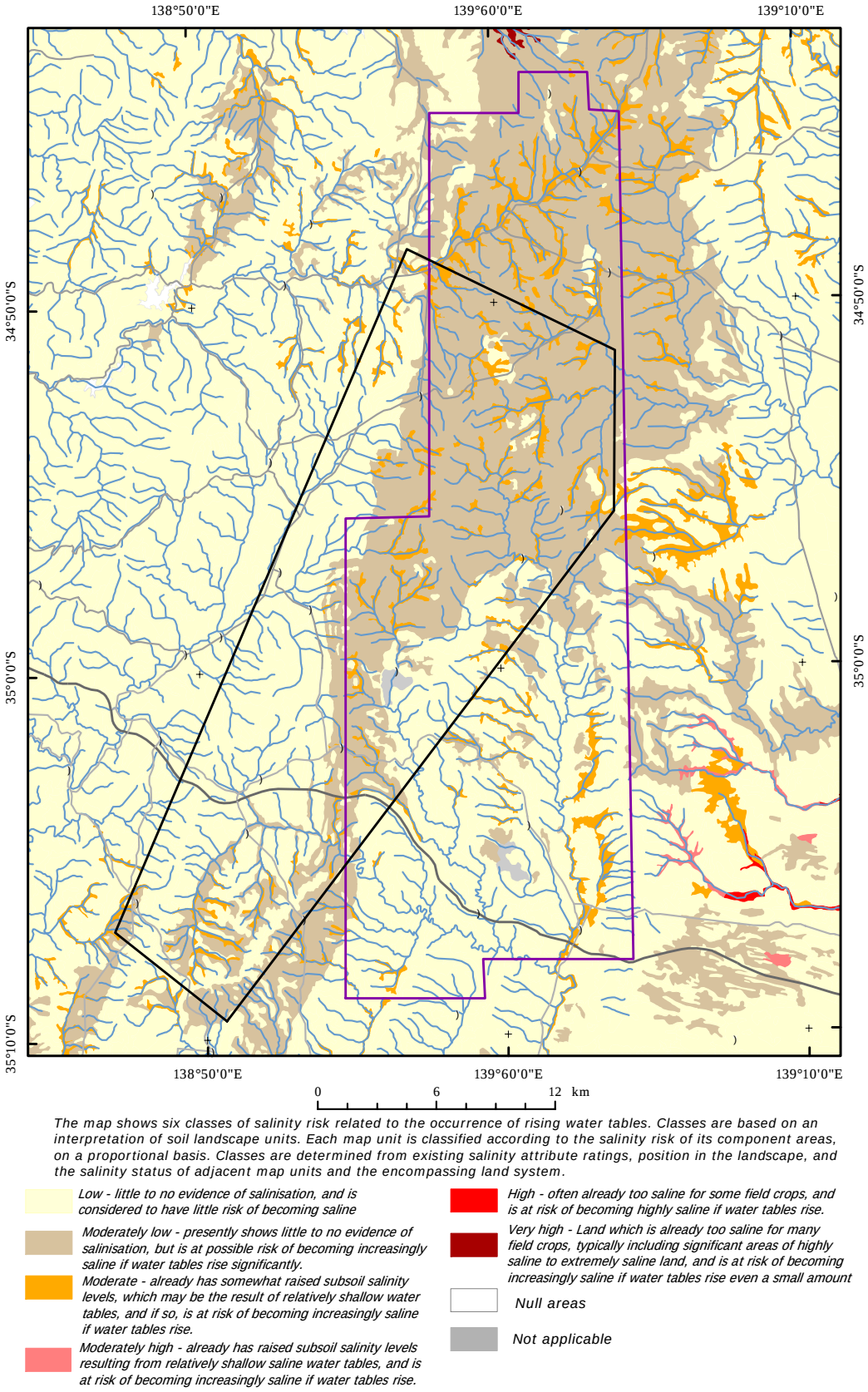

Figure 15. Areas of ranked salinity risk (PIRSA Land Information 2001).

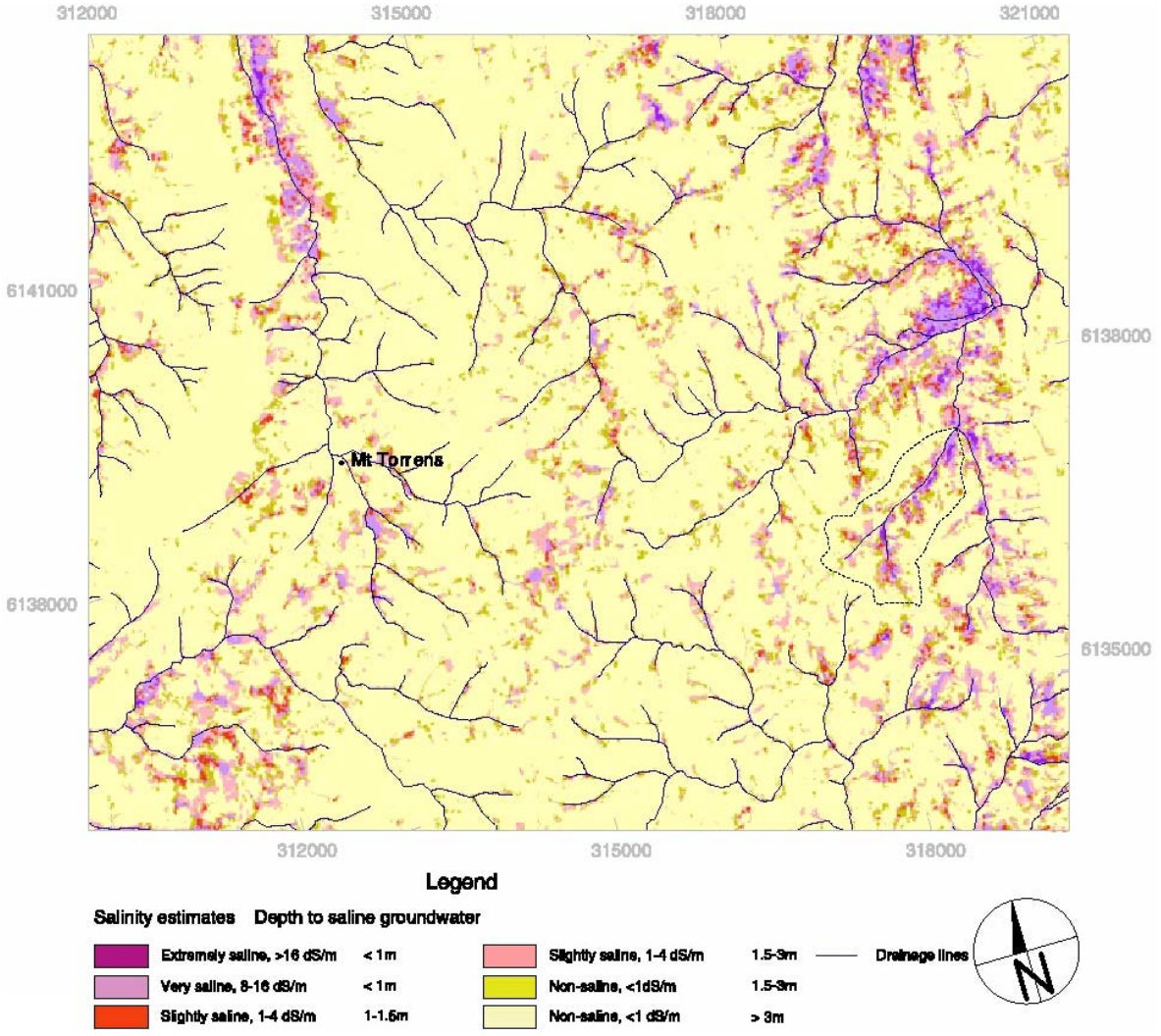

Figure 16. Estimates of salinity for the Mt Torrens area compiled from modelling of soil dielectric, topographic index and 1:50 000 scale PIRSA geological mapping (Fitzpatrick, et al., 1999).

4.2 Expression of salinity in the Adelaide Hills

Several different forms of dryland salinity in the hills have been recognised from a number of studies (Henschke, 1997, 2002; Cox and Davies, 1997; Cox and Reynolds, 1995; Maschmedt, 1993, PIRSA 2001; and Oh, et al. 2000 and Fitzpatrick et al., 1994, 1996 and 1999). Expressions of salinity recognised during the course of this study have been added to those identified from previous studies – they include;

1. Valley floor and drainage lines – corresponding to areas of local discharge. Salts are typically stores in valley alluvium and weathered bedrock beneath the valley floor.

2. Saline seeps along drainage lines as a result of preferential pathways of pressured groundwater flow or perched water tables.

3. Saline seeps at the base of colluvial footslopes (e.g. colluvial and alluvial fans down-slope from the Bremer fault scarp). Seeps typically occur within creeks draining from the fans or at the contact

between the colluvial/alluvial sediment and the underlying bedrock at the base of the footslope or fan.

4. Hillside saline seeps where geological structures impede ground water flow or where local concavities down the hill slope can funnel water and cause small seeps.

5. Break of slope salinity. These areas of salinity typically correlate with transitional or abrupt regolith zones associated with toposequences. For example, seeps can occur at the contact between valley floor sediments and adjacent colluvial footslopes.

6. Salinity associated with pyritic rich bedrock – where accelerated weathering rates due to acid groundwaters lead to the breakdown and release of salts from scapolites and other minerals that contain Na and Cl ions

Vegetation type and condition can often highlight areas affected by land salinisation. Salt affected areas are characterised by the presence of salt tolerant grasses such as sea barley grass. In places stressed vegetation and areas of bare ground or scalding where salts have killed the vegetation and degraded the soil structure are also observed.

5. STUDY METHODS

5.1 Datasets and processing

5.1.1 Magnetics and gamma-ray spectrometry

Magnetic and gamma-ray spectrometry data were collected by Fugro Airborne Survey during June-August 2002 with a flightline spacing of 100 m and a nominal terrain clearance of 60 m. The data was acquired in GDA94, MGA zone 54 and the following Australian Map Grid coordinates define the survey area; 297991E 6111756N; 312728E 6146262N; 323255E 6141179N; 323203E 6133066N and 303639E 6107289N.

A Geometrics G822A magnetometer was used to measure the Earth's magnetic field. The magnetometer recorded approximately 7 m along each flightline with a sensitivity of .001nT. A line spline algorithm was used to produce gridded magnetic data of 20 m cell size resolution for enhancement and display in ERmapper. ERmapper grids were then modelled and integrated with other datasets in ArcInfo GIS.

First vertical and horizontal derivates of the magnetics were produced to highlight major lithological, structural and high frequency features in the data (Figure 17 and 18). The high frequency component of the magnetic image was specifically enhanced to highlight the presence of any near-surface regolith magnetic material (eg. maghemite gravels).

Gamma radiometrics measures the natural radiation from potassium (K), thorium (Th) and uranium (U) in the upper 30cm of the earth's surface. Potassium is measured directly from the decay of ^{40}K. Thorium and U are inferred from daughter elements associated with distinctive isotopic emissions from ^{208}Tl and ^{214}Bi in their respective decay chains, so they are usually expressed in equivalent parts per million eU and eTh. Potassium is more abundant and is expressed as a percentage. Gamma-rays were detected using a 50.3L NaI(T1) crystal pack over 256 channels. A series of data processing and calibration steps were then preformed including NASVD noise reduction (Minty 1997), cosmic, aircraft and radon backgrounds removal, stripping and height corrections. For detail descriptions of

flight acquisition and data processing steps, refer to Furgro Airborne Surveys Pty. Ltd technical report (2002). The flightline data were microleveled for each band and a minimum curvature algorithm was applied to produce grids at 20 m cell size.

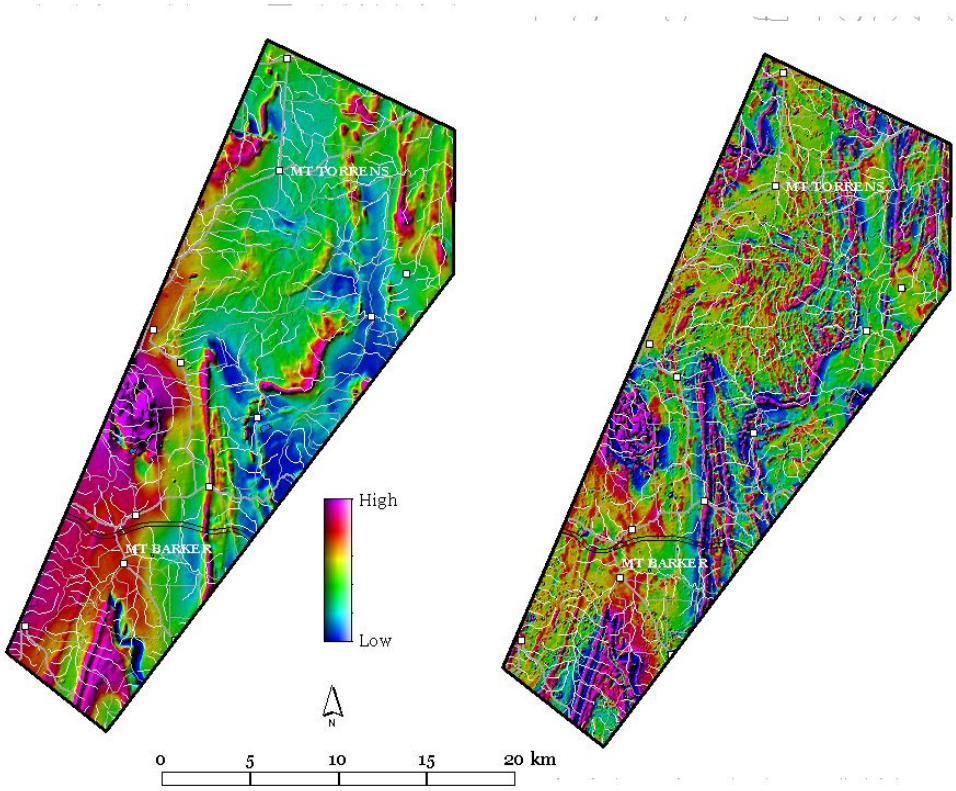

Figure 17. Magnetic intensity (left) and the first vertical derivative (FVD) of the magnetics highlighting magnetic variations and gradients for the Adelaide Hills survey.

Gamma-ray grids were displayed either as, single pseudo-coloured images with red to blue colours relating to high and low gamma-ray values respectively, or as three band colour composite images with potassium in red, thorium in green and uranium in blue (Figure 19 and 20). Images were enhanced with ERmapper software and then incorporated in ArcInfo as GIS thematic layers. Gamma-ray radiation emitted from the ground surface (to a depth of approximately 30cm) reflects the chemical composition of the bedrock, regolith and overlying soil. Gamma-ray imagery therefore shows geochemical variations of K, eTh and eU in exposed regolith and bedrock.

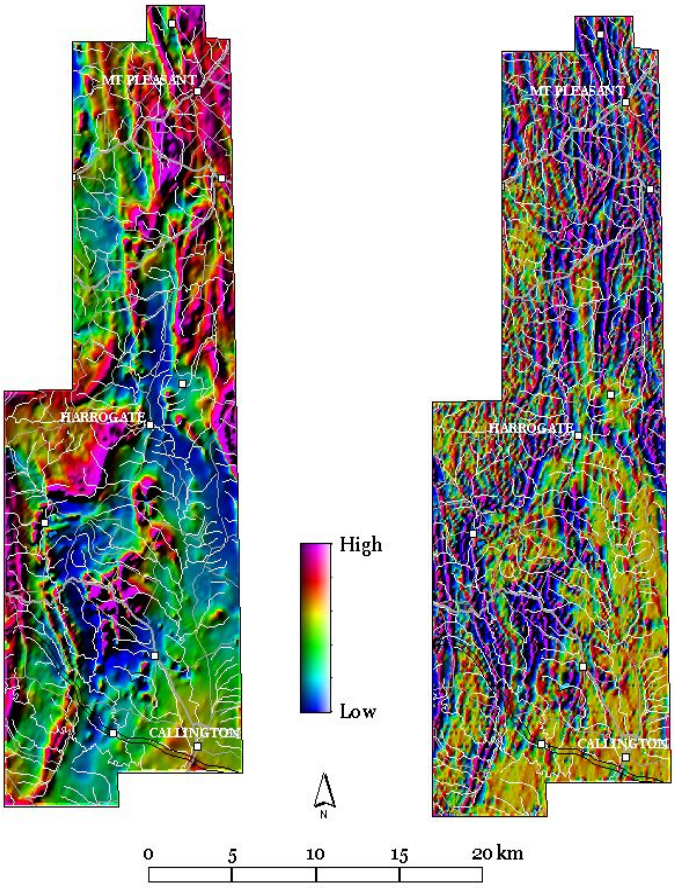

Figure 18. Magnetic intensity (left) and the first vertical derivative (FVD) of the magnetics highlighting magnetic variations and gradients for the PIMA survey.

5.1.2 Ground geophysics – EM31

The EM31 measures apparent conductivity of the upper 3-6m of the regolith. Conductivity depends on soil moisture, soluble salts, temperature, texture particularly the clay content and the nature of the parent material (eg. presence of magnetic minerals). However most of the observed variation in conductivity noted in the EM31 logs relates to the soil moisture and salt content. EM31 surveys have been used extensively in mapping salt affected land and shallow saline ground water tables based on the relationship between high conductivity and salt content in the upper part of the regolith.However, it should be recognised that there is not always a direct correlation between high EM responses and salt concentrations. For example, soils with high clay content and cation exchange capacity can be more conductive than sandy textured soils with similar salt concentrations. Therefore, where there are major variations in soil texture across the survey, consideration should be given to soil type and the effects of soil moisture when estimating salinity using EM31 data.

In this study EM31 transects were used as a guide to map clay-rich regolith materials and salts in the upper 3-6 m of the weathering profile. The EM31 transects assist in validating thematic regolith maps generated from an interpretation of the airborne gamma-ray spectrometry imagery. EM31 measurements were collected at 20 to 40 m intervals along the transects depending on the local

variability in the landscape (relief and regolith). These transects were surveyed orthogonal to streams or valley floors to intersect a range of materials from hill slopes to valley sediments.

5.1.3 Ground geophysics – NanaTem and SmartTEM

NanoTem and SmartTEM are time domain electromagnetic surveying instruments that measure the conductivity of the regolith and bedrock. Two sets of wire loops, one inside the other, are laid down over the ground. A primary field is generated in the larger wire loop that is pulsed or turned off and on repeatedly. The inner wire loop records the small secondary field during the time the primary field is inactive. The nature or behaviour of the secondary field provides direct information on the conductivity or resistivity of the underling material. Secondary eddy currents generated from the primary field will tend to diffuse or decay quickly in resistant materials, whereas in conductive materials the eddy currents circulate around the body and decay more slowly. The decaying secondary field is measured over a number of fixed time intervals after the primary field has been turned off. The response of the secondary field during these time intervals is then used to generate conductivity images of the sub-surface.

The data were acquired at 40m stations, using a 20m loop size, and a 5m in-loop receiver. The data were acquired and processed by Zonge Australia. The derived data were inverted using the Zonge STEMINV routine described by MacInnes and Raymond (2001). The Smooth-model inversion is a robust method for converting Transient Electro-Magnetic (TEM) measurements to profiles of resistivity (or conductivity) versus depth. Observed TEM time and dB/dt magnitude data for each station are used to determine the parameters of a layered-earth model. Layer thicknesses are fixed by calculating source-field penetration depths for each window time. Layer resistivities are then adjusted iteratively until the model TEM response is as close as possible to observed data, consistent with smoothness constraints. The smoothness constraints limit resistivity variation from layer to layer.

The result of smooth-model inversion is a set of estimated resistivities that vary smoothly with depth (see section 6.5). Lateral variation is determined by inverting successive stations along a survey line. Results for a complete transect are presented in pseudosection form by contouring model resistivities (conductivities). For contouring, resistivity (conductivity) values are placed at the midpoint of each layer, forming a column below every station. The columns form an array representing a cross-section of model resistivity (conductivity). Each station was fitted to topography prior to gridding.

Inverting window magnitude data to smoothly varying model conductivities effectively displays the information inherent in TEM measurements. Smooth-model inversion does not require any a prior estimates of model parameters. The data are automatically transformed to resistivity (conductivity) as a function of depth.

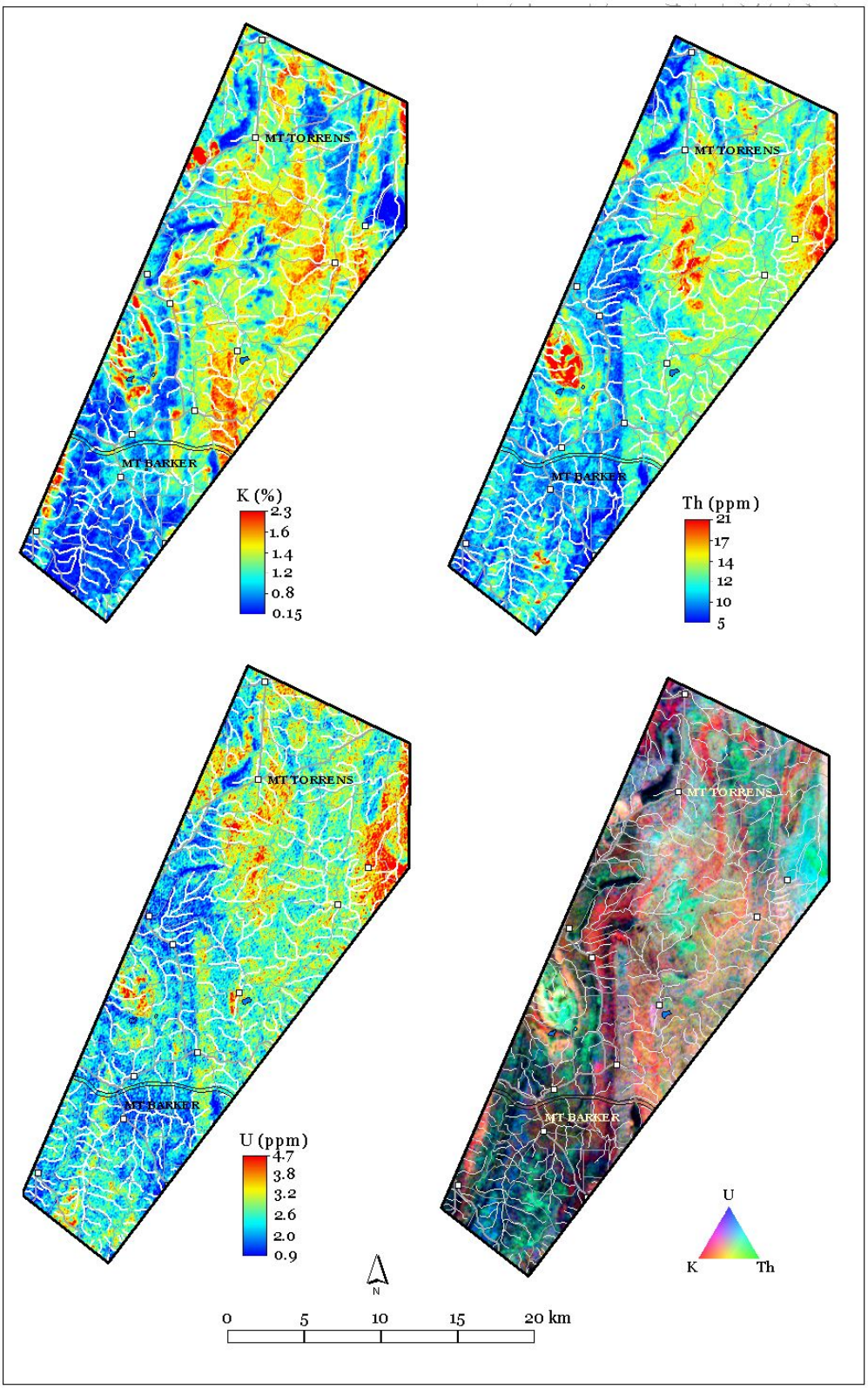

Figure 19. Pseudo-coloured and three band false colour composite image of K, eTh and eU. Adelaide Hills survey.

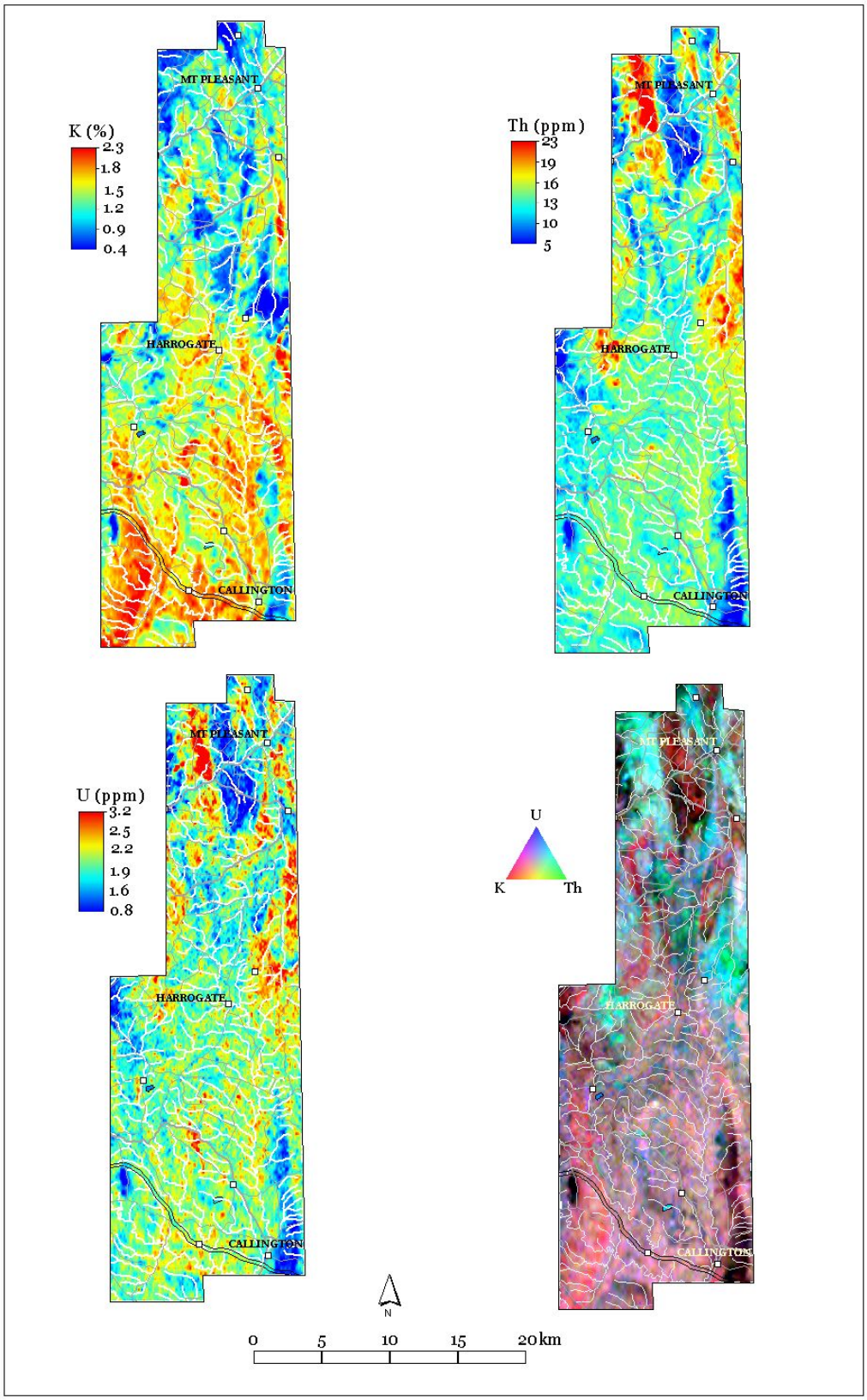

Figure 20. Pseudo-coloured and ternary image of K, eTh and eU. PIMA mining survey.

5.2 Digital elevation model

Any digital display of the continuous variation of relief over space is known as a digital elevation model (Burrough and McDonnell, 1998). Three digital elevation models were used in the investigation. These included elevation data from the airborne survey and topographic map based elevations including spot heights and contours.

A digital elevation model (DEM) is calculated from the aircraft using Global Positioning System (GPS), altitude (flying height - ASL) and a radar altimeter (flying height above the ground). Elevation measurements were collected at 60 m intervals along each flight-line. There was 100m between flight-lines. Tie line levelling and further micro-levelling along each flight-line produced the final levelled terrain model. A line-spline algorithm was also used to produce gridded data with a 20 m cell size for the survey area (Fugro, 2003). The pixel size for the final grid is 20m.

Map based elevation grids were generated at 25 and 10 metres resolutions and were based on 1:50 000 and 1:10 000 scale topographic map information, respectively. The grids were generated by CSIRO Land and Water (Adelaide) using ArcInfo TOPOGRID software. TOPOGRID combines and interpolates elevation values from a range of height attributes including contours, spot heights and drainage lines. Flow directions from drainage lines ensure sensible hydrological gradients in the final grid.

The elevation models were processed to derive a series of surfaces to describe major geomorphological, structural and hydrological characteristics in the study area. Primary terrain attributes including slope, aspect, elevation, roughness and hillshaded relief images were generated to describe major landform elements including catchment morphological, relief, structural lineaments and erosional scarps. Several more sophisticated compound topographic terrain indices (using two or more primary attributes) were also evaluated including a multi-resolution index of valley bottom (MRVBF) and Fuzzy Landscape Analysis (FLAG). Relationships between MRVBF and FLAG with the gamma-ray imagery and regolith landscape models for the main part of the results in section 6.7.

A multi-resolution index of valley bottom flatness for mapping depositional areas (Gallant and Dowling, 2003) was used separate hill slopes from valley floors. The index uses slope to infer flatness and elevation with respect to a local area to infer lowness to delineate valley floors. Different scales of valley bottoms are derived by applying the algorithm and combining the outputs from several resolutions (derived by re-sampling) of the DEM.

Fuzzy Landscape Analysis GIS (FLAG) software (Roberts *et al.* 1997) was used to highlight recharge and discharge sites in the landscape. FLAG generates and combines a number of topographic indices (scaled from 0-1) derived from elevation data using the principles of fuzzy set theory. It has been used effectively in salinity studies, identifying waterlogged soils and areas of recharge and discharge (Laffan 1996, Dowling 2000).
FLAG calculates the following topographic indices:

Topography (HIGH) - an index of high elevations, where the primary assumption is that topography is the surface expression of all factors that have acted on a site over time (including geology, soils, climate, vegetation and land use), often in an inter-related way.

Local lowness (LOWNESS) - deviation of the topographic surface relative to a smoothed topographic surface. This index was used to predict areas of seepage below breaks in slope, assuming that the water table conforms to the topographic surface, except the output is smoother.

Plan curvature (CONCAV) - identifies convergence and divergence of drainage and, therefore, blockages and bottlenecks in water flow.

Contributing area (UPNESS) - the basal area of all adjoining land at higher elevations relative to the area of analysis (that is the area continuously uphill of each point). This lets us evaluate relative height in the landscape (scale values from 0 = highest point and 1 = lowest point).

Two final indices are derived by combining the above:

- Locally 'low' with large contributing area (LOW) – defines the range of areas that are low in the local landscape with large contributing area. These are sites of discharge and by inference salinity where salt stores are near by.

- Concave with large contributing area (CC) - defines areas of convergent drainage with a large contributing area. Again, these are likely wet areas in the landscape.

Locally 'low' with large contributing area (LOW) was the principle output used in this study to highlight potential discharge sites and valley salt stores.

Digital elevation models also had an important role in allowing more effective landscape visualisation. For example combining gamma-ray images with terrain models as 3D perspective drapes facilitated the visualisation and understanding of the relationships between gamma-ray responses and surface morphology (see results section 6.0).

5.3 Sample preparation and drilling

5.3.1 1:5 soil water extracts, conductivity and moisture content

Electrical conductivity of 1:5 soil water extracts were used to estimate the concentration of soluble salts in the soil/regolith. The extracts were prepared by adding 5mls of deionised water to every gram of soil. Approximately 50 grams were used in the analysis. These solutions were then shaken for 1 hour before a conductivity measurement (with internal temperature compensation) was taken. The results are expressed in micro siemens per centimetre. Soil moisture for each sample was determined by oven drying the sample over night and then subtracting the dry weight from the original sample.

5.3.2 Drilling

A total of 17 bores holes were drilled over contrasting regolith-landforms. Holes varied in depth from 4 m in largely unweathered landscapes to over 50 m in highly weathered relict landforms. Two drilling rigs were used. The first was a RAB rig with samples collected every 25 cm for the first 2 m and then at 50 cm intervals to a depth of 14 m and then at 1 m intervals until end of hole. Hole collapses and poor drill sample recovery in areas of deep weathering meant that several of the holes didn't go through the saprolite into the saprock zone of the weathering profile. For this reason a second aircore rig with a larger air compressor was used to obtain a complete profile of the regolith in areas of deep weathering. Samples were collected at 50 cm intervals down hole. A deep drill hole planned for the Mt Barker region was not completed due to wet weather conditions at the scheduled time for drilling.

5.4 Residual modelling (separating bedrock and regolith responses)

The responses or variations seen in gamma-ray imagery relate to both the geochemistry and mineralogy of the bedrock and regolith. Since the soil/regolith response varies according to the parent rock, interpretation of gamma-ray imagery is best done within lithological units. Superimposing lithological units over a gamma-ray image is often helpful when trying to separate bedrock from soil responses. A more sophisticated approach uses residual modelling techniques where geological polygons are used as regions of interest to perform mathematical calculations (Wilford, et al, 2000).

The residual modelling approach assists in separating bedrock and regolith responses from the gamma-ray spectrometric imagery. The approach uses a slope grid from a DEM, geological polygons and individual radioelement grids (K, eTh and eU). The slope grid is used to partition areas in the landscape with relatively high slopes and corresponding high geomorphic process rates from areas with more subdued relief and lower slope angles. Higher erosion rates on steeper slopes are likely to be associated with exposed bedrock and thin soils, so the corresponding gamma-ray response largely reflects the geochemistry of the bedrock. Based on field observations a 6 degree slope threshold was chosen to separate bedrock gamma-ray responses from regolith materials. Once the slope threshold value has been determined, it is used to generate a bedrock response image. All pixels in the gamma-ray image above a selected slope threshold are averaged to give a bedrock signature for each element within each lithological unit. The mean bedrock response is then subtracted from each pixel in the original image to generate residual grids for total count, K, eTh and eU. Radioelement values centred around the mean bedrock response generally relate to thin soils over bedrock or exposed bedrock. They may also correspond to actively eroded and recently deposited alluvium that still retains the radioelement signature of the bedrock. In erosional landscapes these sediments tend to be restricted to narrow corridors along streams. Deviation either above or below the mean value can reflect the weathering of bedrock or the deposition of covering sediments.

6. RESULTS

6.1 Gamma-ray response of bedrock and regolith

6.1.1 Precambrian rocks.

The Precambrian lithologies have lower values for each of the three radioelement (K, eTh and eU) compared with Cambrian rocks. This reflects both geochemical and mineralogical differences between the two rock groups. Lower gamma activity of the Precambrian lithologies is attributed to their relatively high silica content and lower micaceous and feldspathic mineral content (Figure 21, 22 and 23).

Potassium (K) content is generally low in Precambrian lithologies particularly where the bedrock has a high silica content including for example quartzite, siliceous sandstones and siltstones. Units with moderate to high K are associated the Saddleworth Formation (FM) (mudstone, siltstones, shale and some carbonaceous units) with ranges[1] between 2.0 – 3.5 % K; the Tapley Hill FM (siltstone with some dolomite and pyrite) with ranges between 1.5 – 2.3% K; the Ulupa Siltstone with ranges between 1.0 – 1.9% K; the Tarcowie Siltstone (siltstone, minor sandstone and dolomite) with ranges between 1.9 – 2.4% K); the Stoneyfell Quartzite (quartzite, feldspathic sediments and inter bedded shales) with ranges between 1.8 – 2.6 % and high grade metamorphosed sediments (gneiss) associated with the Barossa Complex with ranges between 2.1 – 3.5 %K. These high K values are likely to relate to primary K-bearing rock forming minerals such as muscovite and K-feldspars. Local high K values up to 3.2 % K within the Saddleworth FM may relate to contact metamorphism associated with the Barossa intrusive complex (Figure 21, 22 and 23). Low gamma-ray values (black on the 3 band ternary image) for each of the three radioelements correlate to highly siliceous bedrock including sandstones, siltstone and quartzite (eg. Mitcham Quartzite, Mt Barker). Sufficiently large water bodies (rivers, dams) also appear black in the ternary image, since gamma-rays are attenuated by water.

The eTh content of Precambrian rocks is generally low with ranges typically between 3-10ppm (Figure 21). Exceptions are the Barossa Complex (10-36 ppm); highly weathered ferruginous materials

[1] Radioelement values for each bedrock unit are based on typical ranges where corresponding slopes derived from the DEM were moderate to high. This partitioned areas in the landscape that are actively eroding and where the radioelement responses are likely to correspond with bedrock at or near to the surface.

(discussed in section 6.1.3); Stoneyfell Quartzite with ranges between 10 – 16ppm; the Glen Osmond Slate member (siltstone and minor dolomite) with ranges between 6 – 21ppm and, the Ulupa Siltstone with ranges between 12 – 15ppm.

The eU content of Precambrian rocks is also generally low with ranges between 1 – 2.7ppm. Exceptions are the Barossa Complex with ranges between 2.6 – 6ppm; the Glen Osmond Slate with ranges between 2.8 – 4.5ppm; Stoneyfell Quartzite with ranges between 2 – 3.8 ppm, units within the Saddleworth FM with ranges between 2.0 – 4.8ppm and the Tapley Hill FM with ranges between 2.5 – 4.5 ppm. The Barossa Complex consisting of felspathic schist, genisses and leucocratic granite is therefore high in all three radioelements and appears white in the three band ternary gamma-ray image (Figure 21). Low K and relatively high eTh responses over part of the Barossa Complex rocks relate to the redistribution of the radioelements due to bedrock weathering (see section 6.1.3).

6.1.2 Cambrian bedrock

Metamorphosed Cambrian rocks in the study area are associated with the Blackstairs Passage FM and the Tapanappa FM. The Blackstairs Passage FM consists mostly of meta-sandstones and meta-siltstones with ranges of K typically between 1.1 – 2.4 %, eTh between 1.0 – 14.0 ppm and eU between 1.5 – 3.8ppm. Mineral assembles for the Blackstairs Passage FM include quartz-feldspar-mica (biotite and muscovite). The Tapanappa FM consists mostly of meta-sandstone and greywacke with airborne estimates of K, eTh and eU in the ranges of 1.19 – 2.6 %, 11.2 – 16.5 ppm and 2.9 – 4.0 ppm, respectively. Mineral assemblages for the Tapanappa FM include quartz-plagioclase-microcline-biotite-muscovite. The high K response relates mainly to the abundance of K-mica and K-feldspars in the bedrock. The generally higher K content of these rocks separates them from most of the Precambrian lithologies (Figure 21, 22 and 23). Local pegmatitic intrusions have radioelement values between0 .05 – 0.15 %K, 17 – 26 ppm, eTh and 2.9 – 3.8ppm eU.

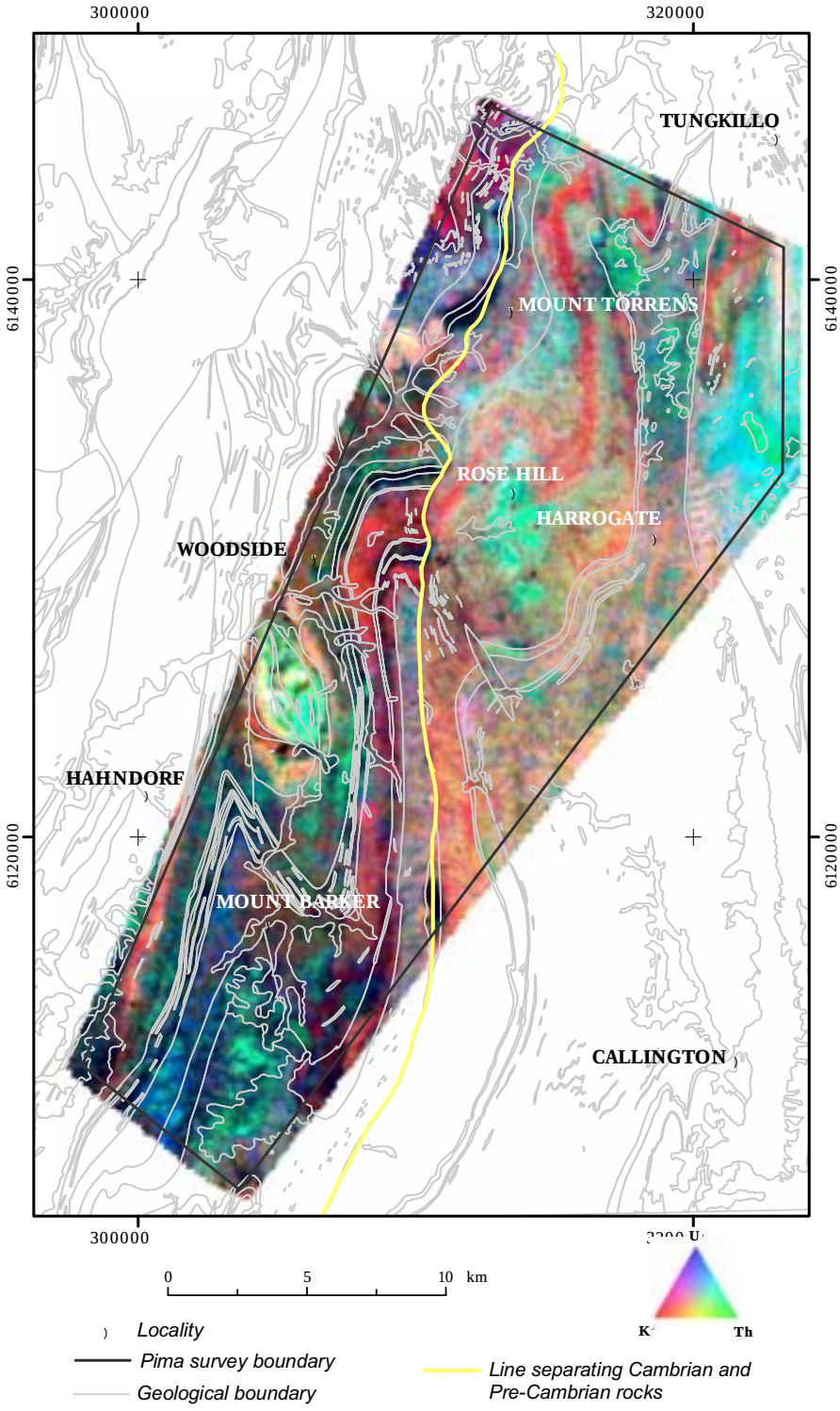

Figure 21. Ternary gamma-ray image (Hills survey) with K in red, eTh in green and eU in blue. Geology units in light grey. Contact between Precambrian (left of line) and Cambrian sediments highlighted.

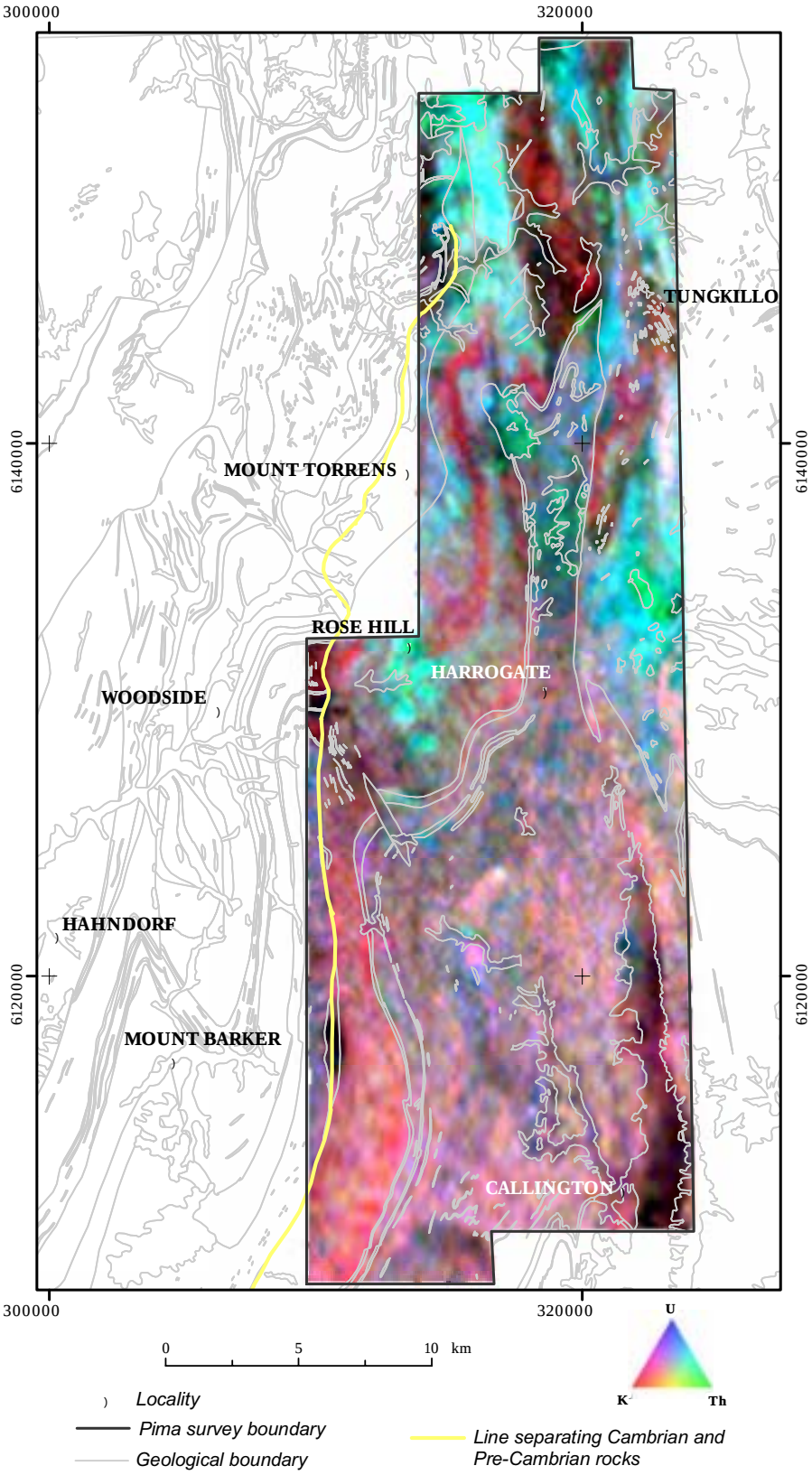

Figure 22. Ternary gamma-ray image (PIMA survey) with K in red, eTh in green and eU in blue. Geology units in light grey.

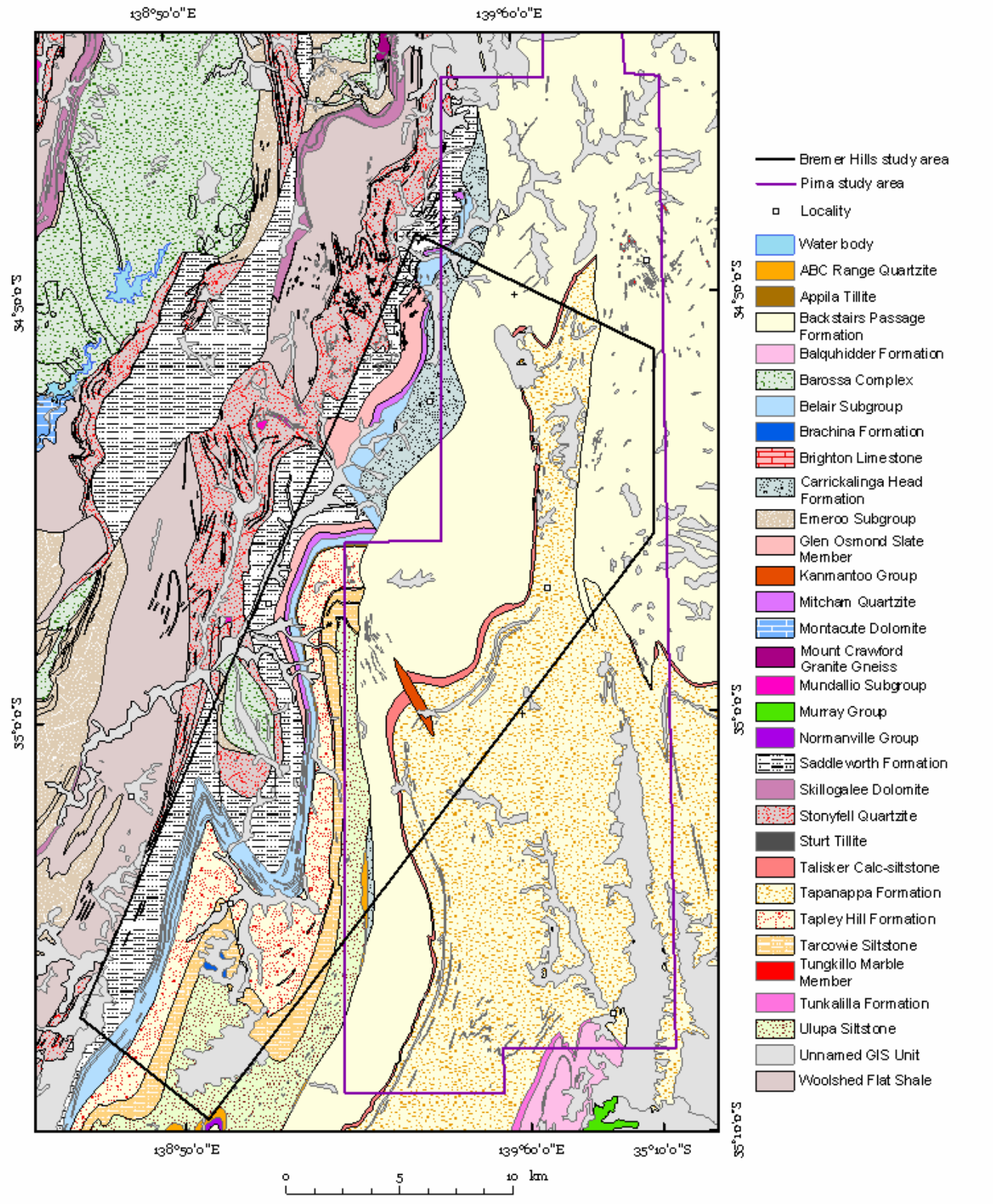

Figure 23. Geological unit names and location of the Hills and PIMA geophysical surveys.

6.1.3 Weathering responses (regolith and soils)

Weathering (soil and regolith formation) modifies the radioelement response from the underlying bedrock. Ferruginous and highly weathered regolith profiles developed on Precambrian and Cambrian lithologies show a significant reduction in K compared to adjacent areas of exposed, fresh to slightly weathered bedrock within the same geological unit (Figure 24). Uranium concentrations show a slight increase from weathered materials compared to the bedrock response. Thorium concentrations in regolith dominated landscapes are more complex. Weathered profiles from south of the Mt Barker township (Figure 24 A) and between Mt Barker and Mt Torrens (Rose Hill - Figure 24 B) show elevated eTh compared the bedrock response. Whereas similar eTh values were found between weathered and bedrock materials in the Hermann's area (Figure 24 C) and in the Muir catchment (south of Tungkillo – Figure 24 D). Potassium concentrations from all sites (Figure 24) show a decrease from the bedrock dominated landscapes to regolith dominated landscapes consisting of thick soils and typically ferruginous and mottled saprolite. The depletion of K and retention or increase of eTh in these weathered profiles gives a distinctive green/blue colour response in the ternary gamma-ray spectrometric image (Figure 25). Similar eTh responses from regolith and bedrock materials (Hermann's and Tungkillo south – Figure 24 C and D) suggests less intense weathering compared to weathering profiles with elevated eTh levels found at Mt Barker and Rose Hill (Figure 24 A and B). Field observations confirm this hypothesis with more outcrop and less weathered saprolite at Hermann's and Tunkillo than at Mt Barker and Rose hill (Figure 26).

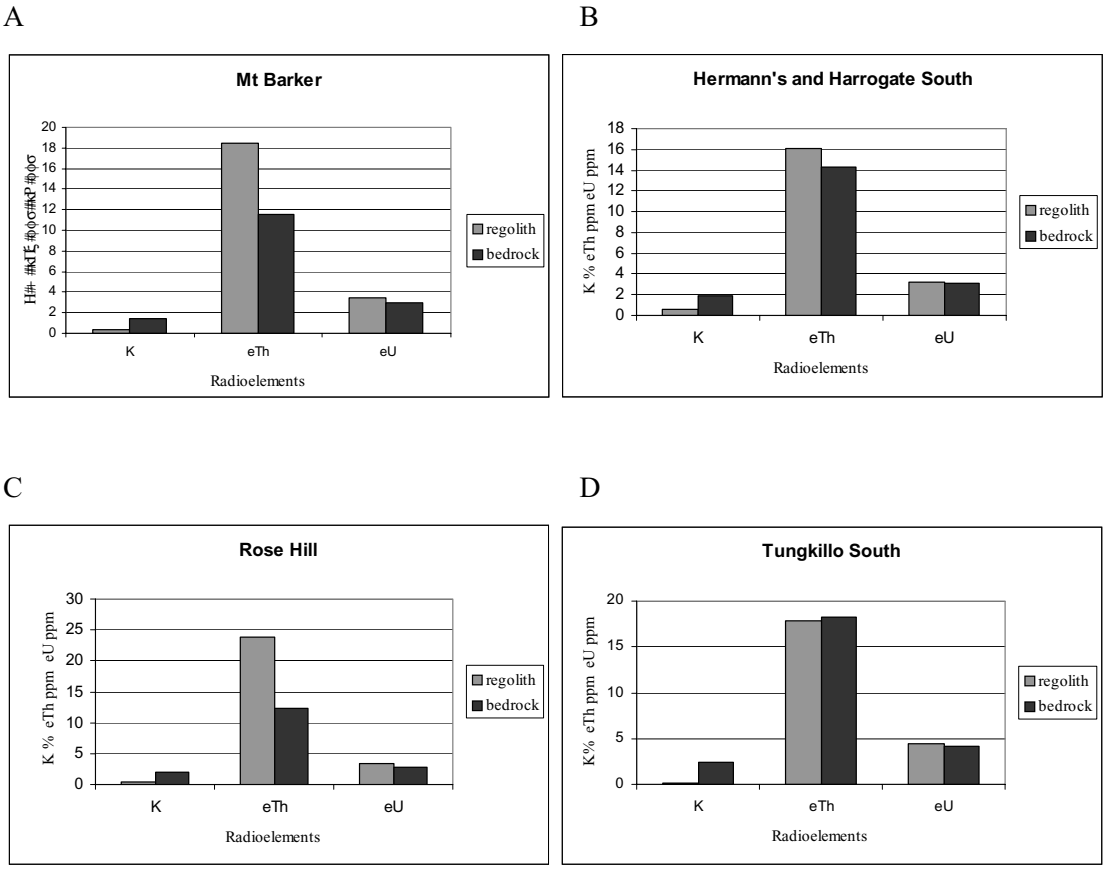

Figure 24. Radioelement responses of bedrock and regolith materials from the selected areas in the study area. Sites include; A - South of the Mt Barker township, B - along the divide between Mt Barker and Mt Torrens near Rose Hill, C - Herrmann's catchment and D - Muir catchment south of Tungkillo.

Loss of K is likely to be caused by leaching from K-bearing minerals (e.g. muscovite and K-feldpars) as the primary minerals in the bedrock weather and soluble cations such as K are lost in solution. Scavenging by iron oxides and absorption onto clays and organic matter are the likely reasons for elevated eTh and to a lesser extent eU concentrations in the upper part of the weathering profile. These relationships are supported by XRD results from drillhole samples taken from deeply weathered profiles south of Mt Barker and north/east of Callington (Table 1). The top of these highly weathered profiles are characterised by a quartz-kaolin mineral assemblages. The profile at Mt Barker also has a high proportion of iron oxides (16% hematite and goethite). The high iron content appears iron nodules and ferruginous mottling within the upper soil layer at the Mt Barker site. At depth the bedrock is less weathered with mica and illite becoming more abundant. These minerals and clays are reflecting more closely the mineralogy of the bedrock which is a micaceous metasiltstone. However, detailed mineralogical and radioelement studies are required to be confident about the distribution of the radioelements and their association with other materials (clays and iron oxides) in the weathered zone. High eU and eTh can also be associated with resistate minerals such as zircon and monazite. Fine grained zircon and monazite are known to occur in the Tapanappa FM (Skwarnecki, et al., 2002) but no heavy mineral separates were done to assess weather these minerals were concentrated in the upper part of the weathering profile where they could contribute to the gamma-ray response.

Well structured, loamy soils developed on metasiltstones, phyllites, slates and fine grained schists (including rock associated with the Tapley FM and Saddleworth FM) between Mt Barker and Mt Torrens are delineated by their relatively high K values and low eTh and eU responses on the ternary image (Figure 21 and 23). These soils are high in quartz (>70% quartz – Table 1) with some mica/illite, smectite, albite and orthoclase. The relatively high K signature of these soils probably relates to the presence of K-mica, illite and orthoclase (orthoclase is a general name for monoclinic potassium feldspar) in the A horizon.

Table 1. Mineralogy based on XRD results for surface soil and drill hole samples.

	Mt Barker 1.0m	Mt Barker 10.0m	Callington HA2 1.0m	Callington HA2 21.0m	Tapley Hill FM site 1	Tapley Hill FM site 2
Quartz	14	48	42	46	72	78
Kaolin	70	16	18	32	9	8
Mica/Illite	-	36	8	16	7	4
Smectite	-	-	7	-	-	-
Hematite	6	-	-	-	-	-
Geothite	10	-	-	2	-	-
Calcite	-	-	18	-	-	-
Gypsum	-	-	-	-	-	-
Albite	-	-	6	-	4	5
Orthoclase	-	-	2	4	7	4
Halite	-	-	-	-	-	-
Rutile	-	-	-	-	-	-
Talc	-	-	-	-	-	-
Amphibole	-	-	-	-	1	1

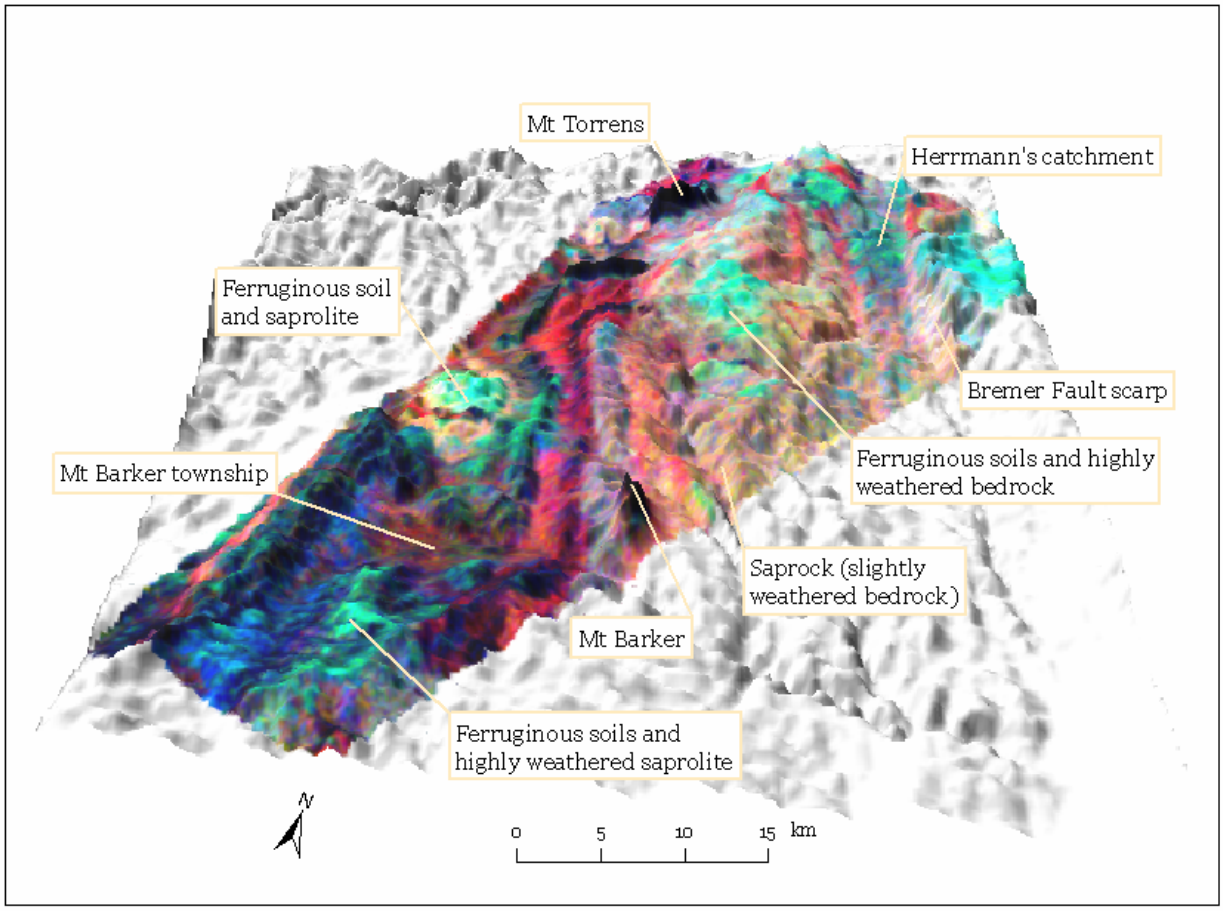

Figure 25. 3D perspective image of the three band gamma-ray data draped over the digital elevation model. The view shows the central-western part of the study area.

Figure 26. Examples of highly weathered bedrock and ferruginous soil south of the Mt Barker township. These are characteristics features of the deeply weathered landsurface.

6.1.4 Alluvial and colluvial sediments

Most alluvial and colluvial deposits in the study area are not of sufficient size to be detected by the airborne survey. Alluvial sediments mainly occur as narrow tracts along drainage lines and colluvial sediments are generally associated with local footslope deposits at the break of slope between the valley floor and the adjacent hills. Where these materials are recognised in the gamma-ray image their radioelement patterns vary. The gamma-ray response of alluvium and colluvium will largely reflect the composition of the source rock or regolith from which they are derived. Sorting of the sediments during transportation and their weathering after they have been deposited is also important. Sediments with similar gamma-ray responses to their source materials (bedrock and weathered bedrock) are a common feature in the study area. This probably reflects landscapes in the Lofty Ranges that are geomorphically active both in terms of high erosional and deposition rates. Therefore, separating bedrock and transported materials in these landscapes can be difficult when only using the gamma-ray imagery. Landscape mapping (e.g. soil-landscape units) and draping the gamma-ray imagery over the DEM can assist in separating alluvium and colluvium from bedrock and residual soils (Figure 25 and 27).

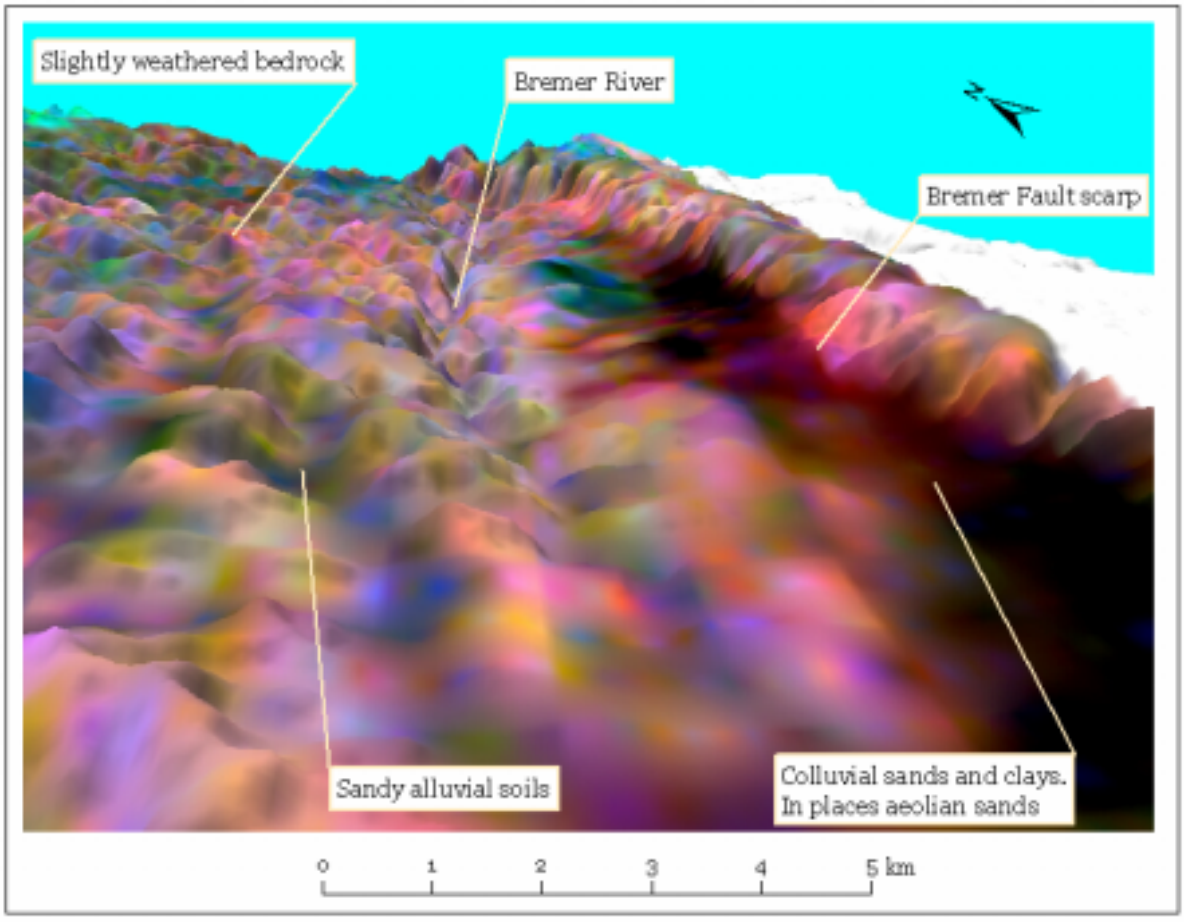

Figure 27. 3D perspective view of the 3-band gamma-ray image draped over the digital elevation model. View angle looking south along the west facing edge of the Bremer fault scarp. Colluvial and alluvial fans developed down slope from the scarp are highlighted. Active parts of the fan have similar radioelement responses to the bedrock. Less active parts of the fans have lost K due to mineral weathering and are partly blanketed by aeolian sands. These fans appear in black tones. Sandy alluvial deposits are in places recognised in the imagery by their dark tones and are separated from much high gamma-ray counts from the surrounding bedrock.

In places (eg. along the Bremer River and some of its larger tributaries) river bedload, overbank and levee deposits are recognised by their low gamma-ray response (Figure 27). Soils on these sediments consist mainly of sandy loams. The high quartz content of these soils is reflected by low gamma responses (eg. quartz has low radioelement count for each of the three radioelements). These quartz rich sediments appear blue in the ternary gamma-ray image (Figure 27).

Relatively large colluvial footslopes flanking the western side of the Bremer fault scarp (Figure 27) have a mixed radioelement response. In places, the colluvial fans have a similar response to the bedrock from which the sediments are sourced. Sediments from this part of the fan are likely to have been actively eroded and deposited. As a result they still retain their bedrock signature. Elsewhere the colluvial sediments appear black in the ternary image indicting low counts of each of the radioelements. Here, K values are typically between 0.7 – 1.0 %, eTh of between 6 – 8ppm and eU of between 0.8 – 1.5ppm, whereas bedrock responses are typically in the range of 1.7 – 2.2 % for K, 12 – 15ppm for eTh and 1.9 – 2.9 for eU. Low K might be caused by the weathering of K bearing minerals in the sediments. Alternative the low K, eTh and eU might be associated with the accumulation of quartz sand at the surface either by winnowing of finer sediments down slope or from sand of aeolian origin accumulating as sand spreads at the base of the scarp. Aeolian sands have been recognised from soil-landscape mapping (Soil and Land Information, 2002) on colluvial footslopes east of Callington.

6.2 Residual analysis – delineating highly weathered regolith

A residual modelling approach was used to separate gamma-ray responses relating to bedrock and regolith materials in the airborne spectrometric imagery. Geological units and slope derived from the DEM were used determine mean bedrock values for each of the three airborne radioelement grids (K, eTh and eU). These mean values there then subtracted from the original gamma-ray grids to derive 'residuals' (see Section 5.4) for a detailed description of the technique). The technique assumes that on steeper slopes the gamma-ray response will relate to the bedrock mineralogy and geochemistry. The residual grids will show gamma-ray responses that are above, equal to or below the predicted average bedrock signature. Since, K is readily lost during bedrock weathering and K-bearing minerals are common in most of the lithologies in the study area – the K residual was used as a surrogate to map or predict areas of highly weathered regolith compared to landscapes that consist mostly of thin soils and exposed largely unweathered bedrock. The K residual image (Figure 31) shows values above the means bedrock unit response in reddish hues and values below the unit response in blue hues. Blue image tones correspond to where K values have decreased from that particular geological unit and in many cases these areas correspond to leached soils and highly weathered saprolite. There are several exceptions to this general rule. The first is where K persists in the weathering profile and is therefore not a good indicator of bedrock weathering or leaching. This situation occurs in soils developed on parts of the Tapley and Saddleworth FM where K is associated with illite (potassium clay) and K-feldspar (samples Tapley 1 and 2 – Table 1). The second exception is where the original bedrock is low in K. Within the study area these rocks also tend to be low in eTh and eU. They include quartzite, siliceous sandstones and siltstones that commonly form hills and ridges (eg. Mt Barker, Mt Torrens and Mt Charles). Because of the overall low gamma content of these lithologies and their characteristically high slopes they can be readily identified and mapped into the K-residual regolith map as an outcrop or shallow regolith class (Figure 31).

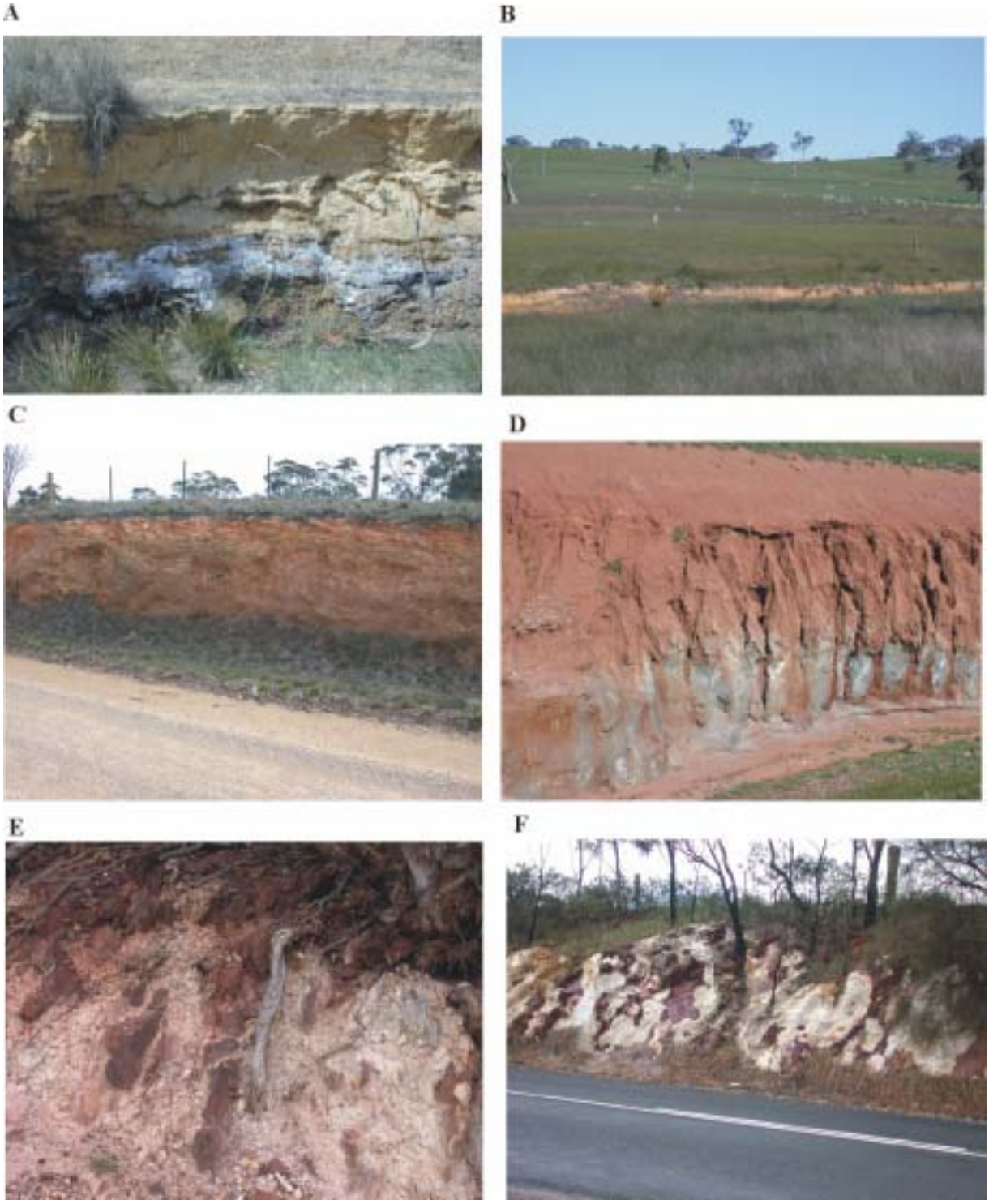

Figure 28. A – Salt crystallising along a channel bank, B – Hermanns creek and catchment. Alluvial sediments buried by very highly weathered saprolite. C – Ferruginous colluvial sediments consisting of poorly sorted lithic fragments, clays and sand. D – Ferruginous colluvial sediments overlying very highly weathered kaolinised saprolite (grey). Photo taken of colluvial footslope down slope from the Bremer Fault Scarp. E – Iron segregations developing within the mottled zone of the weathering profile. F – Highly weathered and mottled saprolite characteristic of the palaeosurface landforms.

Figure 29. A – Trees planted in a discharge zone (South of Tungkillo). B – Ferruginous and cemented alluvial gravels. C – Ferricrete lags used to construct stone walls. D – Ferruginous gravel lags overlying mottled and ferruginous saprolite. These materials typically have high eTh responses in the gamma-ray imagery. E – Mottled and bleached saprolite profile. F – Air-core drill rig used in the drilling program.

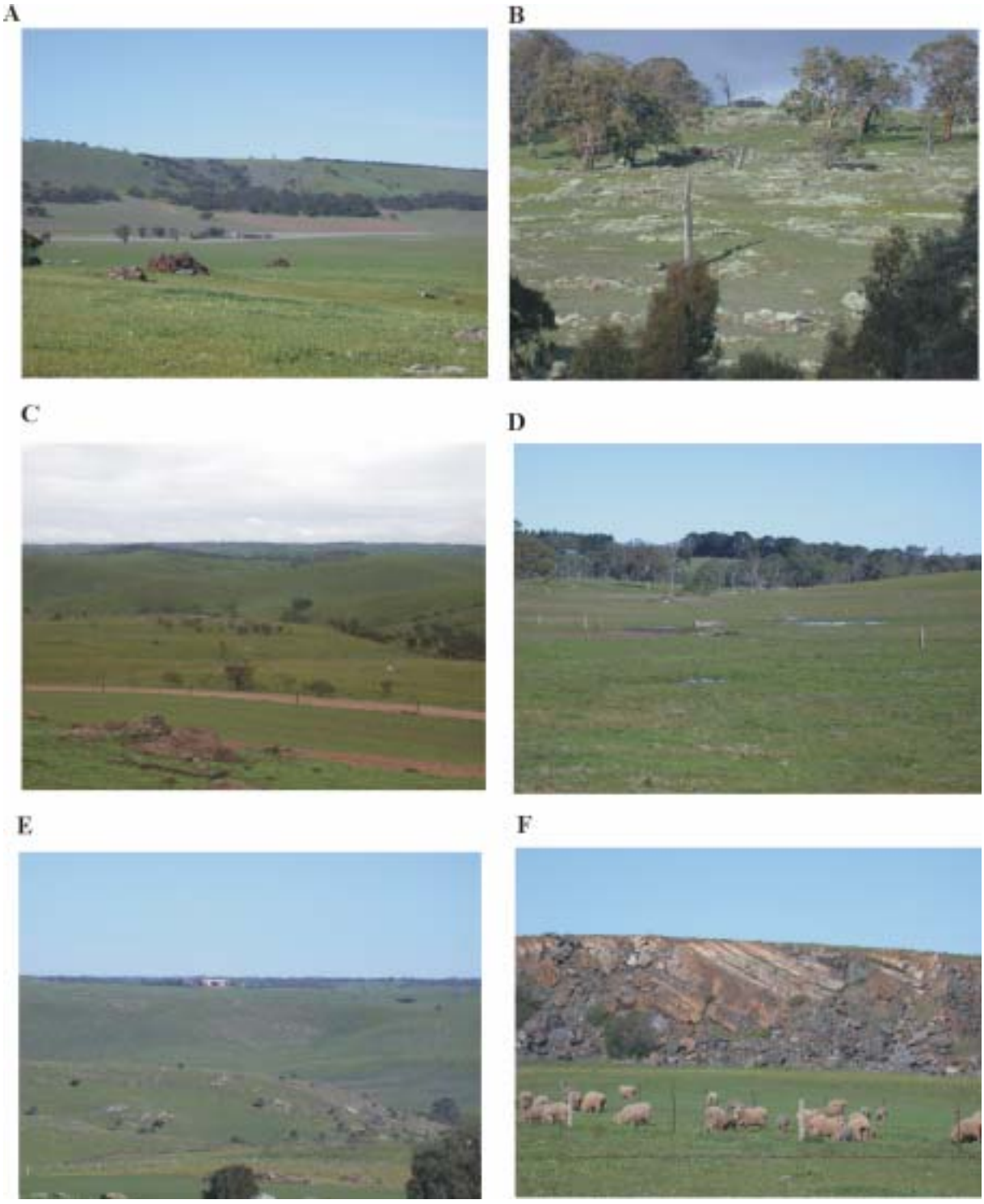

Figure 30. A - Bremer Fault Scarp with colluvial footslopes. B – Thin soil and exposed bedrock. These landscapes typically have high K-residual values. C – Bremer Creek incised into relatively fresh bedrock, photo taken between Harrogate and Callington. D – Highly weathered landform with no surface outcrop. This landscape is typically of the palaeosurface and constrasts less weathered terrain shown in photo B. K-residual vales in these landscapes are low. E - Dissected landforms with skeletal soils over slightly weathered bedrock. F – Cutting through hill showing bedrock to surface. Gamma-ray responses in these terrains reflect the geochemistry and mineralogy of the bedrock.

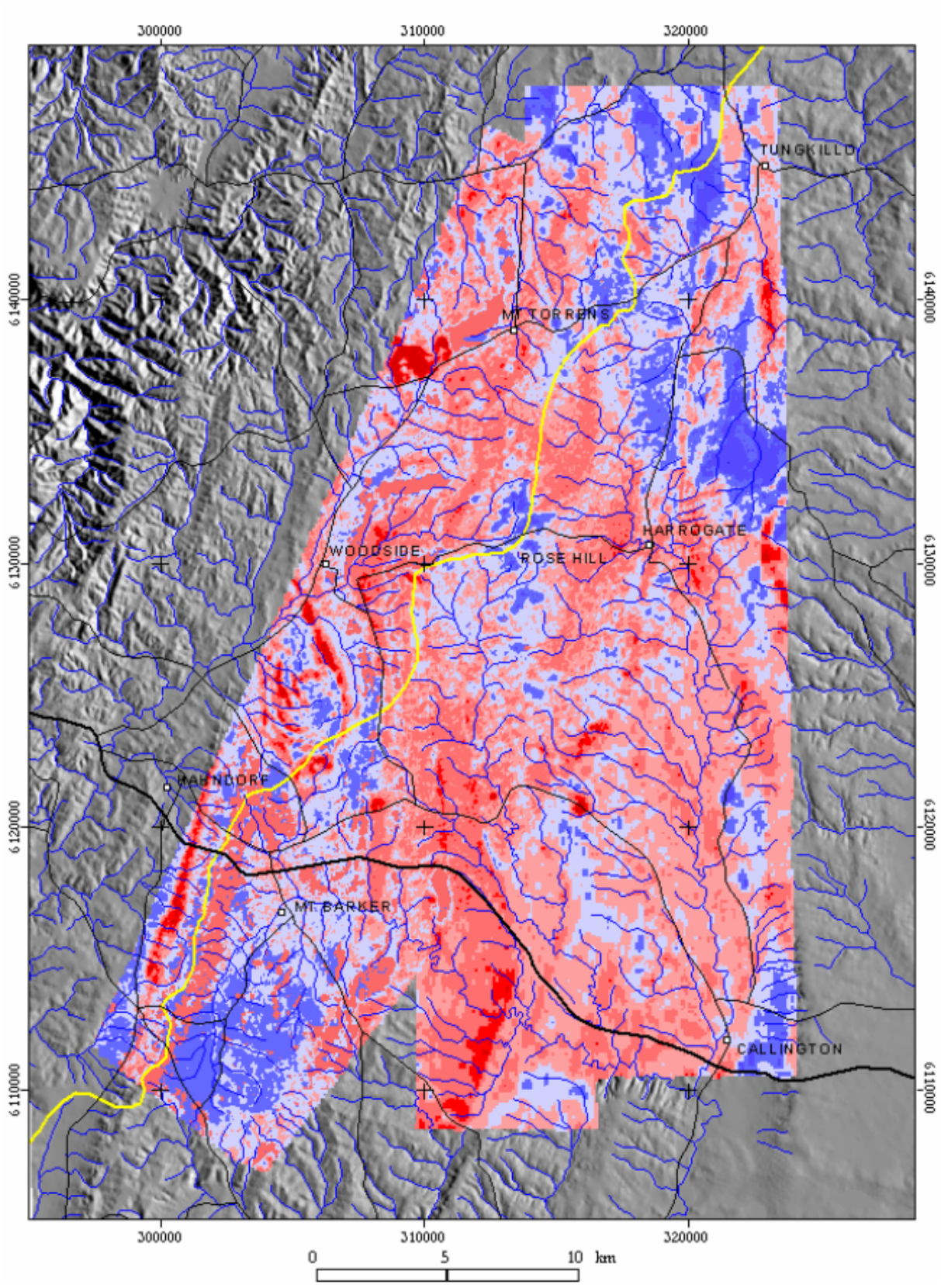

Figure 31. K-residual image (both surveys combined). Red image tones indicate shallow regolith (e.g. numbers above the estimated bedrock mean value) and soils. Blue tones correspond to highly and typically deeply weathered regolith (e.g. numbers below the estimated bedrock mean value). Hard siliceous bedrock (eg. quartzite) materials are identified by low counts in each of the three radioelements and then mapped into the shallow regolith class. Drainage divide in yellow.

6.2.1 K-residuals compared with Tertiary weathering and Pleistocene-Holocene sediments

Areas of predicted highly weathered regolith (blue areas in Figure 31) correlate well with 'lateritic' Tertiary units delineated on geological maps (see Figure 23). These 'lateritic' units include ferruginous lags, gravels, saprolite and mottled clays, and are thought to be part of an older, highly weathered palaeo-surface that developed before the Mt Lofty Ranges were uplifted in the Mid Tertiary. This palaeo-surface is commonly referred to as the 'summit' surface and has previously been mapped over the central part of the Lofty Ranges as discontinuous and scattered, characterised by landforms of relatively low relief. The residual image suggests that the weathered palaeo-surface is more widespread than originally thought based on existing geological maps. Ferruginous lags and nodules and/or highly weathered and typically mottled saprolites delineated by the K-residual image occur mainly south of the Mt Barker township, east and north east of Callington, between Mt Barker and Mt Torrens (along the major drainage divide), east of Mt Torrens and south south-west and west of Tungkillo (Figure 31).

Pleistocene-Holocene alluvial and colluvial sediments consisting of sands, clays and gravels forming fans and footslopes east of the Bremer river and adjacent to and down slope of the Bremer fault scarp, are recognised in the K-residual image by their relatively low K response. This is likely to relate to leaching of K-bearing minerals in the colluvial sediments and abundance of quartz sands at the surface. Some parts of the fans are not well delineated in the K-residual image because of K-bearing minerals in the sediments. These areas might correspond to more active parts of colluvial fan system where the sediments contain K-bearing minerals.

6.3 Correlations with soil-landscape mapping

Generally there is a good correlation between gamma-ray patterns, including the modelled K-residual image, with existing soil-landscape units. This is because radioelement responses reflect surface (20-25cm depth) geochemistry of soil and bedrock materials. Although not the focus of this investigation, ground validated gamma-ray data has the potential to inform on specific soil attributes and can be used to substantially improve existing soil-landscape maps over the study area. Some examples of the correlations between the gamma-ray patterns and soil-landscape units including specific soil attributes are described. Low K and elevated eTh often correlates with ferruginous, highly leached, deep, nutrient poor, acidic soils with a high phosphate fixing capacity. Gamma-ray responses associated with these soils occur on Precambrian and Cambrian lithologies, and in many cases the gamma-ray data could be used to improve the accuracy in mapping these soil types (Figure 32, 33). These soils are also separated in the K-residual image due their very low K content. Low radioelement counts for K, eTh and eU (black on the ternary image) on a variety of different landforms correlate to sandy alluvial soils, aeolian sands and skeletal soils developed on siliceous bedrock (eg. quartzite). Drift sand banks that have accumulated along the edge of the Bremer scarp (east of Callington) appear black in the ternary image and blue in the K-residual image. These soils are infertile and prone to erosion (ref soil-landscape data CD: PIRSA, 2001). Some of the most potentially productive soils in the hills area (PIRSA, 2001), consisting of deep fertile loams with well structured subsoils are recognised in the gamma-ray imagery by their relative high K response and low eTh and eU levels.

The K-residual image can inform on soil thickness and degree of rockiness. In most cases the red response in the K-residual image correlates to shallow stony soils with significant rock outcrop.

Blues image tones correlate with moderate to deep soils of variable texture with little surface bedrock (Figure 34, 35 and 36). Whereas mapped soil-landscape units describe the degree of rockiness as a percentage within each landform unit, the K-residual image has the potential to predict or map this attribute across the landscape.

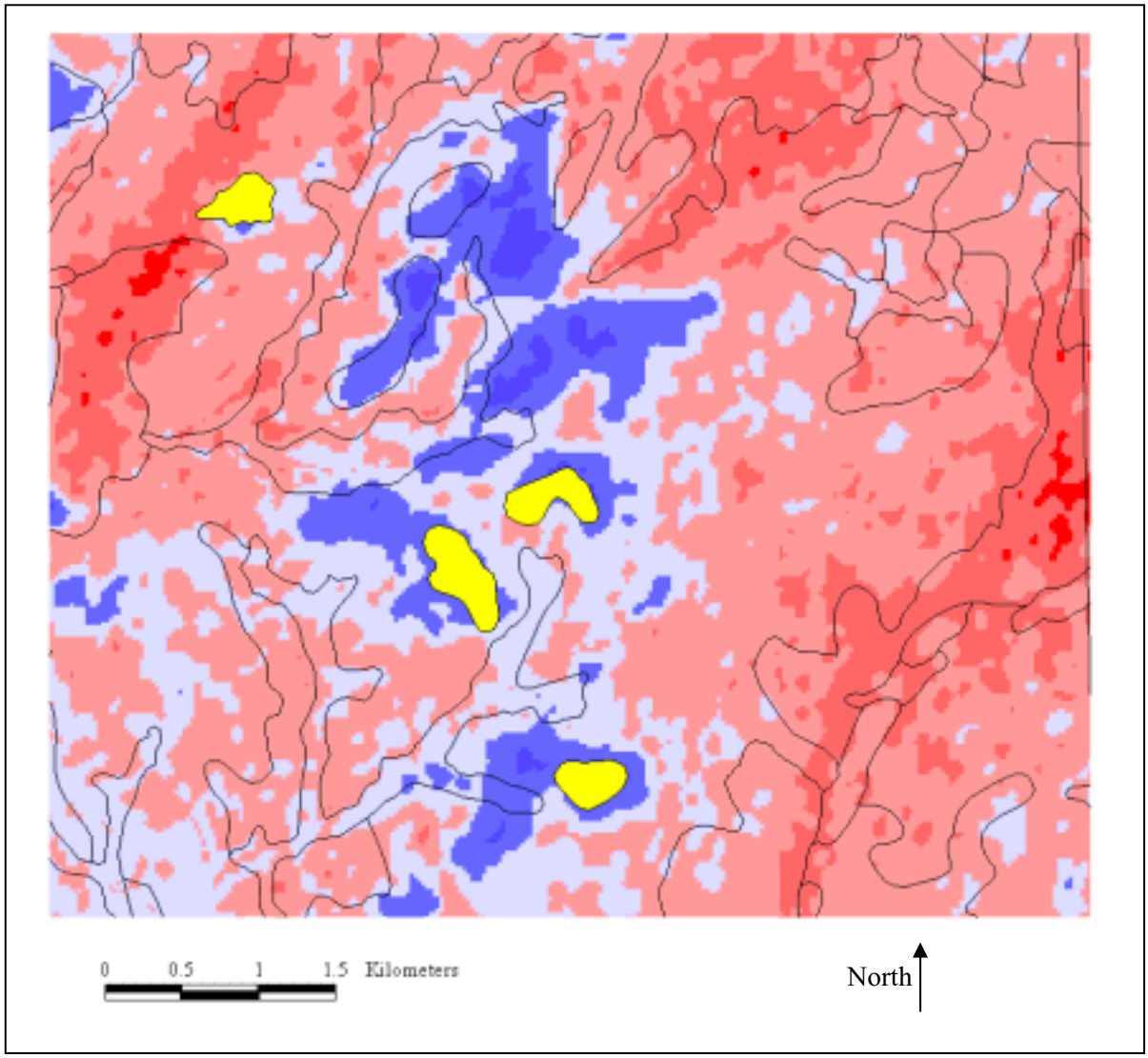

Figure 32. K-residual (blue corresponds to highly weathered bedrock; red corresponds to slightly weathered bedrock) and soil landscape units with highly weathered ferruginous and leached soils highlighted in yellow.

A

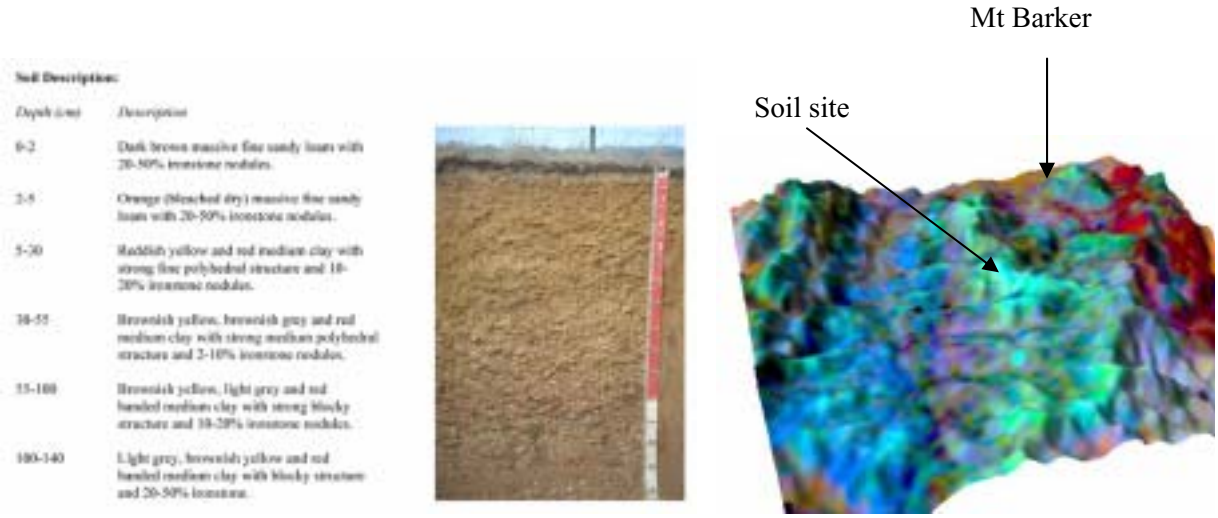

B

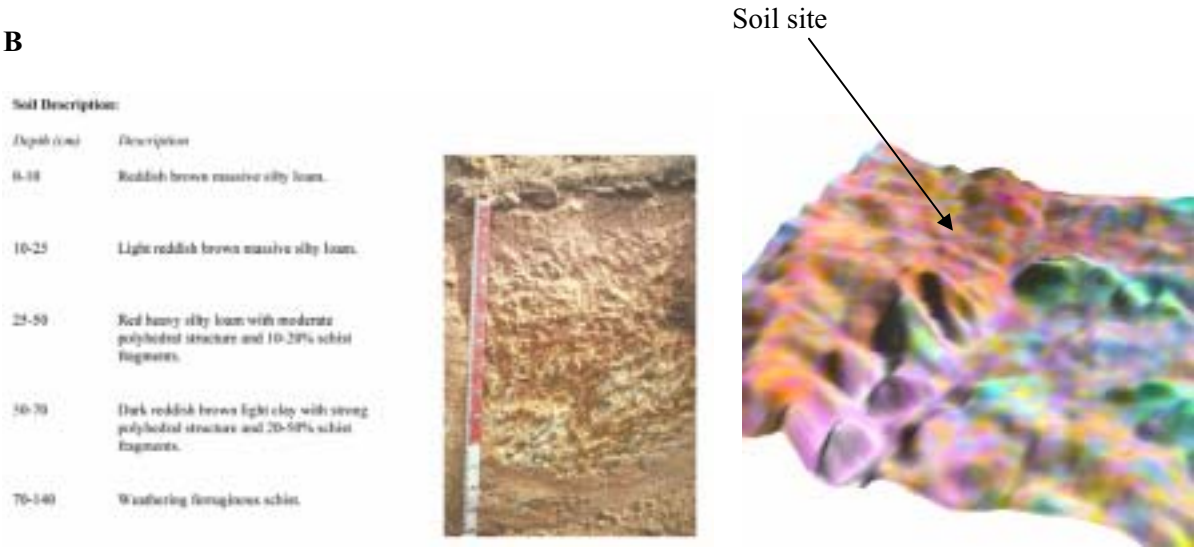

Figure 33. Soil profile descriptions and soil site locations on the ternary gamma-ray spectrometry image (red = potassium, green = thorium and blue = uranium) draped over a digital elevation model. A - highly weathered ferruginous soils and high corresponding eTh and eU image values. Thorium and eU tend to be associated with iron oxides and clays in the weathered profile. B – shallow soil with scattered rock fragments at surface. The gamma-ray response is dominated by potassium. High potassium is largely reflecting the primary mineralogy of the bedrock. (soil profiles from Soil and Land Information, 2002).

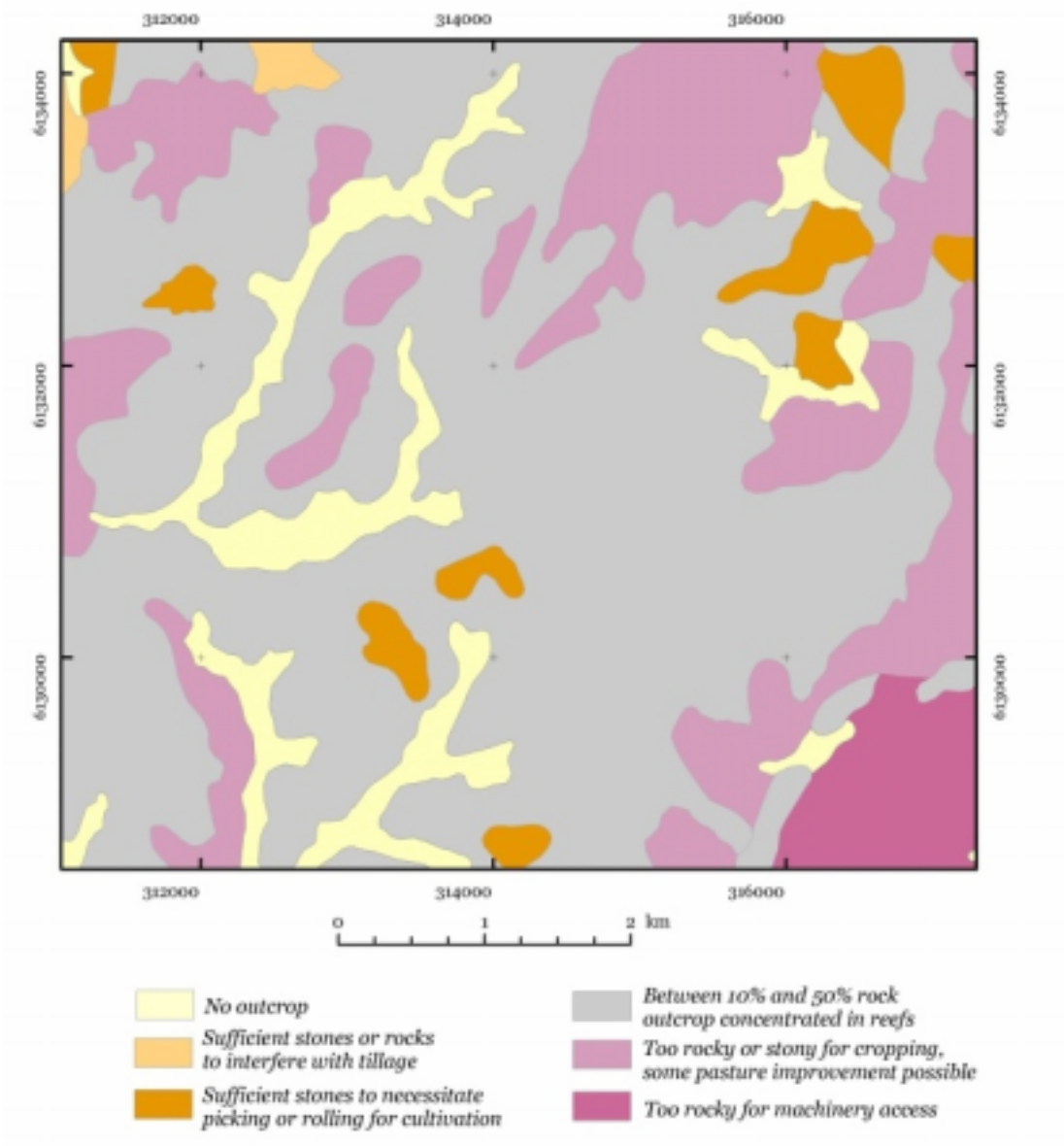

Figure 34. Thematic map showing degrees of rockiness derived from the soil-landscape GIS. For comparison with the K-residual image see Figure 35.

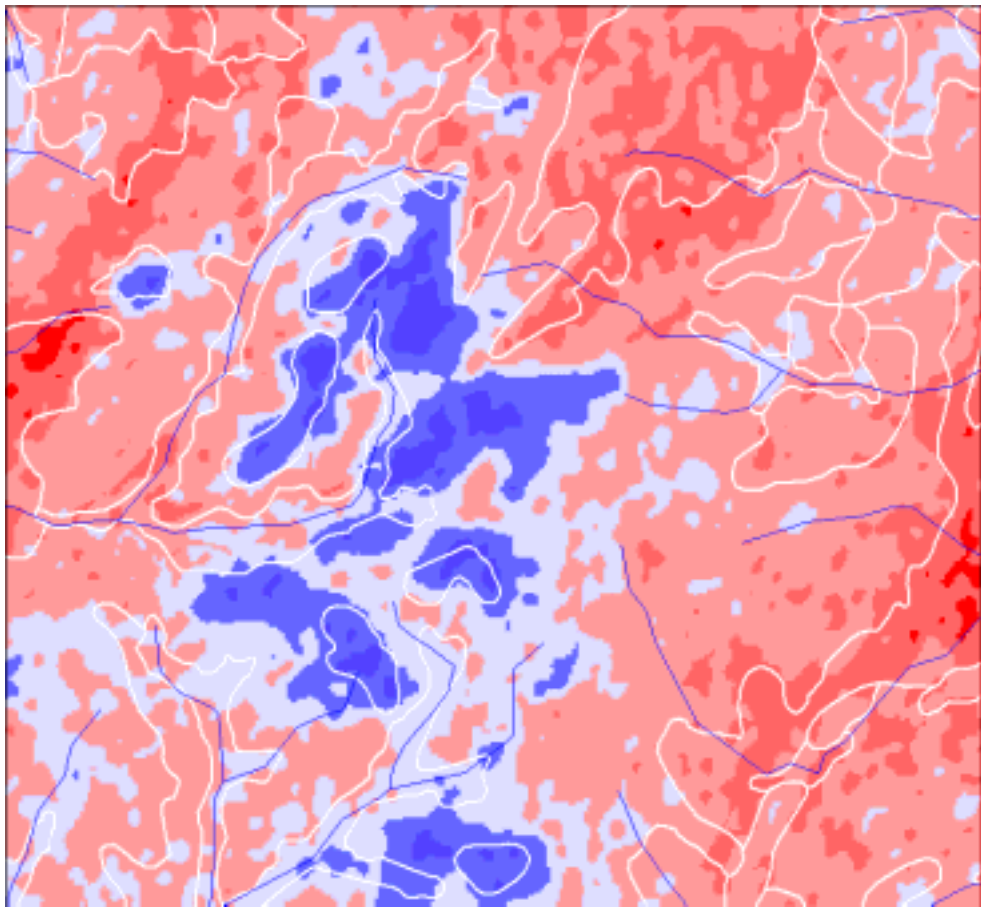

Figure 35. K-residual image over the same location and scale as figure 34. Colours from blue to red correspond with areas of increasing outcrop.

Figure 36. Landscape pictures showing residual soil with little outcrop (has blue response in the K-residual image (left) and bedrock (schist) dominated landscape (has red response in the K-residual image).

6.4 K-residual compared with drill logs

The K-residual image was used to locate a series of drill holes to validate the suggestion that the depth of weathering, the K-residual response and the salt load within the regolith were correlated. Drillholes were located to cover a range of K-residual values and landform types (residual and depositional). Comparison of K-residual values with the maximum depth drilled into the regolith (Figure 37) shows a general trend of increasing regolith thickness with decreasing K-residual value. Negative values indicate greater loss of K (due to bedrock weathering) from the predicted bedrock K response of around zero. Values around zero and above are likely to reflect the geochemistry and mineralogy of the bedrock. Several holes were terminated within the upper part of the weathering profile due to poor sample recovery and groundwater contamination. The relationship of negative K-residual values with thicker regolith becomes clear when only the drill holes that intersected saprock (slightly weathered bedrock) are plotted (Figure 38). K-residual values around -0.4 and above partition generally shallow regolith profiles from more deeply weathered profiles with values less than -0.4. Similar patterns but with a slightly tighter spread are observed when transported regolith materials are excluded and only the results from residual profiles are plotted (Figure 39).

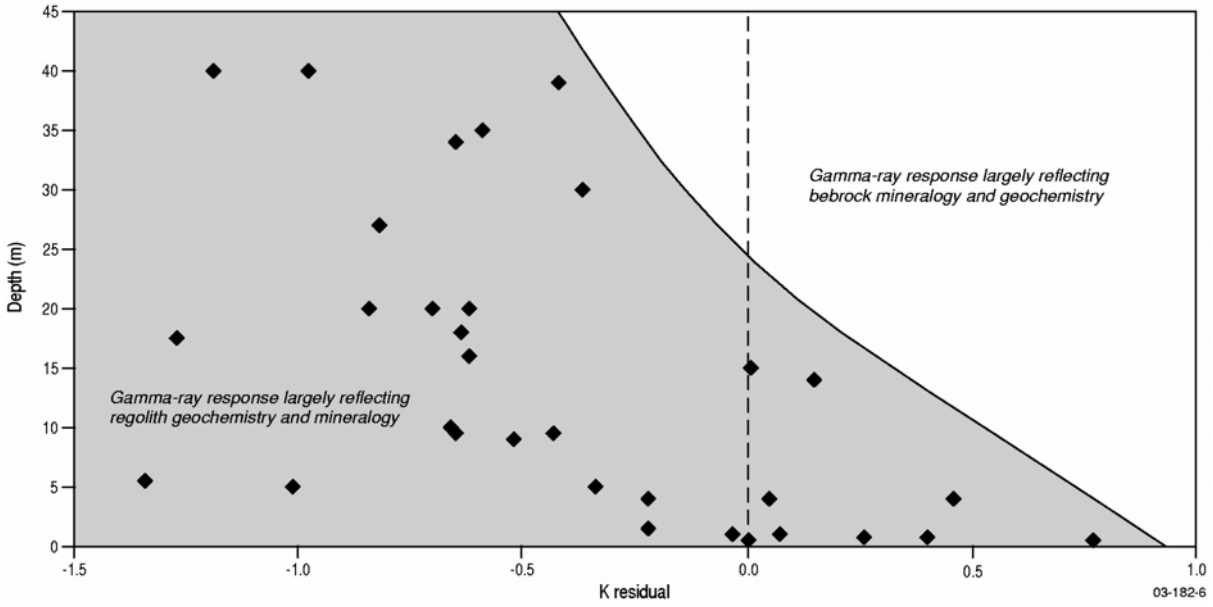

Figure 37. Scatter plot showing the relationship between K-residual response and maximum depth drilled into the bedrock. A general trend exists between thicker regolith and more negative K-residual values. Positive K-residual values reflect the mineralogy and geochemistry of the bedrock. Drill depths are generally lower where the K-residuals are above zero.

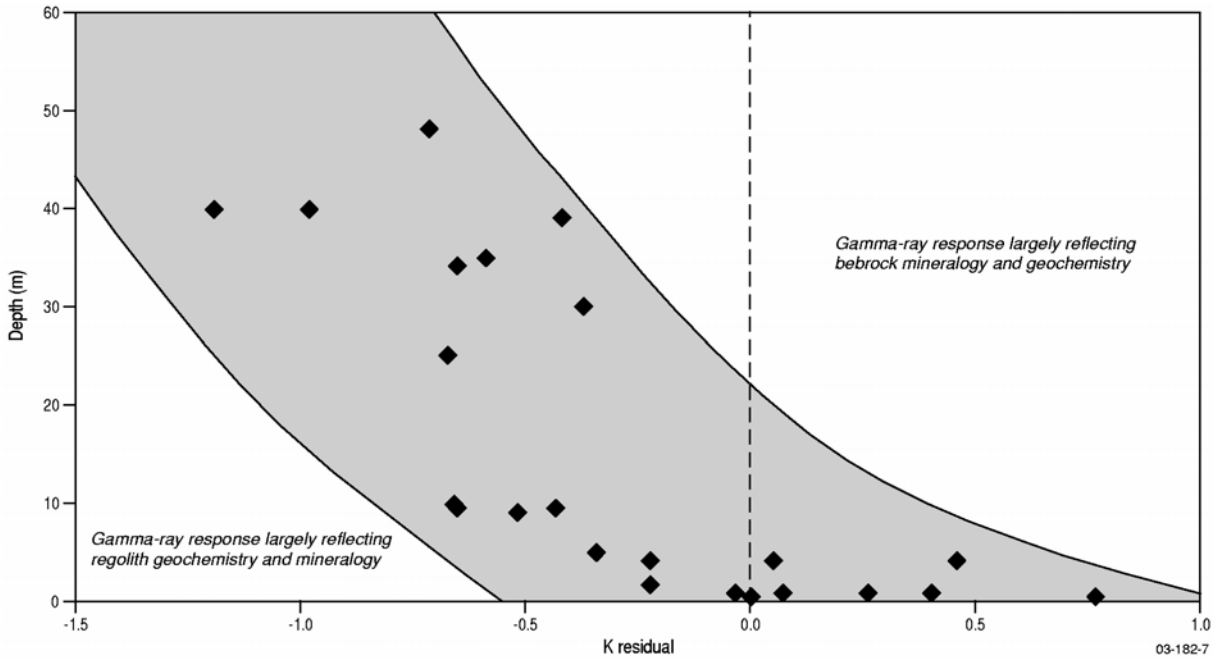

Figure 38. Comparison between K-residual values and only drill holes that intersect saprock.

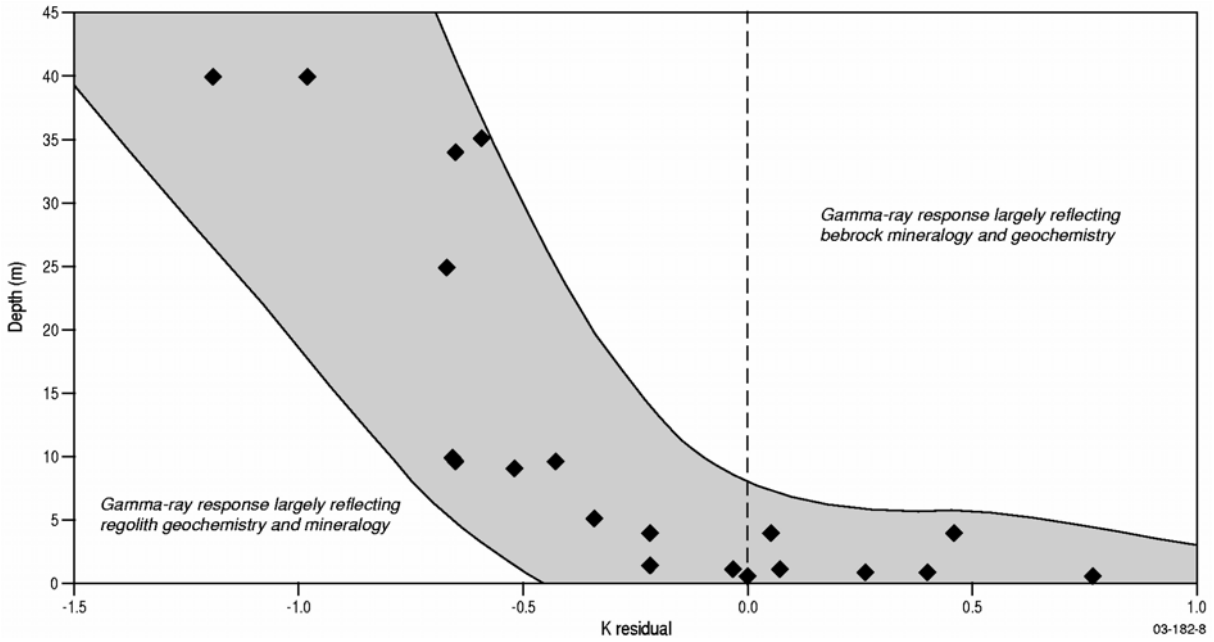

Figure 39. Comparison between K-residual values and only drill holes that intersect saprock and also excluding holes with transported regolith.

6.5 Comparison of K-residuals and Smartem and NanoTEM TEM surveys.

A series of SmarTEM and NanoTEM ground time domain EM (TDEM) traverses were acquired over different landform and regolith types to assist in mapping the distribution and thickness of conductive regolith at depth. Sites were selected using the K-residual image to include landscapes with differing degree of bedrock weathering. The aim was to assess weather the modelled gamma-ray data which measures surface geochemistry (to a depth of approximately 30cm)could be used to predict the nature of regolith materials at depth. These ground TDEM surveys complemented the drilling program by providing a section or image through the regolith to the underlying resistive basement. The traverses were surveyed orthogonal to streams or valley floors to intersect a range of materials from hill slopes to valley sediments (e.g. colluvial and alluvial), as well as local recharge and discharge sites. Stitched conductivity depth sections were then fitted to the topography and presented with a common conductivity scale range to allow relative comparisons between the different surveys. The sections provided information on conductivity structure of the regolith and bedrock to a depth of approximately 60m.

Five Smartem traverses were acquired, including HARSE1 (Figure 40a) which crosses the colluvial fan down slope of the Bremer fault, MT1 (Figure 40b) which traverses the Herrmann's catchment, MB1(Figure 36c) to the south of Mt Barker, MB2 (Figure 41a) east of Mt Barker and HAR1 (Figure 41b) west of Harrington. The positions of these survey lines are shown over the K-residual image in Figure 42. The first three transects (lines HARSE1, MT1 and MB1) are in landscapes predicted by the K-residuals to be highly weathered, the last two sections (lines MB2 and HAR1) are in landscapes predicted by the K-residuals to have a shallow regolith cover.

Sections across landscapes predicted by the K-residuals to be more weathered had higher conductivities than the other two geophysical lines. The resistive layer at the top of the sections is an artefact in the modelling due to limitations of the SmarTEM receiver to resolve early times (eg. shallow responses). Conductivity largely depends on the texture of the regolith, moisture and salt content. Clay substrates, high moisture and salt load will give high conductivity. Based on drilling the regolith in these landscapes is between 30-45m thick and consists of highly weathered and mottled bedrock (results in high clay content and moisture holding capacity). Conductivities range between 200mS/s to over 500mS/m. Sections HARSE1 and MB1 were acquired over similar regolith profiles (both consists of highly weathered metasiltstones) but they show very different conductivity structures. (Figure 40a and c). This is likely to reflect the high higher salt content in the HARSE1 section (see Section 6.8 on regolith salt stores). Sections MB2 and HAR1 are across landscapes dominated by bedrock with local pockets of soil and regolith development. Thin soils and crystalline basement rocks are highly resistive or poorly conductive (less than 80mS/m). In the more resistive areas it may be more appropriate to consider the application of resistivity arrays as an alternative approach.

A

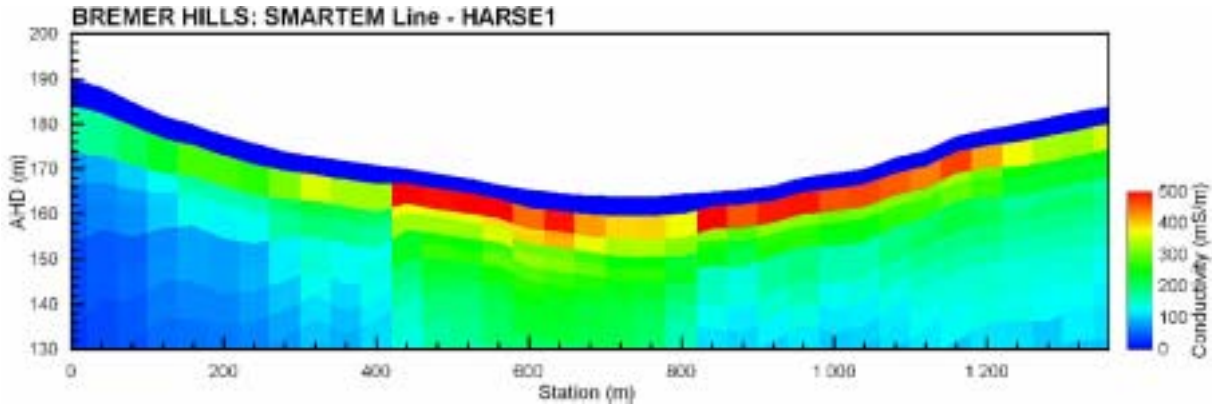

B

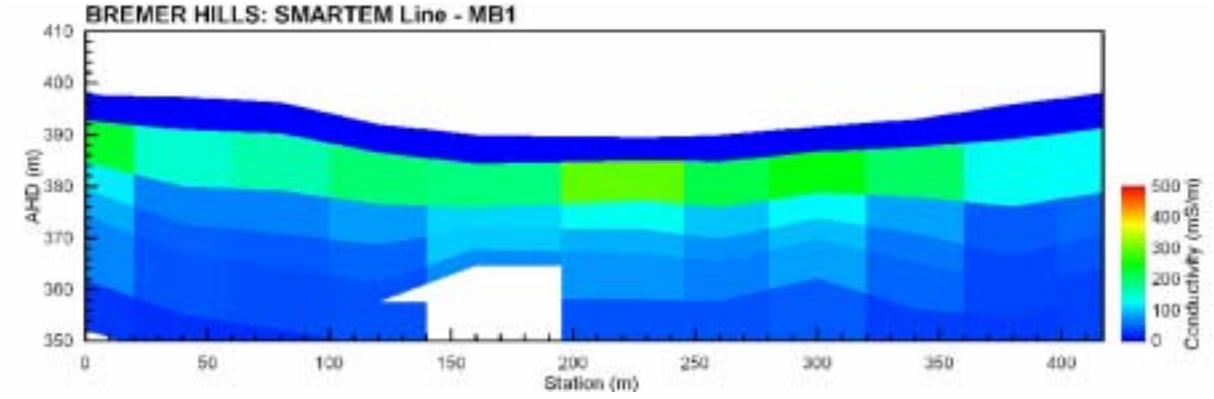

C

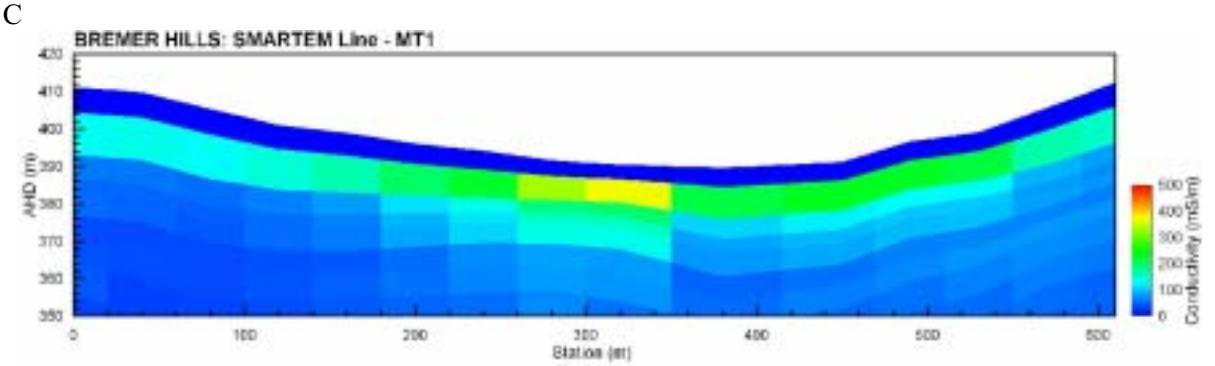

Figure 40. Stitched conductivity depth sections from an smooth Occams inversion of Smartem data for lines A) HARSE1 (N NE of Callington), B) MB1 (S of Mt Barker township) and C) MT1 (Herrmann's catchment). High conductivity in yellow to red hues. Low conductivity in blues shades.

.

A

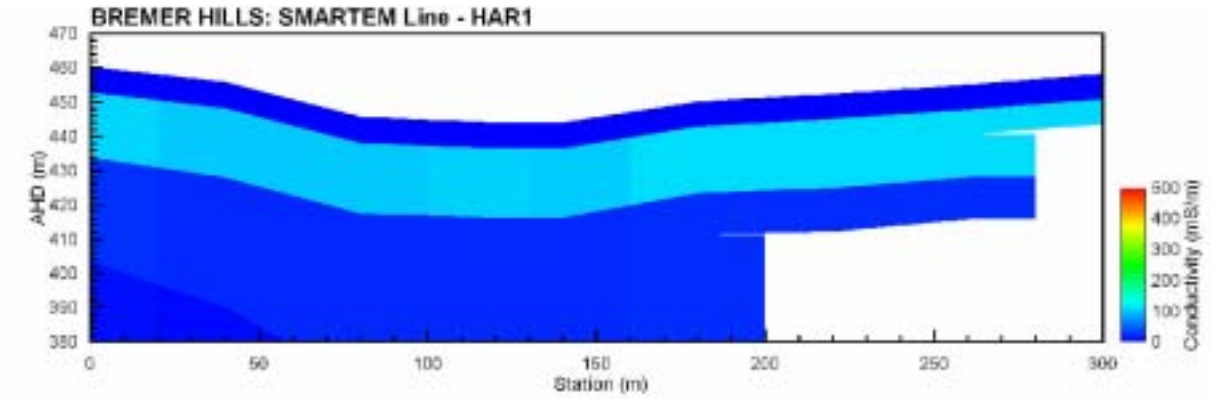

B

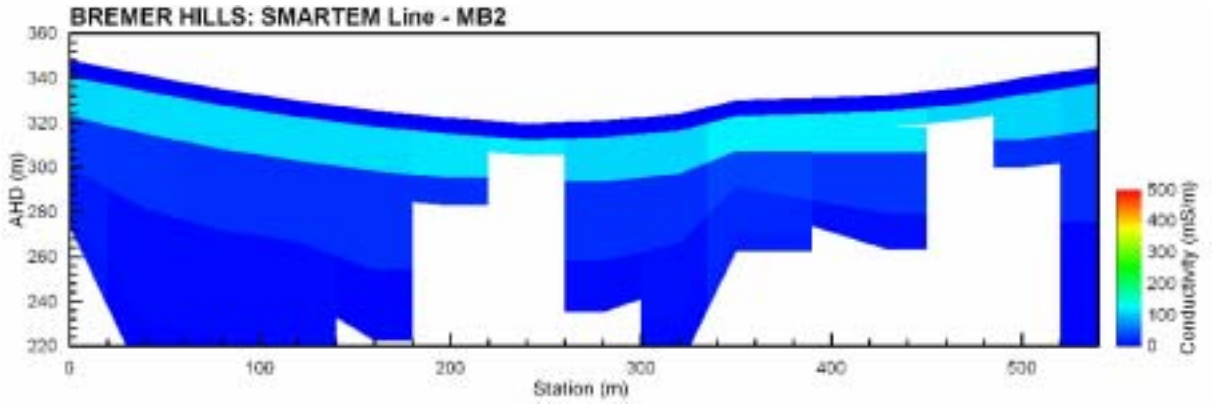

Figure 41. Stitched conductivity depth sections from a smooth Occams inversion of Smartem data for lines A) HAR1 (West of Harrogate) and B) MB2 (East of Mt Barker) High conductivity in yellow to red colours. Low conductivity in blues shades. The pale blue band in both sections is an artefact of the inversion process, and both sections are typified by low conductivities <100mS/m.

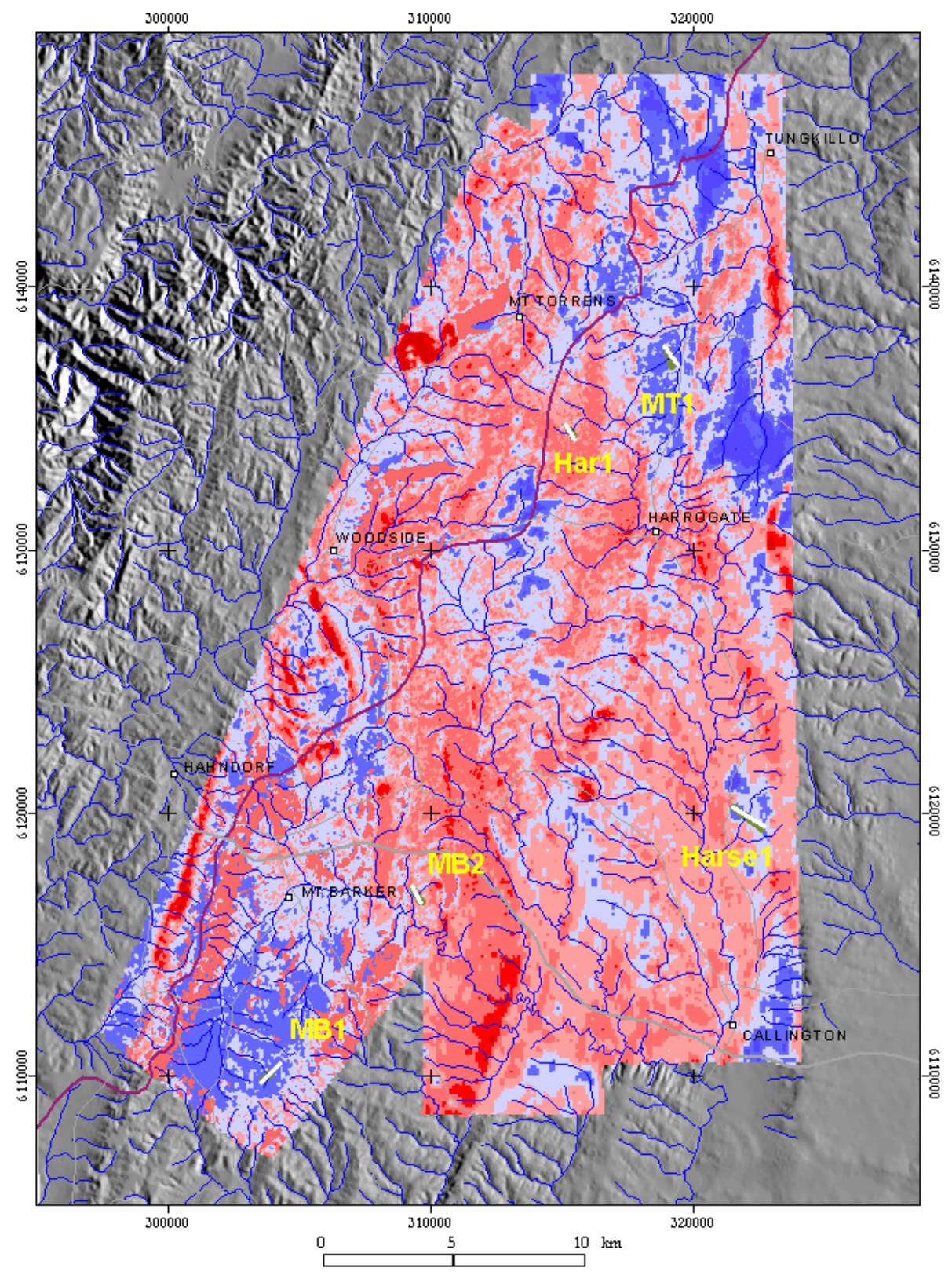

Figure 42. Locations of geophysical survey lines over the K-residual image.

6.6 Relationships between highly weathered regolith materials delineated by the K-residuals and landforms.

In many places the low K residuals, interpreted to relate to areas of highly weathered regolith, correlate with smooth, relatively low relief landforms. These landforms are associated with the partially dissected palaeo-surface or 'summit surface' discussed earlier. The low K-residual response appears to be related to highly weathered soils and saprolite that are preserved in this part of the landscape. As discussed previously, the landforms of the palaeosurface are clearly recognised on the hillshaded, slope and relief derivatives of the DEM. Low K-residual values generally correlate with areas of smooth low amplitude hillshade patterns, low slope and relief (Figure 43).

As discussed in previous sections (section 3.5) the palaeosurface is believed to have developed prior to regional uplift that formed the Lofty Ranges. Uplift of the ranges was associated with a series of major tilt blocks and fault bounding scarps. These fault blocks coupled with the rapid incision of rivers appear to have a significant influence on the the distribution and preservation of the weathered palaeo-surface. The combination of the K-residual image that delineates weathering on the palaeosurface and topographic sections from a high resolution DEM provide further insights into the distribution of the older parts of the landscape, tectonic movements and geomorphic processes over the Adelaide Hills.

Highly weathered materials associated with the palaeosurface are found on both the upper and lower parts of the tilt blocks (Figure 44). Highly weathered regolith is also preserved along drainage divides that frequently correspond to the upper part of the tilt blocks (Figure 45, 46, 47, 48 and 49). Preservation on divides and on the upper part of tilt blocks is likely to be associated with lower rates of geomorphic activity associated with relatively short stream flow lengths and stream erosion capacity. Preservation of highly weathered regolith on the lower parts of the tilt blocks is likely to be because of low base levels and associated erosion rates. In places the lower part of the tilt blocks are buried by colluvial and alluvial sediments that protect the underlying saprolite from erosion. Some of the lower faulted blocks were inundated by the sea and Miocene marine carbonates were deposited. Remnant outcrops of Miocene limestones and Fe-indurated river channel gravels occur on local rises near to the edge of the Bremer Fault scarp north of Callington. Landforms along the major drainage divide east of Woodside and the Herman's catchment are examples of highly weathered palaeosurfaces preserved on both the upper and lower parts of faulted blocks.

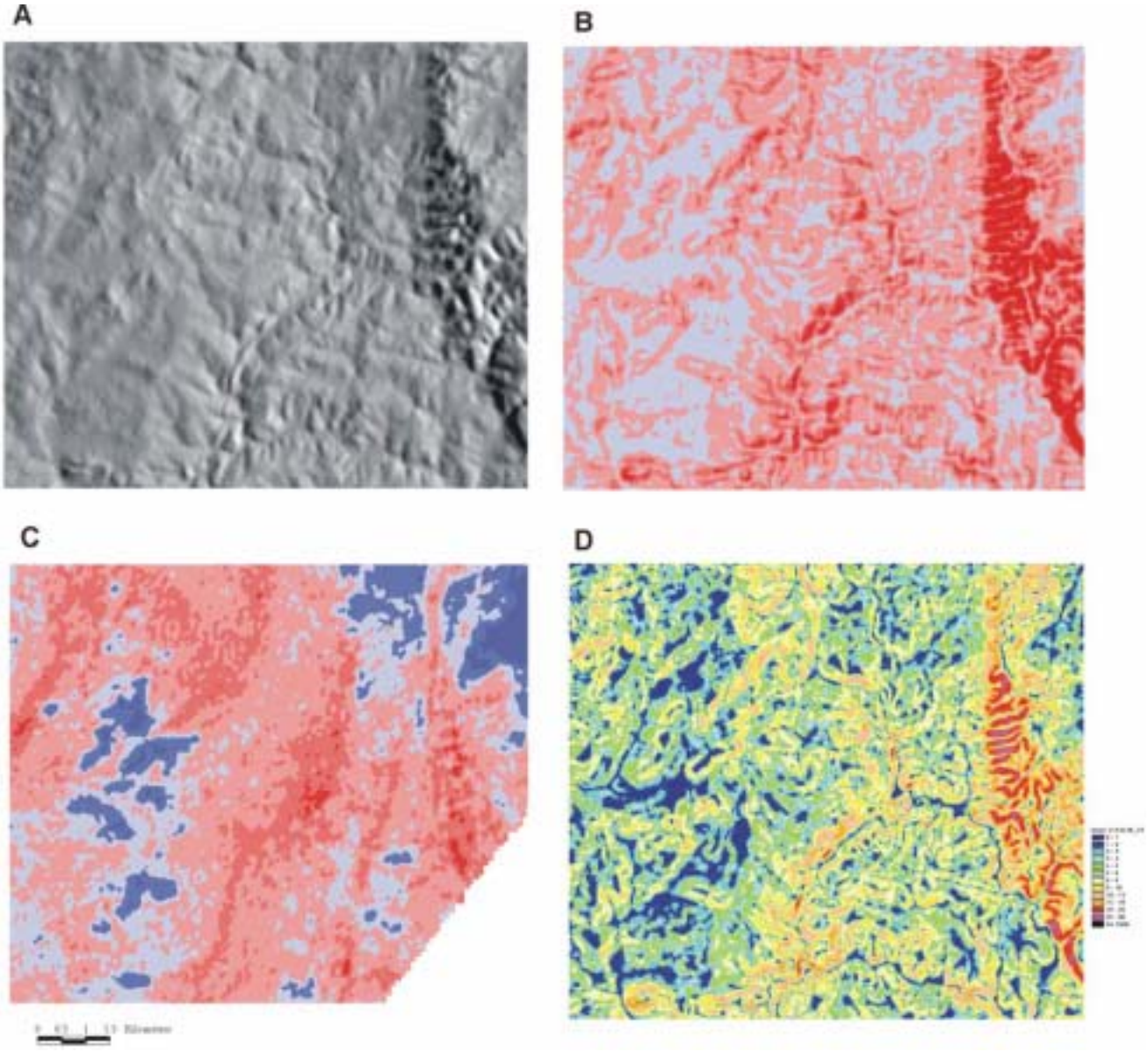

Figure 43. A – hillshaded DEM, B- relief (low grey – high red hues), C - K-residual image (highly weathered regolith in blue – less weathered in reddish hues) and D - slope (low slopes blue – high slopes in reddish hues).

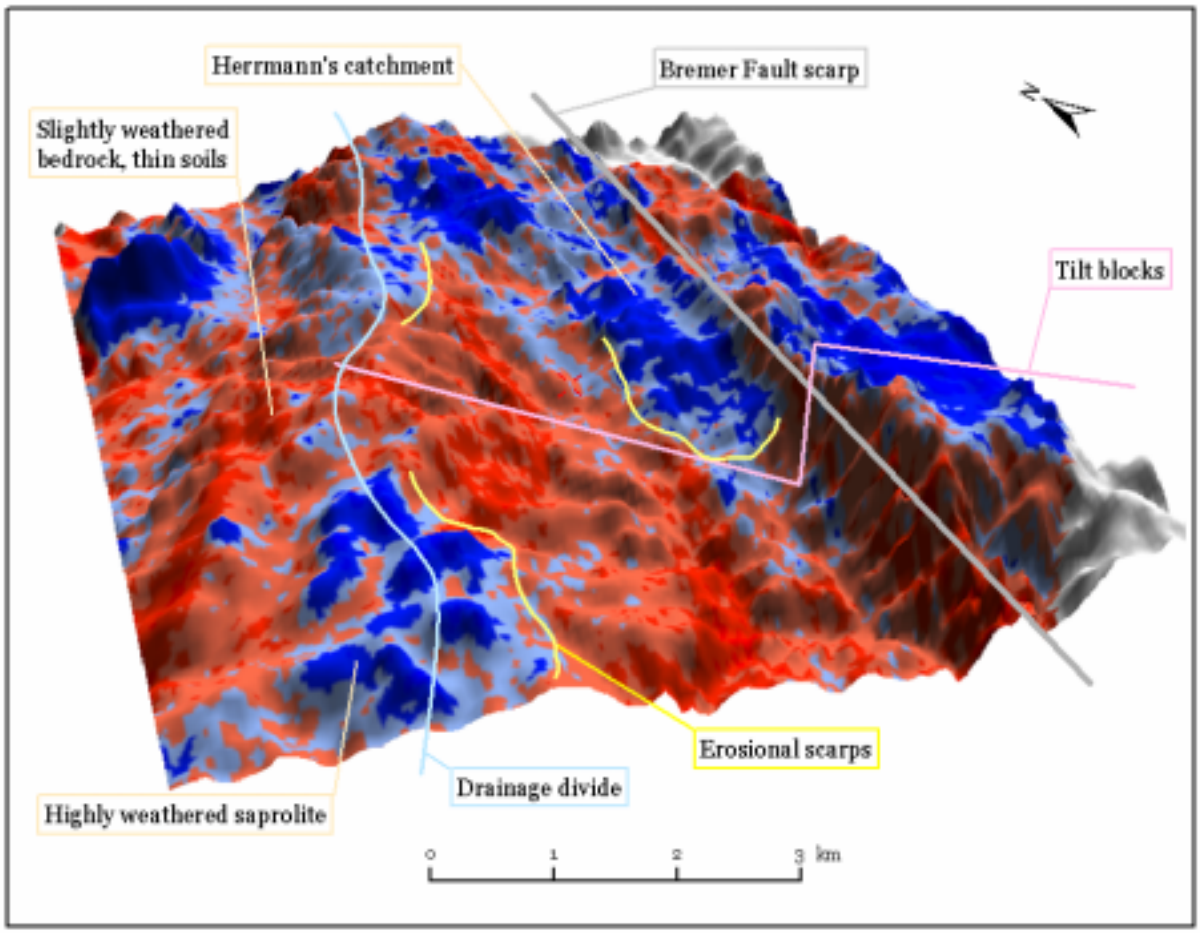

Figure 44. 3D perspective view of the K-residual draped over the DEM. Major fault blocks, fault scarps and minor erosional scarps are highlighted. Highly weathered regolith is preserved on the upper and lower parts of the fault blocks. Erosional scarps typically form the bounding edge of the weathered surface.

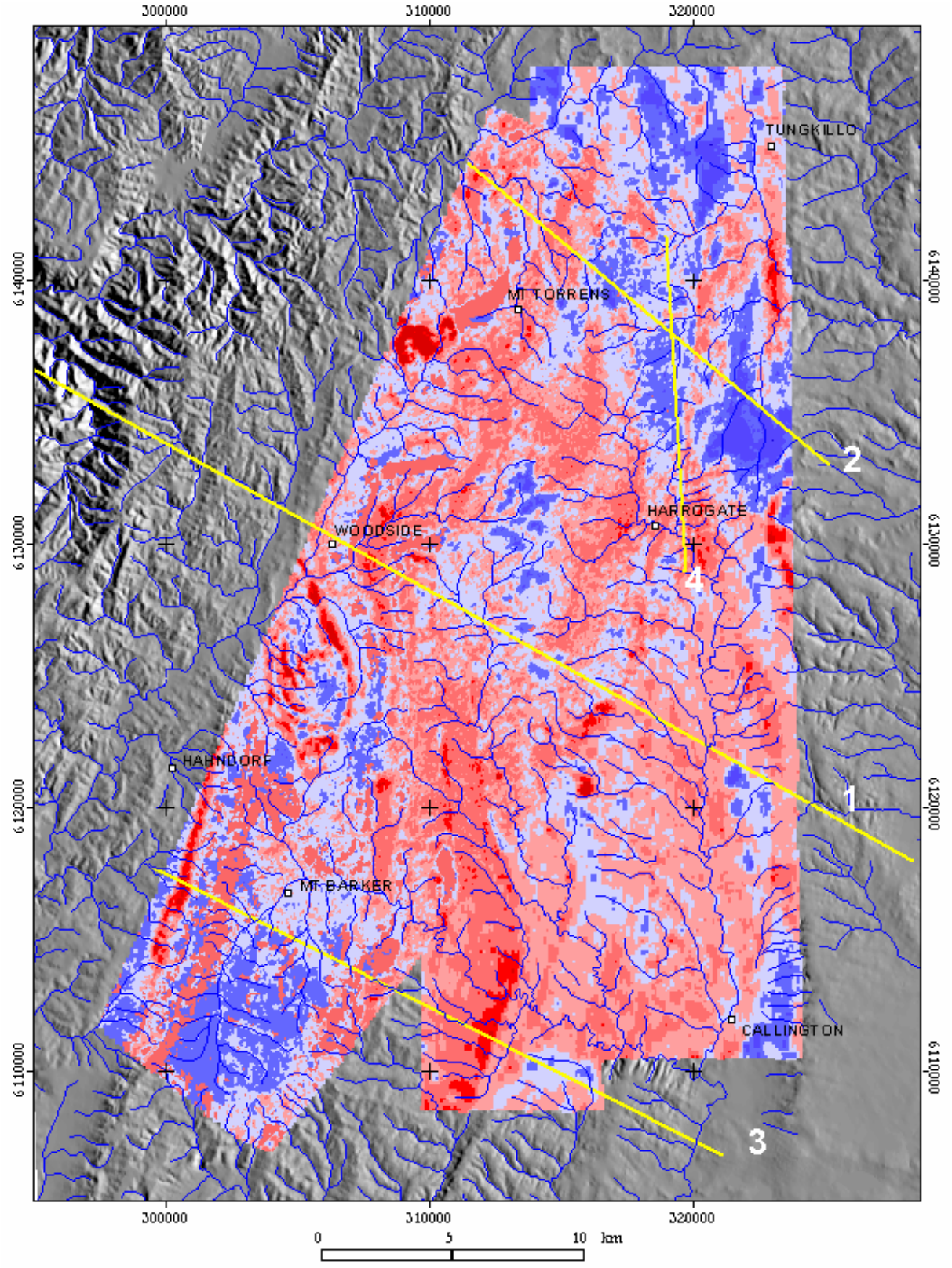

Figure 45. Location of topographic x-sections over the K-residual image.

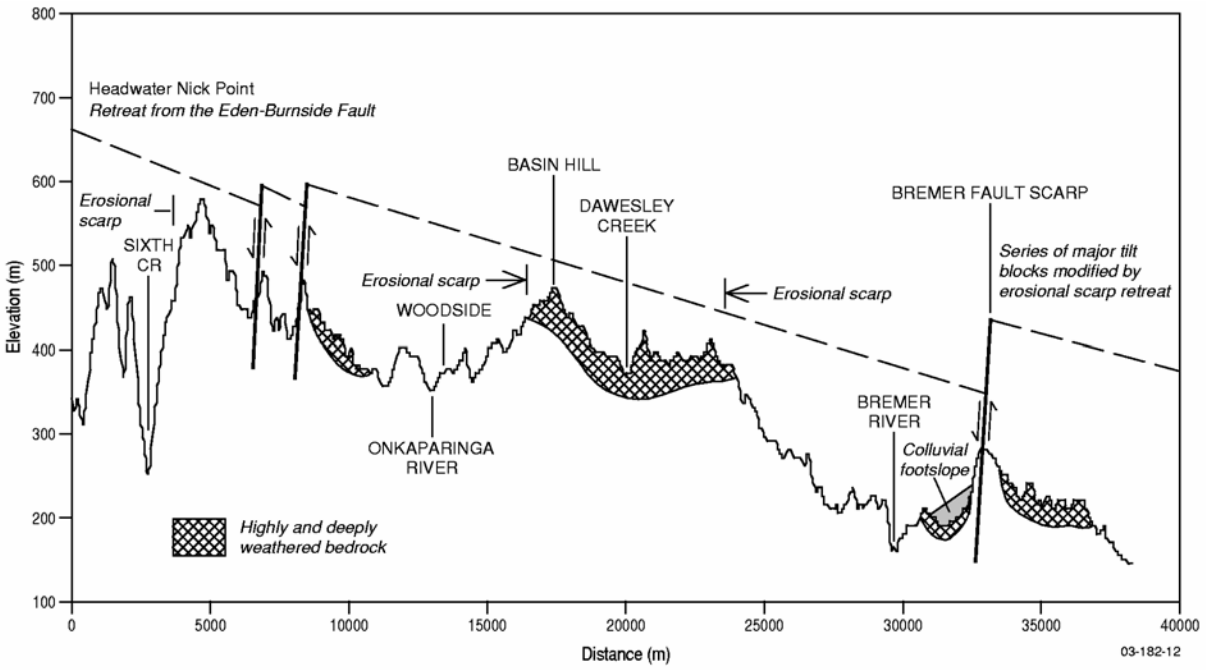

Figure 46. Topographic x-section 1 highlighting a series of easterly tilted fault blocks. Major fault scarps are associated with these fault blocks (e.g. Bremer Fault) as well as a series of local scale parasitic faults within the larger tilt blocks. Deep weathering associated with the palaeosurface is preserved on both the upper (often coincident with drainage divides) and lower parts of the tilt blocks. Headward erosion associated with a series of erosional scarps is actively eroding the older weathered palaeosurface. The portrayed thickness of weathered materials is schematic and not to scale. (Indicate which end is which on the sections)

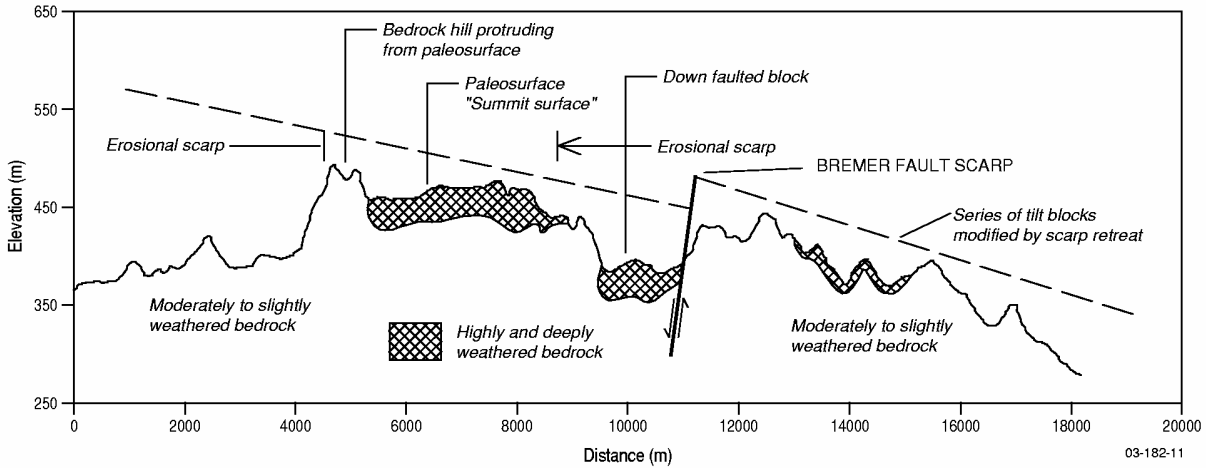

Figure 47. Topographic x-section 2 highlighting a series of easterly tilted fault blocks. Major fault scarps are associated with these fault blocks (e.g. Bremer Fault). Deep weathering associated with the palaeosurface is preserved on both the upper (often coincident with drainage divides) and lower parts of the tilt blocks. Headward erosion associated with a series of erosional scarps is actively removing material from the older weathered palaeosurface. The Herrmann's catchment is located in the down faulted block centre of section. Thickness of weathered materials not to scale.

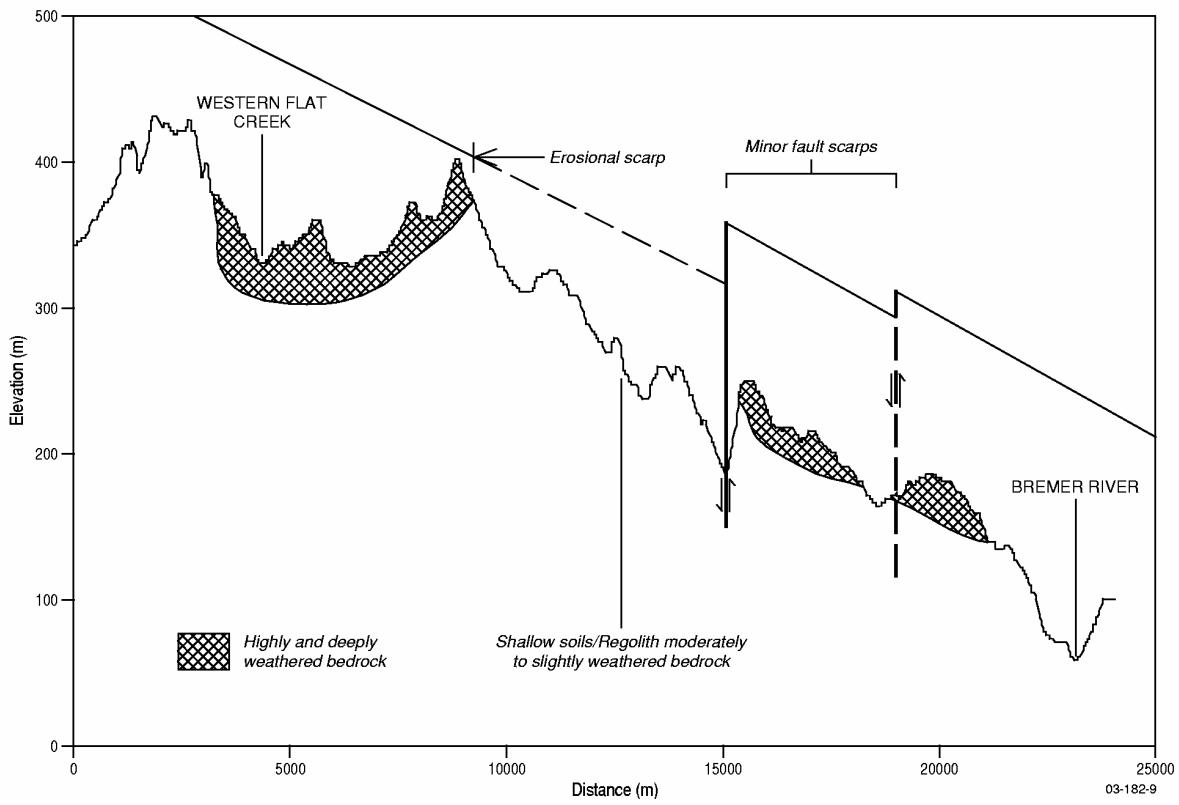

Figure 48. Topographic x-section 3 highlighting a series tilted fault blocks. Deep weathering associated with the palaeosurface is preserved on the upper sections of the tilt blocks (often coincident with drainage divides). Local erosional is now stripping materials from the palaeosurface. Thickness of weathered materials not to scale.

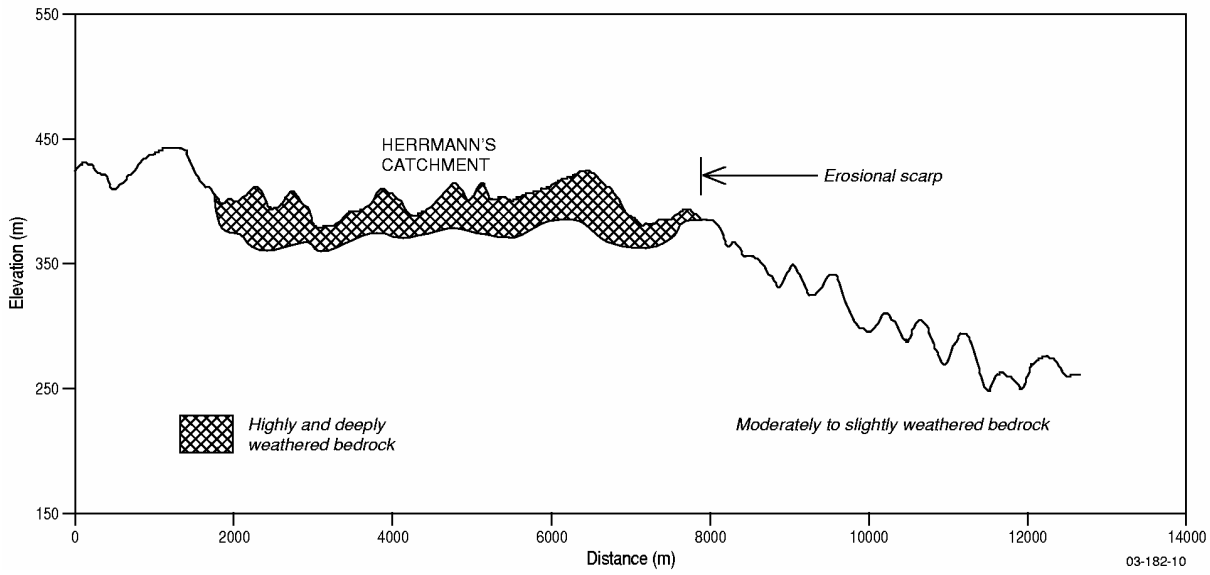

Figure 49. Topographic x-section 4 between Harrogate and the Herrmann's catchment. Headward incision associated with an erosional scarp is removing deeply weathered regolith. Moderately to slightly weathered bedrock is exposed below the scarp edge. Thickness of weathered materials not to scale.

In addition to the major tilt blocks and fault scarps, are a series of erosional scarps have been identified in the study area. These scarps highlight areas of active erosion, and are associated with nick point retreat from the major fault scarps and headward erosion of streams over the tilt block surface (Figure 49, 50). The erosional scarps have contributed to the development of a complex mosaic of materials with different ages and degrees of weathering. In general, older, typically more weathered and Fe indurated regolith materials, occur above the scarp. Below the scarp edge less weathered regolith are more common. In many places the erosional scarps delineate the edge of the more weathered palaeosurface landforms that is now being actively eroded in response to regional uplift. Along topographic section 4 (Figure 49) a series of photographs (Figure 51) show a progressive decrease in bedrock weathering away from the scarp edge. As the scarps retreat, they leave behind a diachronous surface with younger materials closest to the edge and older materials away and down slope from the scarp.

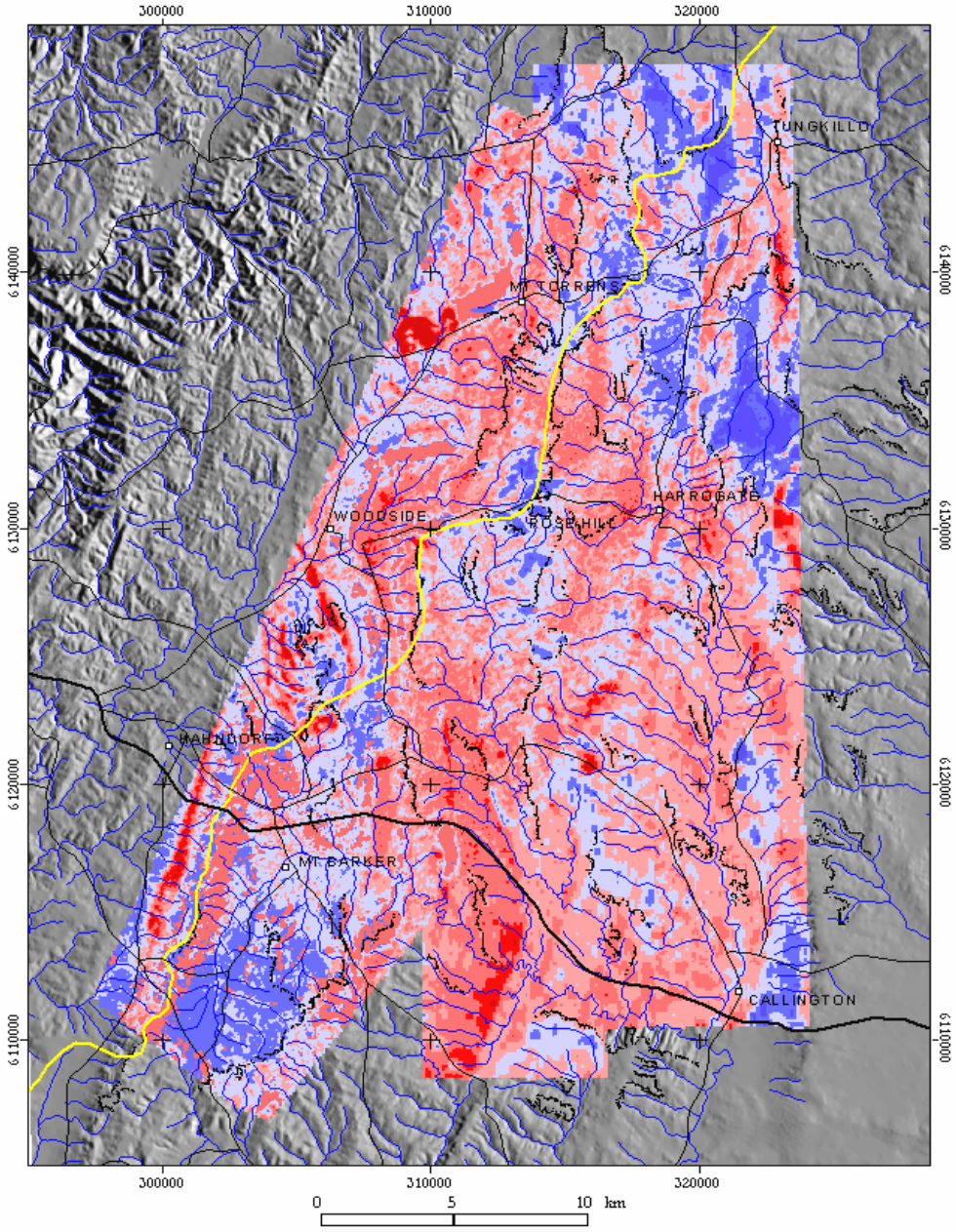

Figure 50. Distribution of erosional scarps over the K-residual image. The erosional scarps were compiled and digitised from a hillshaded image of the digital elevation model.

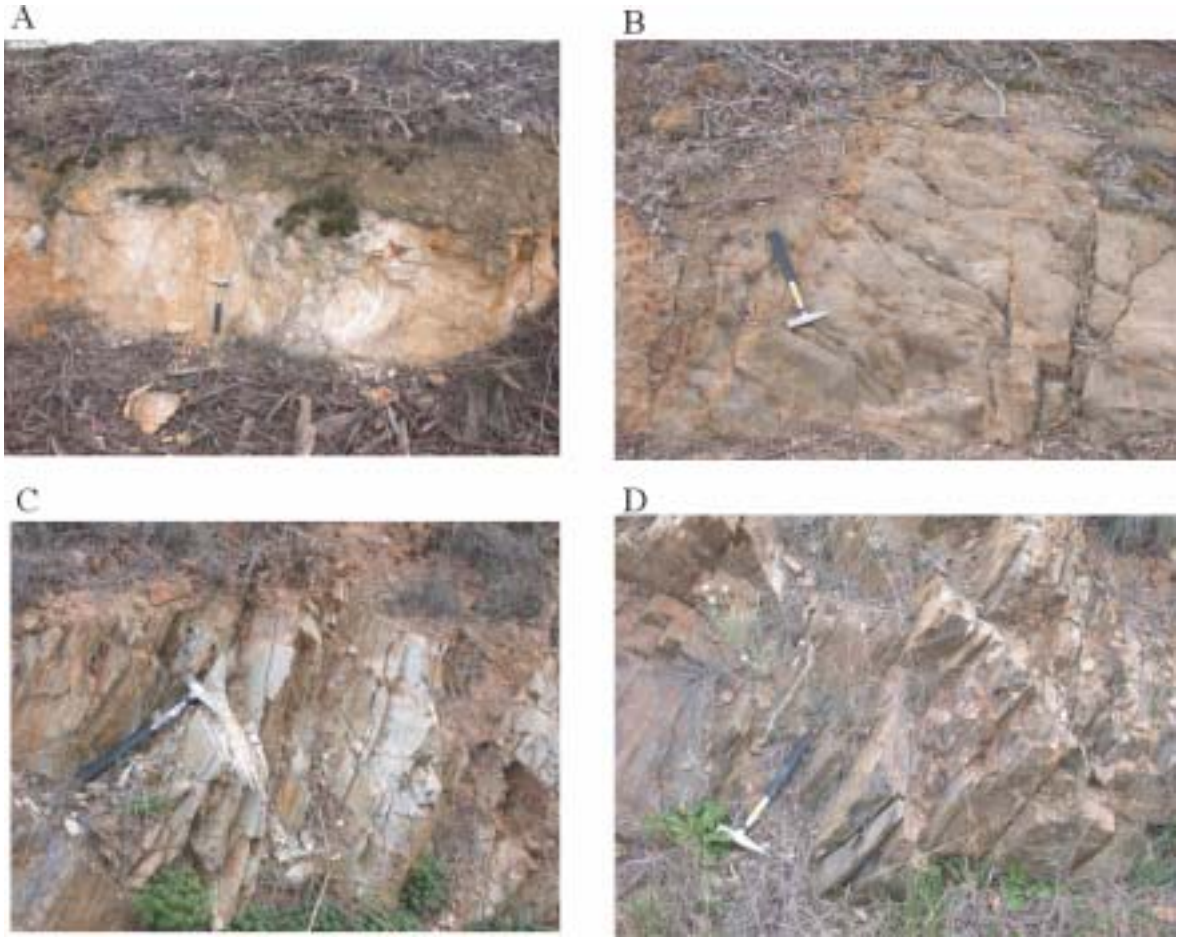

Figure 51. Series of photographs showing decreasing degrees of bedrock (metasiltstone) weathering from the top of the erosional scarp (A) to the base (D). Photographs are taken parallel to section 4 Figure 49.

6.7 Surface hydrology characteristics

In erosional landscapes, hill slope morphology exerts a major control on distribution of surface and near surface water flow (e.g. surface runoff and through flow). The 25m resolution digital elevation model was processed using two algorithms to extract key hydrological and geomorphological characteristics of the study area. The first algorithm is called Fuzzy Landscape Analysis GIS (FLAG) (Roberts *et al.* 1997). FLAG was used to map likely recharge and discharge zones. The second algorithm is called Multi Resolution Valley Bottom Flatness (MRVBF), which was used to map low lying depositional areas in the landscape.

6.7.1 FLAG

FLAG was used to generate an index that describes locally low areas with a large contributing area (LOW). The LOW index is similar to a topographic wetness index and is used to highlight areas of surface wetness and discharge in the landscape (Figure 48a). Over the Hills study area 'LOW'

partitioned areas along creeks and streams including valley floors and sides from, mid slopes, ridge lines and hill crests. This effectively separated, at local scales, areas of potential recharge and discharge. In many cases LOW highlighted areas of local discharge and waterlogging. It was expected that the LOW index would be a good surrogate for mapping and extrapolating areas of potential saline discharge based on salt scalds mapped from aerial photographs in the northern part of the study area (Henschke, 1997), particularly as most of the scalds occur along drainage lines or valley sides. Although most of the mapped salt scalds corresponded to areas delineated by the LOW index there were many situations where this was not observed (Figure 52a). The prediction of salinity or saline discharge is greatly improved when the radiometric K-residual image is combined with the LOW index (Figure 52b). The K-residual separates weathered catchments (low K-residual values) from bedrock dominated catchments (high K-residual values, blue image hues). The valleys in low K-residual areas have lower slope gradients both along and perpendicular to the drainage line. Known salt scalds generally occur where the K-residual and LOW intersect. Areas where the two datasets intersect are interpreted as saline groundwater discharge sites sourcing salt from the regolith in poorly drained, sluggish valley systems. These landscapes have a higher capacity to store water and through evapo-transpiration processes salts are concentrated in the upper part of the regolith. In comparison, areas of mapped saline discharge that occur in bedrock incised valleys with little apparent regolith development (positive K-residuals) are likely to discharge relatively fresh water (e.g. these landscape have a lower capacity to store water and hence salt). Further field testing and validation is needed to test these interpretations.

*6.7.2 **Multi Resolution Valley Bottom Index (MRVBF)***

The MRVBF index provided an excellent first pass separation of valley floors and low lying depositional alluvial plains from hill slopes and ridge lines. It was sensitive to local changes in valley flatness and the corresponding valley shape. V-shape valleys with relatively steep sides and narrow corridors of alluvial/colluvial sediment along and adjacent to the valley floor had low MRVBF values (Figure 53). Conversely, broader valleys with gentler slopes had a higher MRVBF values (Figure 53). In most places these broader valleys tended to have a more extensive and thicker fill of alluvial and colluvial sediments. The broader valleys mainly coincided with low K-residual values and older landscapes associated with the palaeo-surface described earlier (section 3.5). Examples of the broader valley systems can be seen around the Mt Barker area and along the drainage divide between Mt Barker and Mt Torrens. These broader valleys tend to have relatively low stream gradients compared to other streams (Figure 56).

The MRVBF algorithm was also useful in highlighting bedrock constrictions or bottle necks along river channels. Bottle necks along drainage lines are recognised as a sudden change in width indicated by the flatness index (Figure 54). In many places the constriction point corresponds to a nick point[1] in the stream. The nick point separates relatively low stream gradients above the nick point from steeper gradients below. This is illustrated in the Mt Barker and Dairy Flat catchments (Figure 55 and 56). There is a corresponding correlation with the radiometrics image where the less incised landscapes above the nick point have radioelement values reflecting more, possibly thicker regolith materials (eg. low K and often elevated eTh) compared with bedrock-related responses that tend to dominate below the nick point.

[1]A nickpoint is a point of abrupt change in the longitudinal profile of stream due to a change in base level (eg. uplift in the Hills).

A B

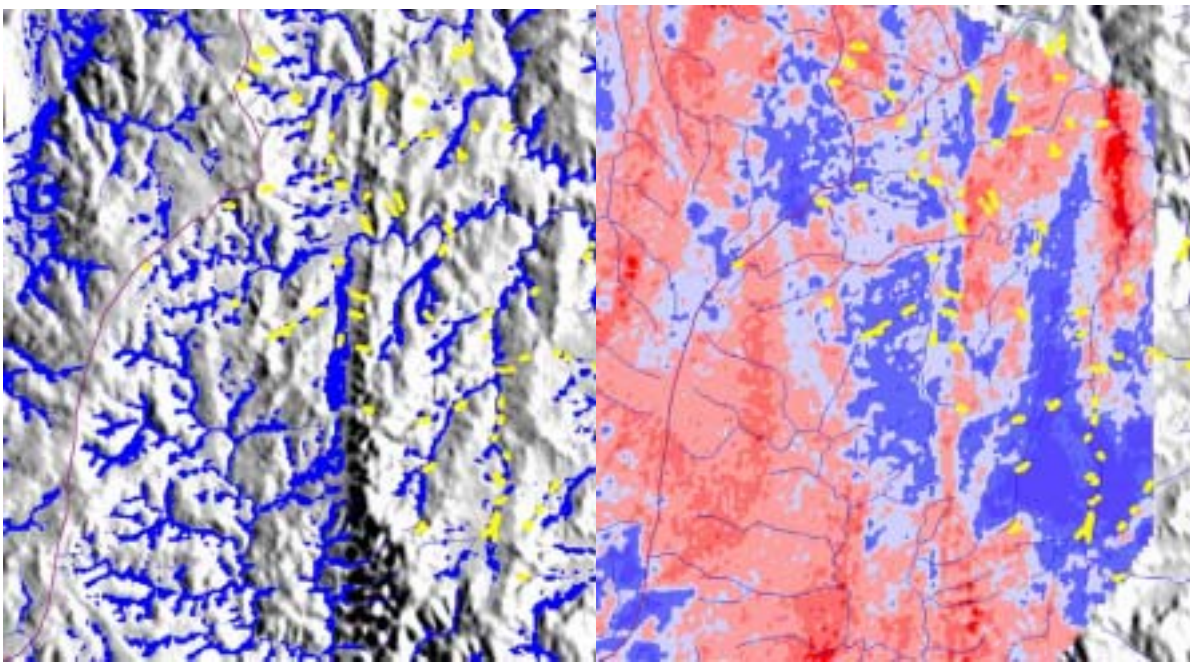

Figure 52. A - Flag index LOW, drainage lines and mapped salt scalds over hillshaded DEM. Example taken form the northern part of the study area. B - K-residual image highlighting weathered landscapes in blue and less weathered in red.

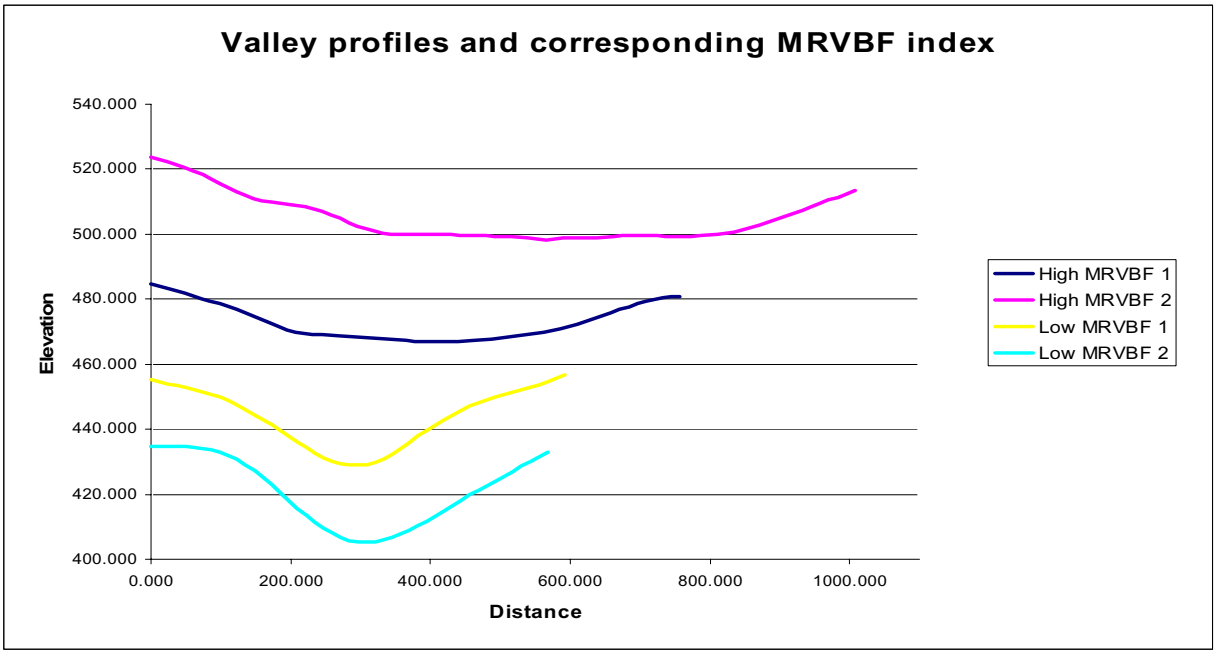

Figure 53. High and low MRVBF values compared to valley profiles. High MRVBF values correspond to low relief landforms associated with the palaeo or "summit" surface. Low MRVBF values are associated with areas of active erosion and stream incision.

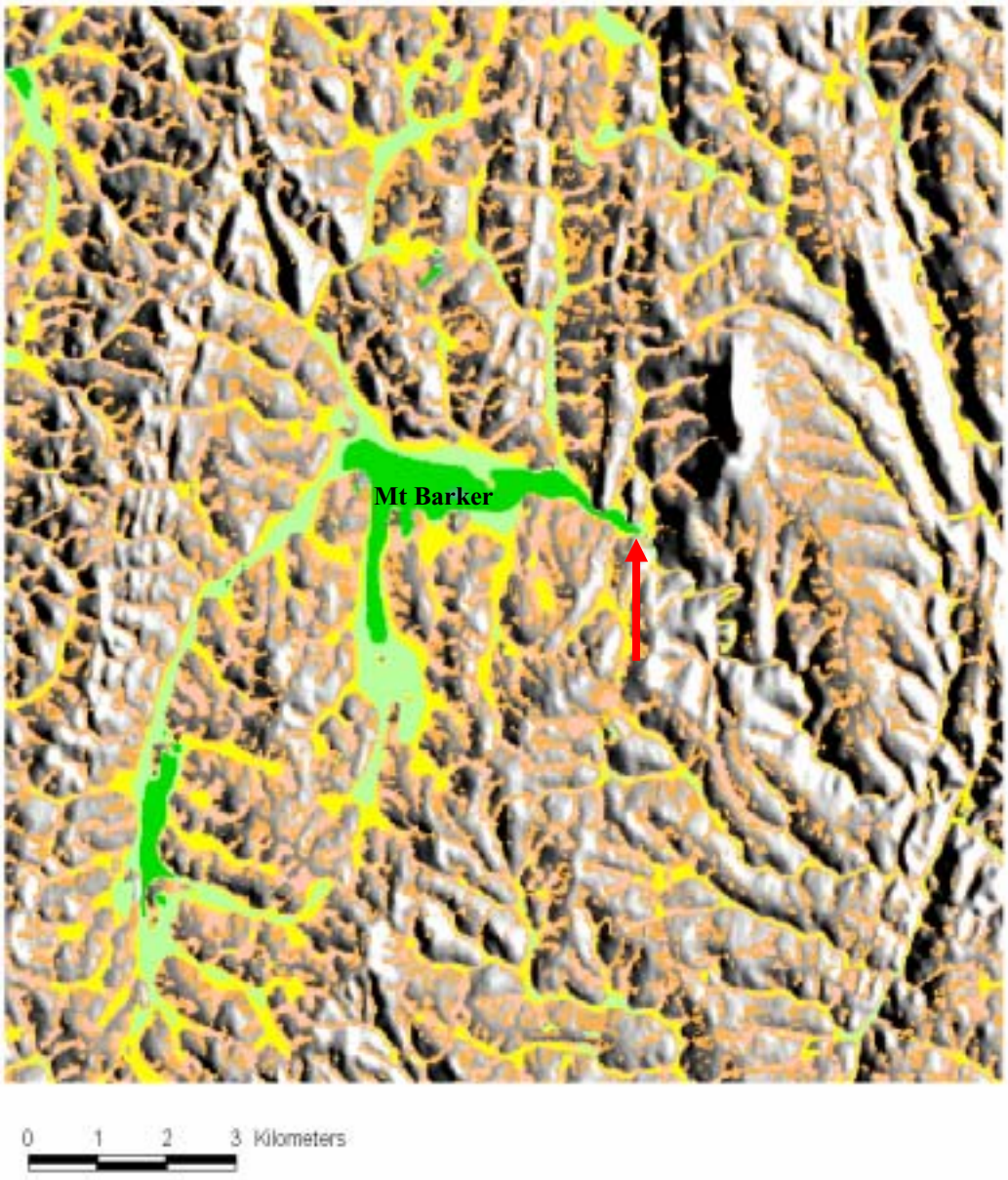

Figure 54. MRVBF over the Mt Barker area. Broad flat valleys are indicated in green and yellow hues. Bottlenecks or constriction in drainage are readily identified by the terrain index. These constrictions are typically associated with nick points (red arrow) in the stream or river.

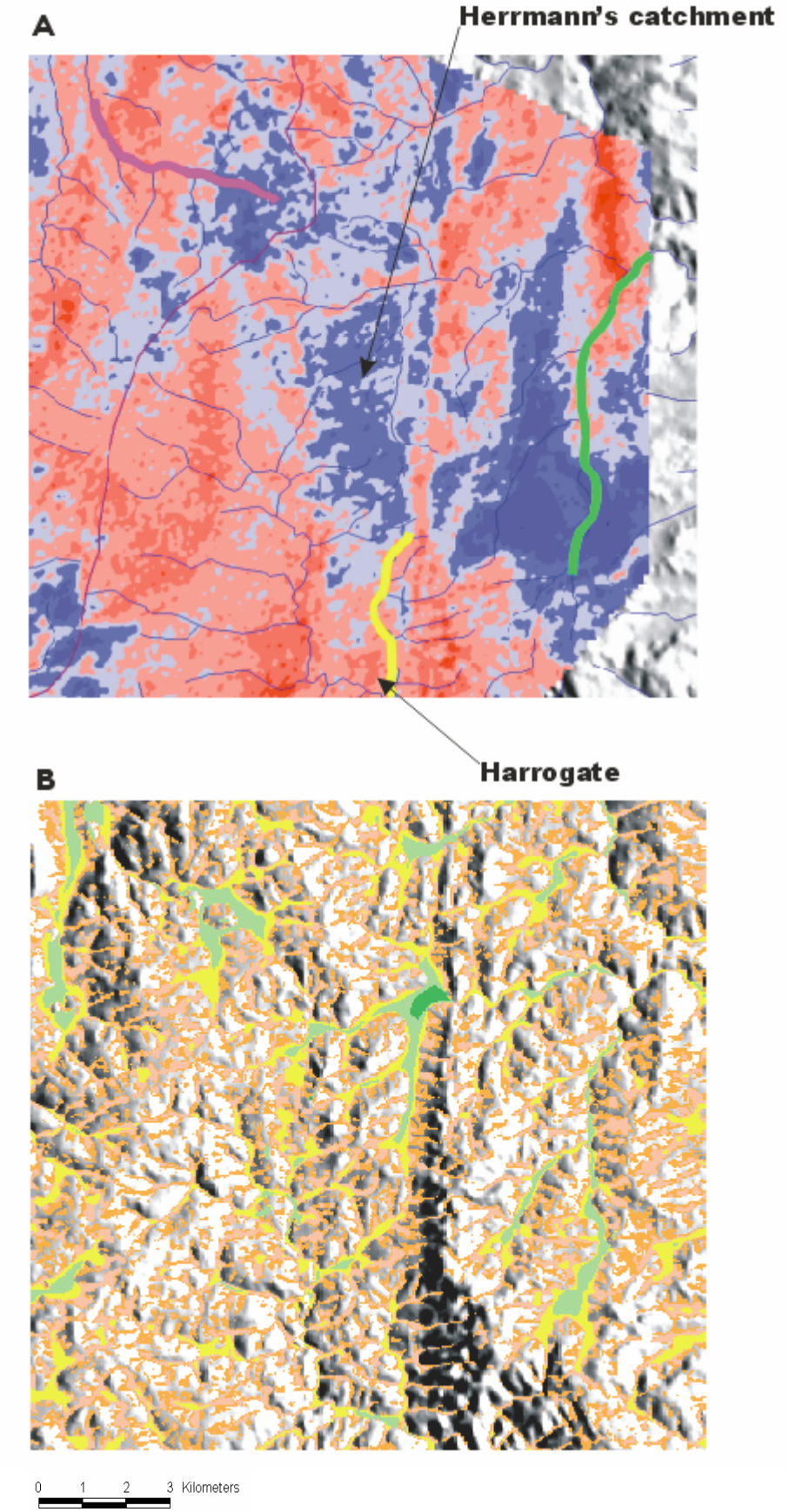

Figure 55. K-residual (A) and MRVBF (B) for the northern part of the study area.
Includes Dairy Creek and Herrmann's catchment. The longitudinal profiles of rivers highlighted in A are shown in figure 56.

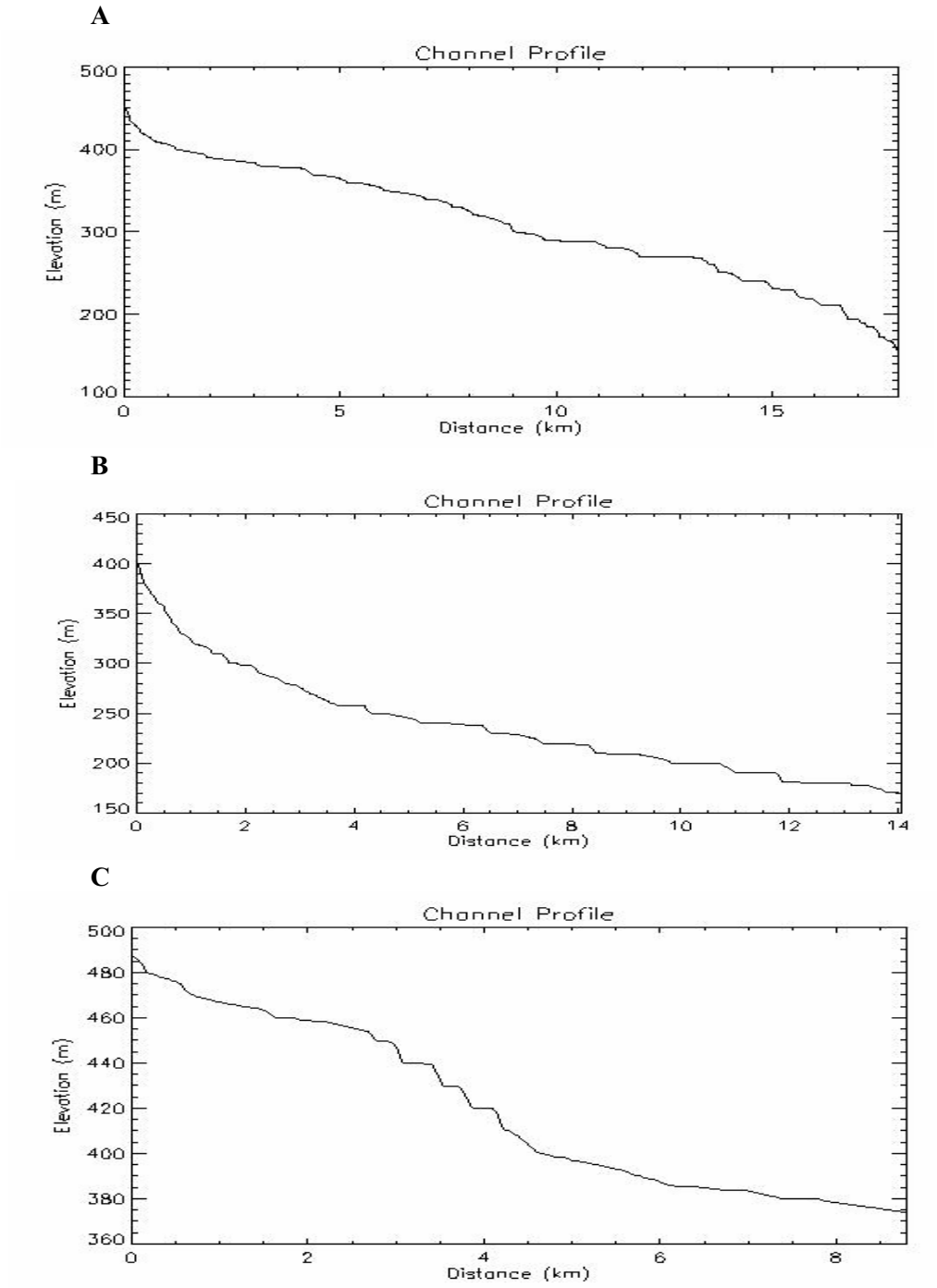

Figure 56. Stream profiles. A – Corresponds to the green line in figure 54a, B – yellow line and C – purple line. Lower gradients associated with the upper part of profile A and C correspond to the low relief palaeosurface. The break in slope (particularly visible in profile C) correlates to nick point retreat and steepening of the stream gradient. Profile C – is reflecting headwater erosion and scarp retreat as the tributaries of the Bremer River erode northwards into the highly weathered Hermann's catchment and associated landforms. In general lower stream gradients are associated with low K-residual image values and with broader valleys as indicated by MRVBF.

6.8 Regolith salt storage

The electrical conductance (EC) of the aqueous extracts measured in the drill samples are assumed to represent the amount salt stored in the regolith. This assumption is supported by hydrological investigations in the Keynes catchment (Cox and Reynolds, 1995) just north of the study area that found a high correlation ($R^2 = 0.98$) between EC and chloride concentration (Figure 57).

EC depth profiles (appendix A) have been classified according to the shape and pattern of salt concentration with depth. These classes or categories include;

1. Shallow Recharge profiles (T6, N1, T4, T5, HD5) with an evaporation peak at or near the surface and then a rapid decrease in salt content with depth. Overall the salt content is low. These profiles are associated with generally thin soils and saprolite over bedrock. Surface and near surface runoff is expected to be high. These profiles are found in recharge areas (e.g. hill slopes).

2. Moderately deep Recharge profiles (B4, T3, T9) with an evaporation peak at or near to the surface and then a gradual increase in salt concentration with depth. The salt trend suggests salts are being leached down through the profile. These profiles are characteristic of groundwater recharge zones.

3. Deep, leached Recharge Profiles (B1, B2, B3, B5, B6, B8, HA6, T8, T7, HA1, HA9) with an evaporation peak at the surface and a uniform low to moderate salt content with depth. This trend suggests that either salts were never concentrated in the profile or that salt have been leached below the depth drilled. Since most of the holes terminate within the saprolite and don't intersect the saprock (e.g. not a complete weathering profile) the latter explanation is probably more likely. These profiles are characteristics of recharge areas associated with hill slopes and hill crests.

4. Bulge Profiles (HA2, HA3, HA4, HA5, HA7, T2, B7, HD4, HA8, T1) with an evaporation peak at the surface and a salt bulge at depth. This is suggestive of salts being concentrated in a fluctuating water table zone within the regolith. These profiles are associated with groundwater discharge sites including valley floors, lower valley slopes and the base of colluvial fans. A profile bulge is also associated with areas covered by native woodland vegetation (T2). The bulge probable coincides with the depth of root zone. Transpiration of soil water would over time concentrate salts within this zone. In places multi-bulges probably reflect variations in texture and moisture content through the regolith profile.

Based on the EC and chloride correlation shown in figure 57 and an assumed bulk density of 1650 kg m^{-3} determined from measured drill core (Cox and Reynolds, 1995) tones of salt per hectare were calculated for the upper 5 metres of regolith and for the total depth drilled (Table 2). Across the study area a poor relationship was noted between K-residual values that were used to predict regolith depth and the amount of salt stored in the profile. (Figure 58). The highest salt stores are associated with discharge sites and colluvial footslope deposits, particularly on the eastern side of the study area (Figure 59). Both recharge and discharge sites on the western side of the study area have generally low salt stores.

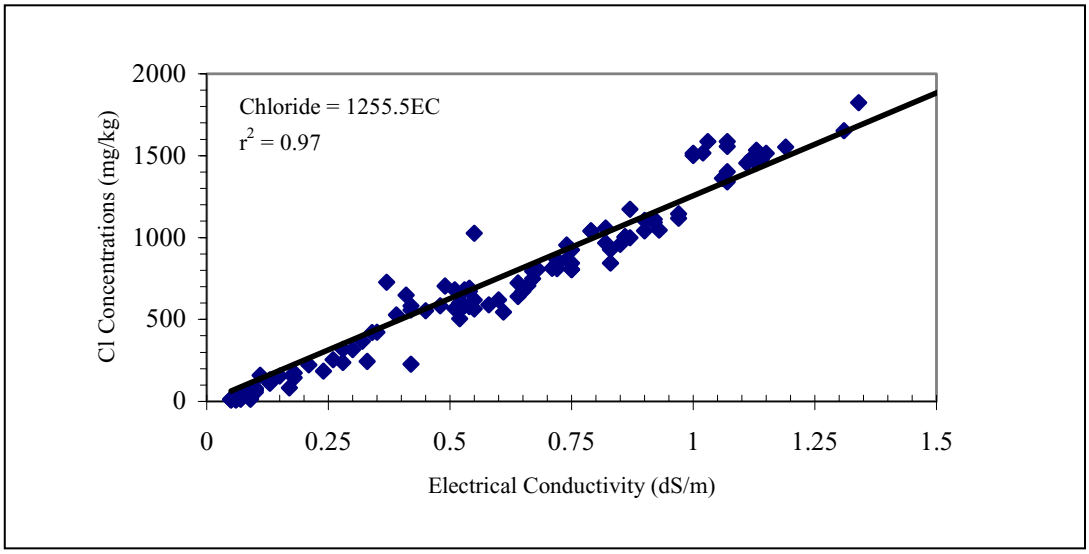

Figure 57. Correlation between EC and chloride from the Keynes catchment (Cox and Reynolds, 1995).

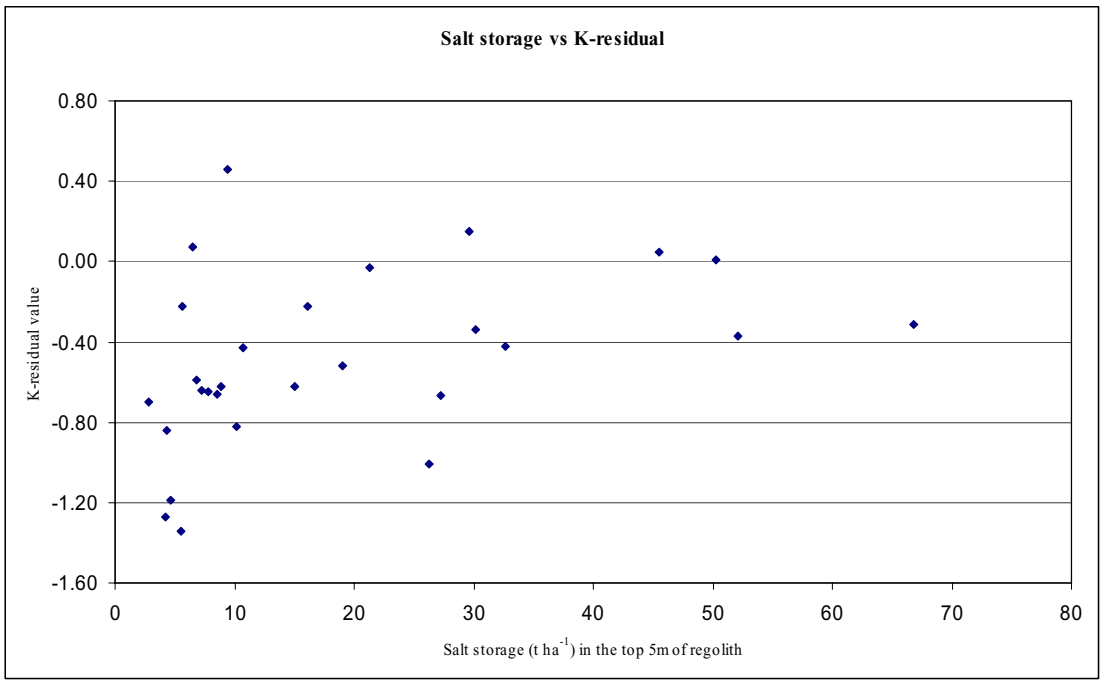

Figure 58. Relationship between salt store (t ha $^{-1}$) and K-residuals (low numbers = thicker regolith).

Table 2. Salt storage within the regolith aquifer for the upper 5m and over the total depth drilled.

Drill Hole Name	Salt storage over the upper 5m of the regolith aquifer (t ha^{-1})	Salt storage over the total depth drilled (t ha^{-1})
B1	4	12
B2	3	10
B3	9	25
B4	10	28
B5	8	20
B6	6	7
B7	19	51
B8	11	22
HA1	33	258
HA2	67	537
HA3	52	466
HA4	30	150
HA5	50	147
HA6	21	147
HA7	46	46
HA8	27	89
HA9	7	69
HD4	5	113
HD5	30	30
N1	9	9
T2	15	126
T3	7	165
T4	8	8
T5	16	16
T6	6	6
T7	26	26
T8	4	12
T9	6	6

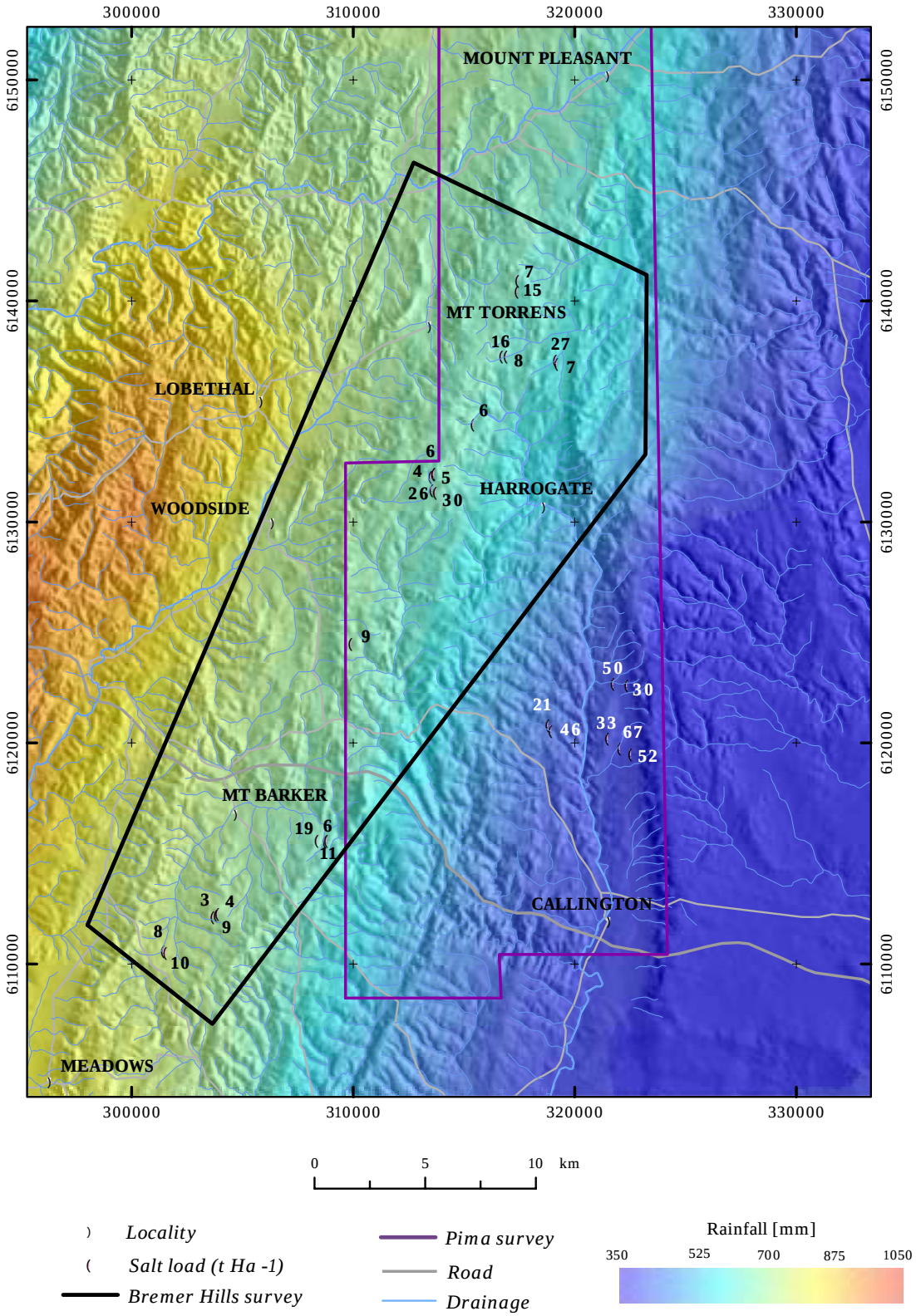

Figure 59. Salt stores (t ha $^{-1}$) in the upper 5m of regolith over average annual rainfall grid. Hillshaded DEM embedded into the rainfall grid to provide a topographic context.

6.9 Salt stores and rainfall

A significant relationship (R^2 = 0.67) was found between salt storage in the regolith aquifer and average annual rainfall (Figure 60). The sharp rainfall gradient across the study area ranging from over 1000mm in the west to less than 350mm in the east, influences the amount stored salt in the regolith. Most of the salts appear to have been or are being flushed from regolith profiles on the wetter western side of the study area, whereas, higher salt stores are associated with regolith materials over the drier eastern region. Appreciable amounts of salt have also been noted in relatively shallow regolith profiles on the eastern side contain (HA7, HA8).

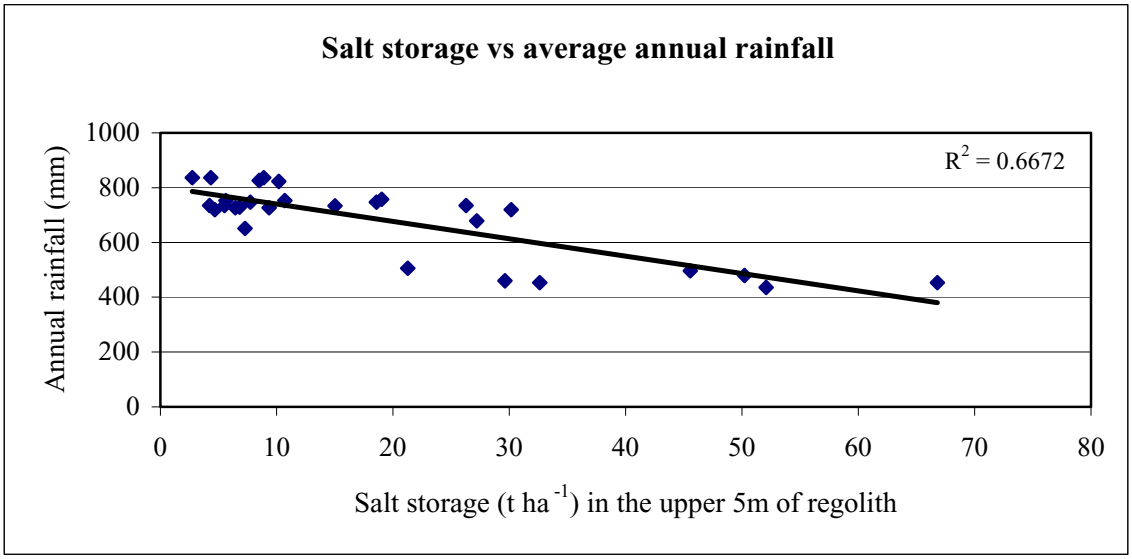

Figure 60. Correlation between salt storage (t ha $^{-1}$) and annual rainfall.

6.10 Salt mobilisation

A systematic investigation of the relationships between existing stream EC measurements and the K-residual image (Figure 61) was not undertaken. In many cases existing stream EC measurements were not at sufficient scale to be compared with the K-residual image. Stream EC measurements provide a snap shot in time and can change temporally depending on the amount of surface and base flow into the stream. Also the EC measurements don't inform on the total salt exported from a stream. Nevertheless, generally the higher stream ECs correspond to regions of deep weathering delineated by the K-residual image, including for example the Hermann's, Tungkillo and parts of the Mt Barker catchments. Where some detailed stream measurements were taken a clear relationship was found

between catchments with thick regolith and higher stream EC values or salinities (Figure 60). The regolith dominated catchments also showed evidence of sluggish drainage with water-logging and groundwater seeps common along the valley floors. The sluggish drainage probably relates to the high amount of clay in the regolith and the relatively low topographic and associated hydrological gradients (both perpendicular and along the drainage lines) that are characteristic of these highly weathered catchments.

.

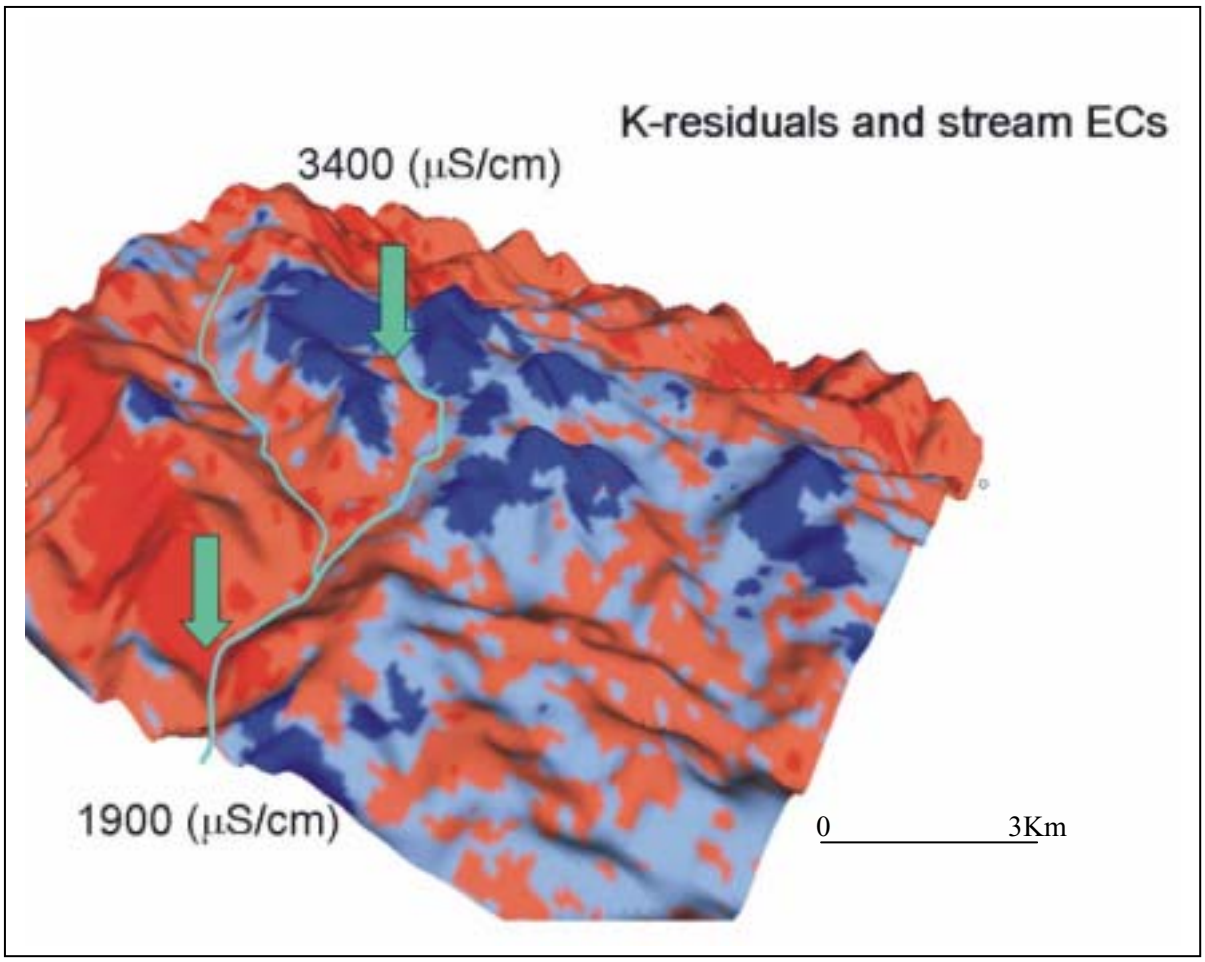

Figure 61. Streams draining through areas in the catchment dominated by thick regolith are generally more saline than stream draining watersheds with shallow regolith. In this example the highest salt stores and stream salinities are in the upper part of the catchment (K-residual image: blue = thicker regolith). As the streams drainages through less weathered parts of the catchment (red) the water becomes more diluted with less saline waters. In this situation remedial action would target the upper part of the catchment.

7. DISCUSSION AND CONCLUSIONS

The combined interpretation of airborne gamma-ray imagery and digital terrain attributes in conjunction with field based studies using ground geophysics and drilling have led to an improved understanding of regolith-landforms and controls on the distribution of salt across the study area. A synthesis of the main findings from this study is presented in a series of 3D conceptual models from different regolith, landform and rainfall regions within the study area. These are intended to illustrate the relationships between regolith, landform, climate and hydrogeomorphic processes as they influence the distribution and mobilisation of salt across the Hills area. (Figure 62, 63, 64 and 65).

The modelling and interpretation of gamma-ray spectrometric imagery has provided a rapid first pass delineation of thicker, better developed regolith profiles from landscapes that are dominated by relatively shallow soil and slightly weathered bedrock. The basis for this is related to how the radioelements are redistributed in the landscape following pedogenesis and bedrock weathering. K is leached from the regolith profile whereas eTh and eU often increases in concentration near the surface due to their association with iron oxides and clays. Changes in the relative distribution and abundance of these radioelements during weathering are used to separate the regolith and associated geomorphic/weathering processes from bedrock materials. The residual modelling approach uses the relative loss of K within each bedrock unit as a surrogate for estimating the degree of bedrock weathering and the thickness of regolith developed across the landscape. The approach works best in erosional landscapes where the bedrock contains K-bearing minerals. For the study area, most of the lithologies were suited to the application of this technique. Lithologies containing little or no K (eg. quartzites, highly siliceous sandstones) could be mapped due to their characteristic low gamma ray counts in each of the radioelements. However, the residual analysis method cannot separate regolith and bedrock responses where the bedrock contains no K or where K is retained in the weathered zone (eg. K associated with illite clays). Since it uses the known geology, errors in the position of the geological boundaries can generate artefacts in the product. These assumptions and limiting conditions need to be considered and understood when interpreting the results, and when applying the methodology in other regions. Ground validation of the residual gamma-ray patterns is regarded as an essential prerequisite for its effective application.

In the Hills area, the loss of K, as highlighted in the K-residual image, has delineated weathering profiles up to 45m deep. Since gamma-rays are emitted from only the top 20-30cm of bedrock or soil the surface characteristics of many soils in the area appear to be diagnostic of an underlying thick regolith. Soils that are typically highly leached (very low K) and ferruginous (iron nodules and lags) appear to be related to these thicker weathering profiles The K-residual image was more effective in predicting thicker regolith profiles where they have developed in situ, rather than in situations where they are covered by transported sediments. Apart from mapping areas of thicker regolith, the gamma-ray imagery is also useful for mapping a range of soil types and attributes. In general there was a good correlation between soil-landscape units and the observed gamma-ray responses. In many places the gamma-ray image can be used to modify soil-landscape unit boundaries or inform on the variability of particular attributes within soil units. Since similar gamma-ray responses can occur on different lithologies or landscapes, their interpretation is most effective when combined with an understanding of geological and landform units (e.g. erosional vs depositional landforms).

In the Hills area, highly weathered, thick regolith is associated with an old deeply weathered palaeo-surface often referred to as the “summit” surface. Whilst still the subject of controversy, its origin is generally it is thought to be that of an old landscape of relatively low relief which dates back to the Mesozoic and prior to the uplift that formed the hills. Where this palaeo-surface is still preserved, regolith profiles reflect long standing processes that have been active from the Mesozoic to the present day. The K-residual image is able to map the distribution of the palaeo-surface with greater accuracy than shown on existing soil and geological maps. Preservation of the palaeo-surface is more

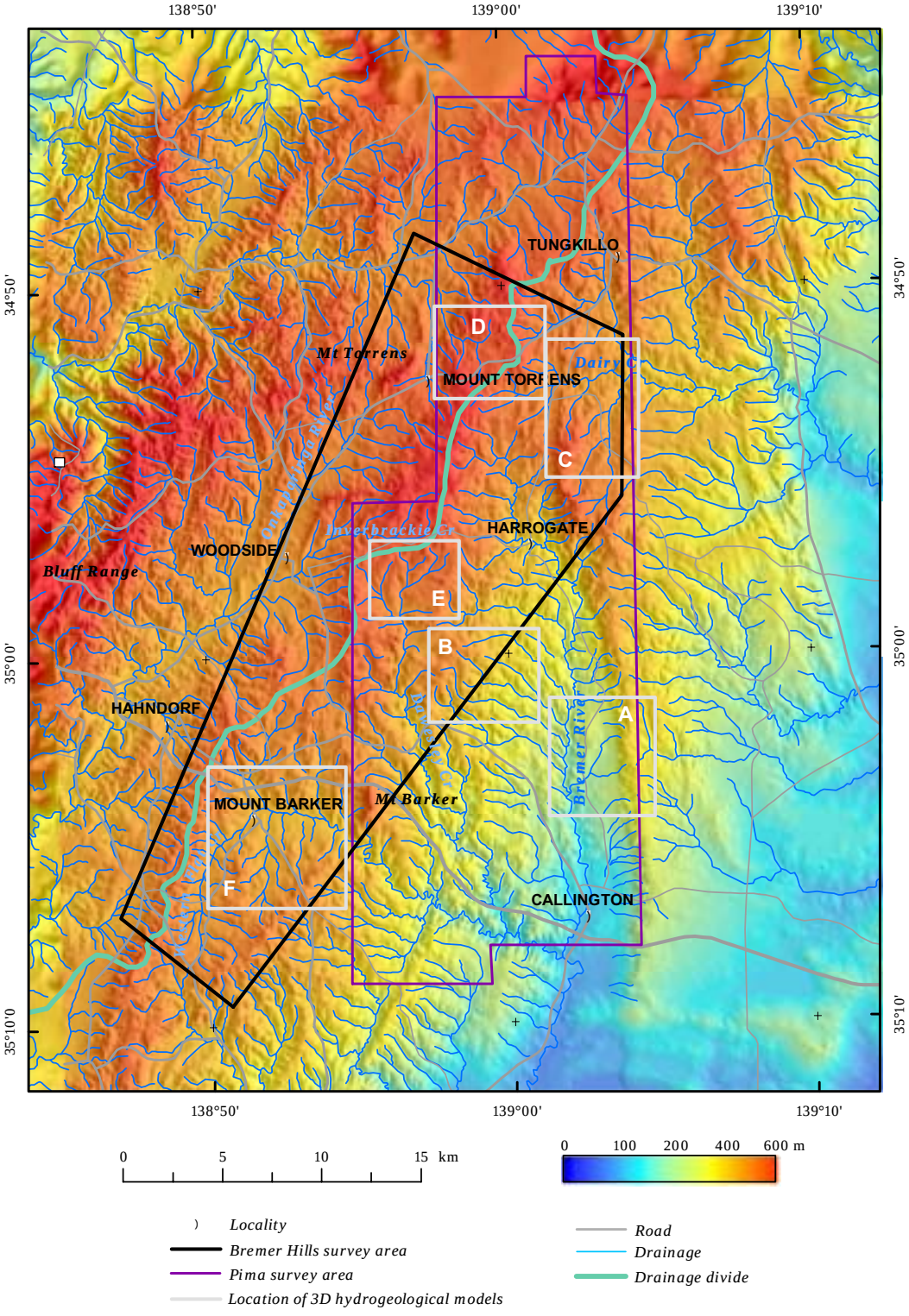

Figure 62. Location of 3D hydrogeomorphic conceptual models.

wide spread than indicated from previous mapping. Generally deeper weathering and thicker regolith profiles are associated with this palaeo-surface. Uplift, block faulting and erosion (scarp retreat and

valley incision) has resulted in a complex landscape where deeply weathered regolith profiles are juxtaposed with areas of thin soil and exposed bedrock.

Most of the weathered materials (leached and ferruginous soils, mottled sediments and kaolinised and mottled saprolite) have characteristically low K and elevated eTh. Exceptions are in landscapes associated with the Hermann's catchment and the Muir catchment south of Tungkillo. While, these catchments have low K radioelement responses, they exhibit eTh concentrations similar to the unweathered bedrock. This is thought to reflect a landscape that was either never deeply weathered (e.g. weathering sufficient to leach K but where thorium is not associated with the development of ferruginous duricrusts) or was deeply weathered and then partially stripped, exposing less weathered materials at the surface. Twidale and Bourne (1975) have described the development of an etch plain in the Tungkillo region, which formed by partial stripping of the weathered bedrock and exposure of an irregular weathering front. Whether the radioelement relationships found around Tungkillo and Hermann's relate to this landscape model requires further investigation.

Terrain modelling using MRVBF was not as effective, nor appropriate in identifying the older weathered landscape, with a poor correlation noted between the MRVBF index and depth of weathering. This was attributed to similarities in the local relief of the palaeosurface and the more contemporary landscape. However, MRVBF index was particularly useful in delineating valley fill sediments and broad valley fill systems that in places are associated with older landscapes in the area. The valley index effectively highlighted local constrictions or bottle necks along drainage lines. In many places these bottle necks coincided with stream nick points where broader valley profiles and thicker alluvial sediments occur above the nick point, compared with steeper valley profiles and thin alluvial deposits below. By contrast, the K-residual image was less useful in depositional areas particularly where the sediments had similar signatures to the bedrock from which the sediments were derived. Therefore the K-residual image and MRVBF index complemented each other and together were effective in mapping thicker regolith profiles (including residual profiles and sediments) and valley constrictions.

In respect of the distribution of salt in the study area, several factors were recognised as being important. These include thickness and composition of regolith, rainfall, stream gradients and constrictions or barriers to near surface groundwater flow. Regolith thickness governs the capacity of the landscape to store cyclic salts (e.g. those salts derived from rainfall). Weathering increases the capacity of the landscape to store salts because clays generated by the breakdown of primary rock minerals have generally much higher porosities and lower permeabilities than the original bedrock. In addition weathering is important when considering the release of salts into the groundwater from the break down of salt bearing minerals in the bedrock. Fitzpatrick et al. (1996, 2002) has identified the weathering of scapolite, a bedrock mineral that contains sodium and chloride ions, as a source of groundwater salts in the Hermann's catchment. Although most of the salts in the Hills area are of oceanic origin (Cox et al, 2002, Smitt, 2004) salts derived from bedrock weathering may be important at local catchment scales, particularly where the bedrock contains sulphides (pyritic units of the Tapanappa and Talisker FM) that can cause accelerated weathering of the bedrock (Fitzpatrick et al. (1996). However, even in areas of disseminated reduced sulphur minerals $S04^{2-}/Cl$ ratios and $^{34}S_{so4}$ of saline seeps are similar to atmospheric aerosols values (Smitt, 2004). In either case delineating areas of deep weathering is important for both origins of salt in the landscape.

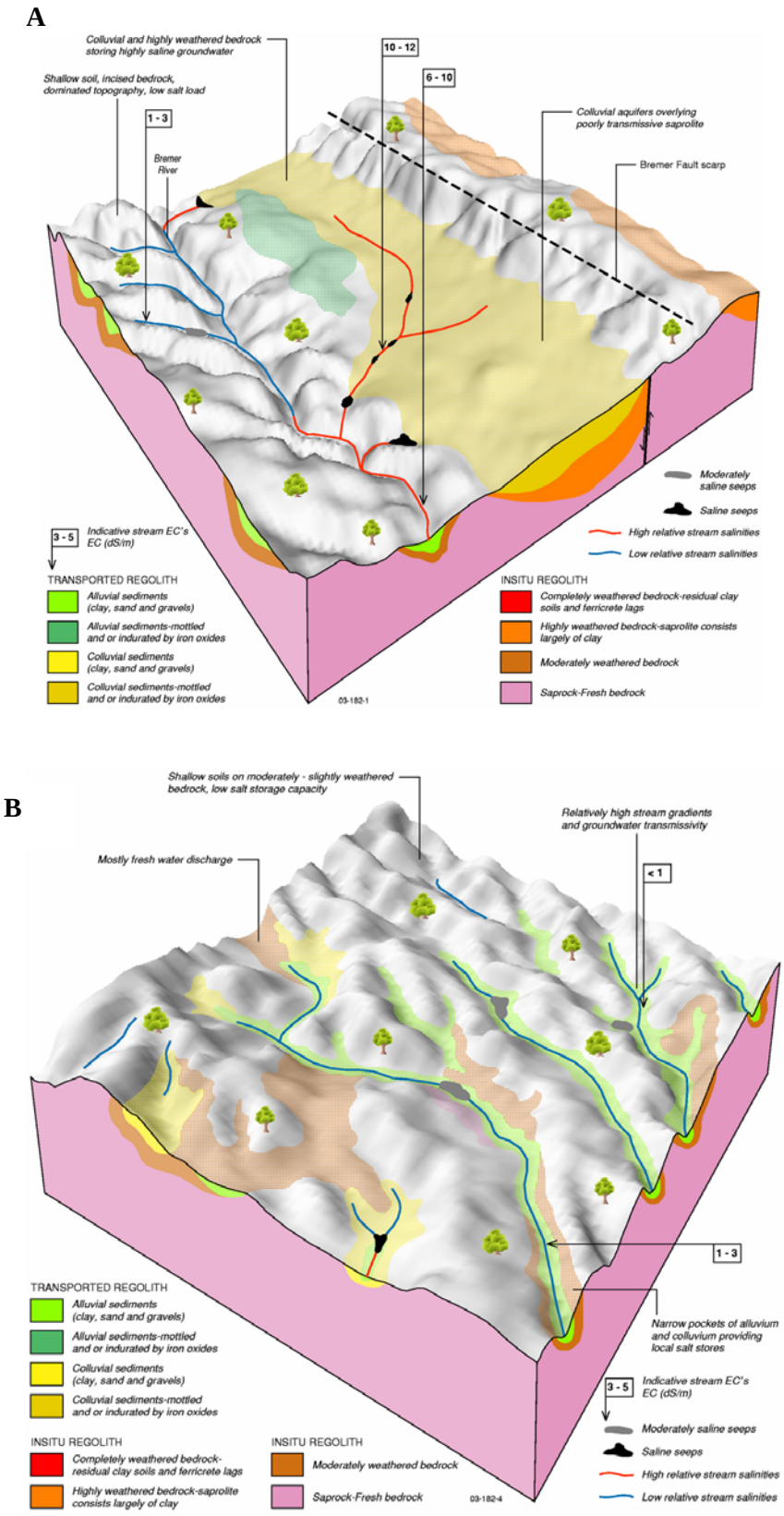

Figure 63. 3D hydrogeomorphic model based on the integration of information on the regolith, hydrological processes, salt stores, rainfall, stream EC and landforms. Refer to Figure 61 for the location of models A and B.

C

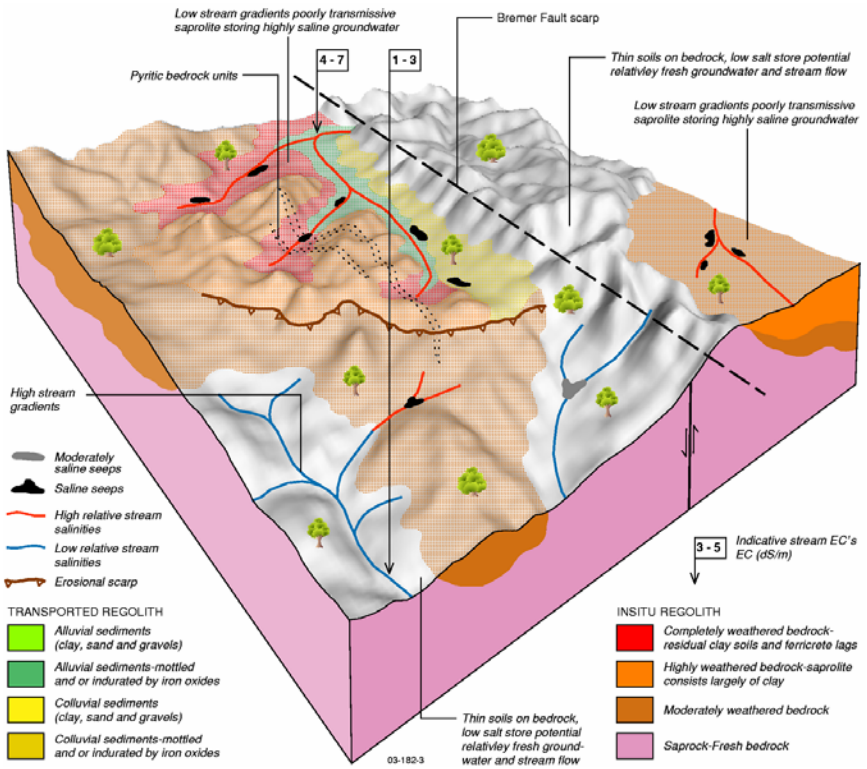

D

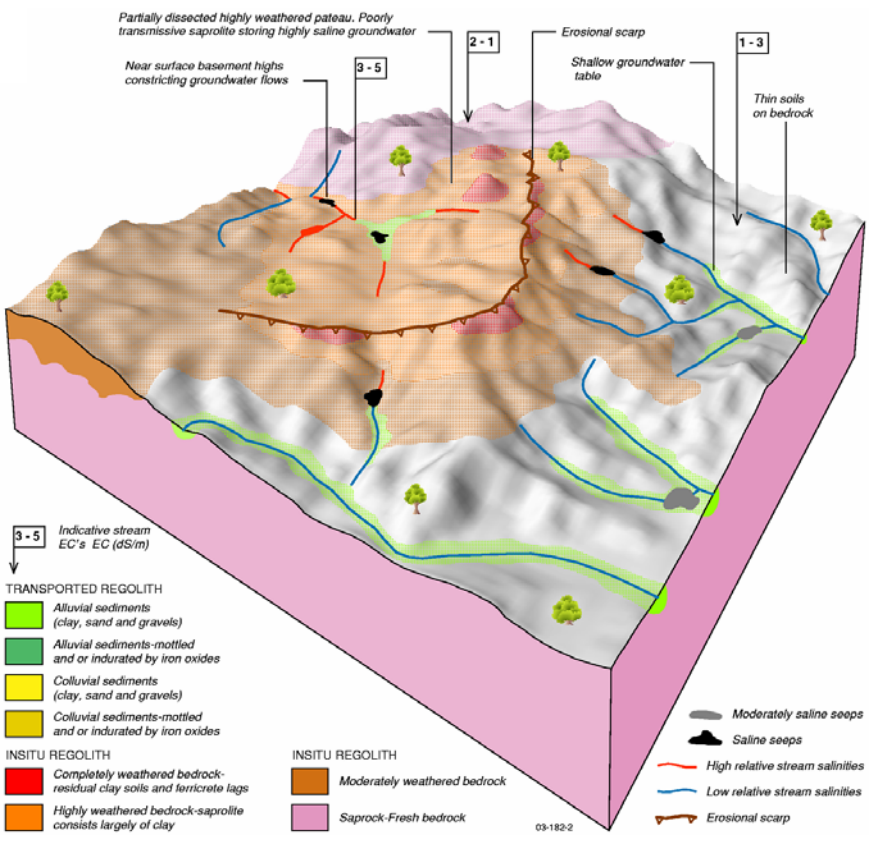

Figure 64. 3D hydrogeomorphic model based on the integration of information on regolith, hydrological processes, salt stores, rainfall, stream EC and landforms. Refer to figure 61 for the location of models C and D.

E

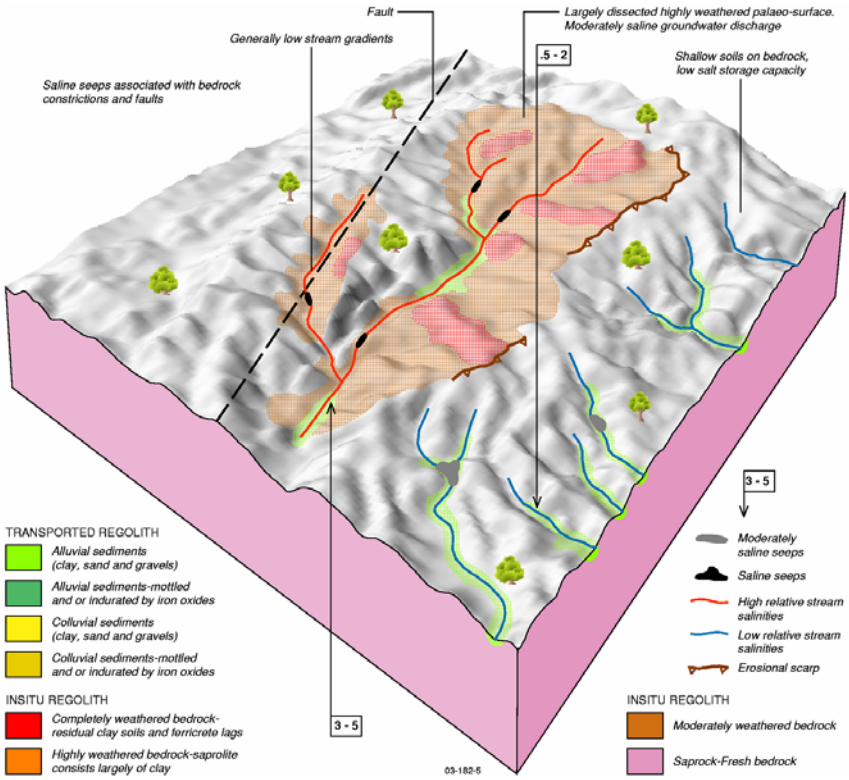

F

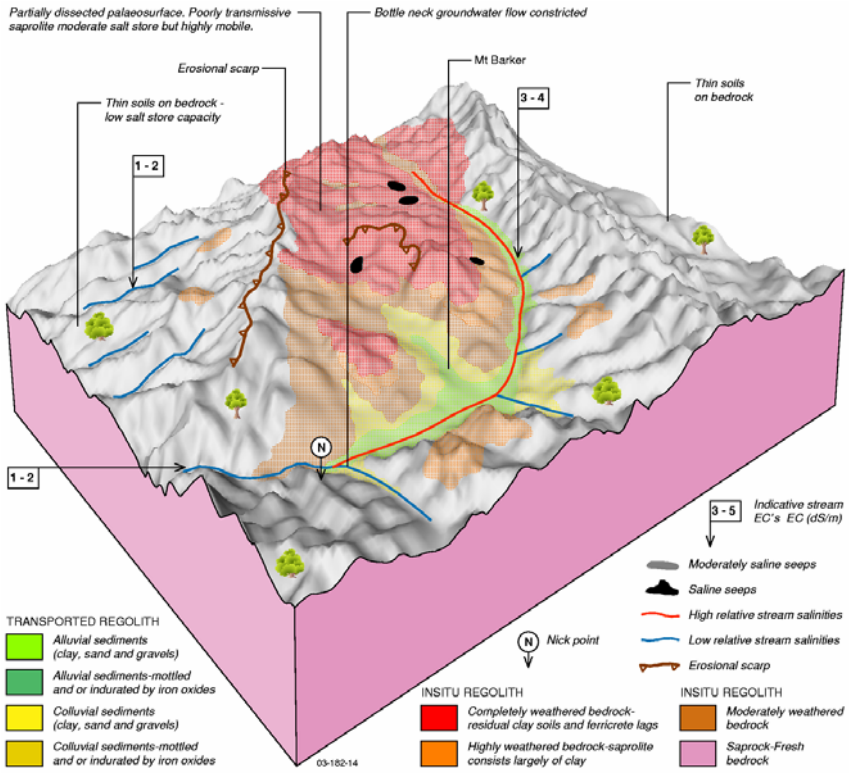

Figure 65. 3D hydrogeomorphic model based on the integration of information on regolith, hydrological processes, salt stores, rainfall, stream EC and landforms. Refer to figure 61 for the location of models E and F.

There is a poor correlation between regolith thickness as indicated by the K-residual image and salt storage. Instead we find a good correlation between rainfall and salt storage. The thickness and composition of the regolith might determine the capacity of the landscape to store salts, but rainfall largely determines the rates of recharge and groundwater fluxes which in term largely determines the concentration of salts in the profile. The influence of rainfall on the storage of salt is particularly strong in the study area due to the very sharp rainfall gradient between the western and eastern sides of the Adelaide Hills. When comparing similar regolith profiles across the study area those profiles in the high rainfall zone (western side of the Hills) have considerably lower salt stores than profiles on the drier eastern side. For a given area (e.g. similar rainfall), high salt stores are associated with valley alluvium, colluvial fans and highly weathered bedrock. Eastward as rainfall decreases, the salts in these regolith materials progressively increase. The highest salt stores are associated with discharge sites in weathered landscapes (valley floors, base of colluvial fans) on the eastern side of the study area. The lowest salt stores are associated with thin soils and regolith in areas of high rainfall. These thin regolith landscapes have a limited capacity to store salts and are regularly flushed by rainfall.

Stream gradients and valley constrictions have a major control in determining how the landscape drains. Relatively low stream gradients and broad valleys are typically associated with highly/deeply weathered palaeo-landscapes identified in the K-residual image. These landscapes have a higher potential to store salts due to relatively low hydrological gradients (sluggish hydrological systems) compared to actively eroding landscapes with steeper valley profiles and hydraulic gradients.

The highest salt stores are not the areas in the landscape where the most salt is being discharged into streams. The highest salt stores are found in regolith materials on the drier eastern side of the study area, yet the highest salt flows into the streams are associated with Western Flat Creek in the Mt Barker catchment (Ecker, 1998). Drilling in the Mt Barker catchment would suggest that although the salt loads in the regolith (certainly in the upper part of the weathering) are relatively low, the salts are highly mobile and being flushed into the groundwater and streams due to the high rainfall in the area. On the eastern side of the study area, the dominant process is one of salt accession in the weathered profile. Henschke (1997) alluded to similar relationships, recognising that deep weathering was a potential source of stored salts, but that high rainfall prevented the accumulation of salts in the upper part of the regolith profile. The Mt Barker catchment has some of the highest salt output:input ratios in the region (Ecker, 1998). This suggests that high salt exports are in deeply weathered parts of the landscape with the highest rainfall.

Preliminarily studies have found that for a given area with similar rainfall, the highest EC values are associated with streams that drained through the regolith dominated parts of the catchments. Stream ECs then reduce as they drain through areas with a shallow regolith cover. The most sudden changes in stream EC measurements were associated with stream nick points as they often separate weathered and less weathered parts of the catchment.

Insights into the distribution of regolith materials, hydrogeomorphic processes and relationships between regolith and salt are summarised in a series of 3D hydrogeomorphic conceptual models (Figure 63-65). These models show the distribution of regolith materials across the landscape based on the interpretation of gamma-ray spectrometry and digital terrain attributes. The relationships between regolith, rainfall, stream EC and EC profiles has been used to infer salt storage and stream salinities. These conceptual models cover regions with different rainfall and regolith-landform characteristics and are intended to form the basis for predicting how different parts of the catchment behave from a hydrogeological perspective.

In the Hills region, airborne gamma-ray data provided a great deal of information on the characteristics and distribution of soils and regolith materials. They also provided further insight into weathering and geomorphic processes. These data have the potential to improve existing soil-landscape and geological maps of the region. When integrated with field observations, ground geophysics and drilling, the combination of modelled gamma-ray imagery and terrain derived indices

have provided an improved understanding of the relationships between regolith materials, landscape processes and salinity. Attributes derived from the processing of the geophysical imagery and digital elevation model can be used to develop more robust and spatially explicit hydrogeomorphic models or maps of the region. However, as with all remotely sensed datasets, gamma-ray imagery requires ground validation and its application should be predicated on an understanding of the strengths and limitations of the technology.

8. RECOMMENDATIONS:

Discussion with stakeholders and catchment groups is needed to determine how the results from this work might be incorporated into whole-of-catchment management plans. Recommendations for future research need to evolve from discussions with catchment groups if it is to target local requirements.

Information presented in this report on regolith thickness, salt storage, salt mobilisation and the relationships between rainfall and the accumulation and leaching of salts in the regolith can now be used in generating more spatially explicit hydro-geomorphic units (HGUs) over the region. The HGUs would be used to classify the region into a series of sub-catchments with similar salinity patterns and associated hydro-geomorphic processes to assist catchment management. Thematic maps of regolith thickness and salt stores should also be used in developing more robust groundwater flow system models that assess the cumulative impact of land use change in catchments (e.g. through the use of CATSALT or equivalent models).

9. ACKNOWLEDGEMENTS

I wish to thank Jim Cox, Craig Liddicoat, Mark Thomas, Chris Henschke and Chris Smitt for support in the field and in providing datasets as well as an opportunity to exchange views and debate issues. Special thanks to Tim Munday who reviewed and improved the report and Heike Apps and Joe Mifsud for the production of GIS maps and figures. Thanks to Andrew Fitzpatrick for processing the airborne magnetics.

This study was made possible through funding support by the SA and Commonwealth Governments through the National Action Plan for Salinity and Water Quality, and CRC LEME.

John Wilford publishes with the permission of the CEOs of Geoscience Australia and CRC LEME.

9. REFERENCES

Alley, N.F., (1977). Age and origin of laterite and silcrete duricrusts and their relationship to episodic tectonism in the Mid-North of South Australia. *Geological Society of Australia. Journal, 24:107-116.*

Beasley, R., 2001, The application of geophysics in catchment assessment in northern New South Wales, Salinity, Land Management and New Technologies Conference, Bendigo 18-21 February.

Belperio, A. and Flint, R.B., (1992). The Geological and geomorphological framework of Kangaroo Island. South Australia. *Department of mines and Energy Report Book, 92/1.*

Bierwirth, P., 1996 – Investigation of airborne gamma-ray images as a rapid mapping tool for soil and land degradation – Wagga Wagga, NSW, AGSO, Record 1996/22.

Bird, M.I and Chivas, A.R., (1993). Geomorphic and paleo-climatic implications of an oxygen-isotopic chronology for Australian deeply weathered profiles. *Australian Journal of Earth Sciences, 40:345-358.*

Bourman, R. P. 1973. Geomorphic evolution of southeastern Fleurieu Peninsula. MA. thesis, The University of Adelaide, Adelaide (unpubl.).

Bourman, R.P and Lindsay, J.M., (1989). Timing, extent and character of late Cainozoic faulting of the eastern margin of the Mt Lofty Ranges, South Australia. *Royal Society of South Australia. Transactions, 113:63-67.*

Bourman, R.P., (1993a). Perennial problems in the study of laterite: a review. *Australian Journal of Earth Sciences, 40:345-358.*

Bourman, R.P., (1993b). Modes of ferricrete genesis: evidence from south-eastern Australia. *Zeitschrift fur Geomorphologie, 37:77-101.*

Bourman, R.P., (1995). A review of laterite studies in southern South Australia. *Royal Society of South Australia, Transactions 119(1), 1-28.*

Bourman, R.P., Milnes, A.R. and Oades, J.M., (1987). Investigations of ferricretes and related surficial ferruginous materials in parts of Southern and Eastern Australia. . *Zeitschrift fur Geomorphologie, 64:1-24.*

Burrough, P.A. and McDonnell, R.A. 1998. *Principles of Geographic Information Systems.* Oxford University Press.

Clark, R and Mitchell, N., (1987). Annual Rainfall-Runoff relationships in Mount Lofty Ranges Catchments near Adelaide, SA. *E & S Report 87/19.*

Cook SE, Corner RJ, Grealish G, Gessler PE, Chartres C.J., 1996 - A rule-based system to map soil properties. *Soil Science of America Journal* 60, 1893-1900.

Cook, P.G., Walker, G.R., Buselli, G., Potts, I.W. and Dodds, A.R., (1992). The application of electromagnetic techniques to groundwater recharge investigations. *Journal of Hydrology, 1992, Vol 130.*

Cox, J., McEwan, K., Davies, P., Smitt, C., Herczeg, A and Walker, G., 2002. Salt Transport in the Bremer Hills, SA, Report for NAP South Australian Salt Mapping and Management, CSIRO Land and Water, Technical Report 50/02.

Cox, J.W. and Davies, P.J., (1997). Groundwater and perched water trends in the Hermann's sub-catchment South Australia. CRC for Soil and Land Management: Technical Report 1/97.

Cox, J.W. and Reynolds, M.B., (1995). Hydrogeological results from the Keynes catchment SA (stage 2). CSIRO Division of Soils, Technical report 5/1995.

Cox, J.W., Pitman, A., Fitzpatrick, R., Henschke, C.J. and Bourne, J., (1995). Waterlogging and salinity research: Keynes catchment, Keyneton. Notes prepared for Keyneton Catchment field day, 17th November 1995.

Daily, B., Firman, J.B., Forbes, B.G and Lindsay, J.M., 1976. Geology, In Natural History of the Adelaide Region (ed. Twidale C.R.T, Tyler. M.J and Webb, B.P), Royal society of South Australia.

Daily, B., Milnes, A.R., Twidale, C.R. and Bourne, J.A., (1979). Geology and Geomorphology. In: Tyler, M.J., Twidale, C.R. and Ling, J.K., (Eds), Natural History of Kangaroo Island. *Royal Society of South Australia. Occasional Publications, 2:1-38.*

Daily, B., Twidale, C.R. and Milnes, A.R., (1974). The age of the lateritized summit surface on Kangaroo Island and adjacent regions of South Australia. *Geological Society of South Australia. Journal, 21:387-392.*

Dauth, C., 1997 – Airborne magnetic, radiometric and satellite imagery for regolith mapping in the Yilgarn Craton of Western Australia, Exploration Geophysics, Vol 28, pp199-203.

Dayle, B., Twidale, C. R. & Milnes, A.R. 1974. The age of the lateritized summit surface on Kangaroo Island and adjacent region of South Australia. *Journal of Geological Society of Australia* 21, 387-392.

Dowling T I 2000 *FLAG Analysis of catchments in the Wellington Region of NSW*. CSIRO Land and Water, Consulting report 12/00, Canberra

Fenner, C. 1930. The major structural and physiographic features of South Australia.*Royal Society of South Australia, Transactions* **54**, 1-36.

Fitzpatrick, R W; Bruce, D A; Merry, R H; Davies, P J; Spouncer, L R; Bishop, L, and Maschmedt, D. Soil landscape quality assessment at catchment and regional scale - Mt Lofty Ranges Pilot Project. 1999; National Land and Water Resources Audit Interim Technical Report.

Fitzpatrick, R.W. and Naidu, R.., (1990). Preliminary schematic cross-section model through the saline catchment near Harrogate showing two groundwater systems and the formation of saline sulphidic soils (CSIRO, internal document).

Fitzpatrick, R.W., Cox, J.W, Fritsch, E. and Hollingsworth, I.D., (1994). A soil-diagnostic key to manage saline and waterlogged catchments in the Mount Lofty Ranges. South Australia. *Soil Use and Management 10:145-152.*

Fitzpatrick, R.W., Cox, J.W. and Bourne, J., (1997). Managing waterlogged and saline catchments in the Mount Lofty Ranges, South Australia: A soil landscape and vegetation key with on farm management options. Catchment Management series. CSIRO Publishing, Melbourne.

Fitzpatrick, R.W., Fritsch, E. and Self, P.G., (1996). Interpretation of soil features produced by ancient and modern processes in degraded landscapes: V. Development of saline sulfidic features in non-tidal seepage areas. *Geoderma 69: 1-29.*

Fitzpatrick, R.W., Naidu, R., Fritsch, E. and Hollingsworth, I.D., (1992). Dryland salinity processes and remedies in the Mt Lofty Ranges sub catchments: End of Grant Report (CDS6). CSIRO Division of soils Technical Report 100/1992.

Fitzpatrick, R.W., Skwarnecki, M. and Raven, M., (2002). Contribution of Saprolite and pyrite weathering to salinity in the Mount Torrens region South Australia. In Priess, V.P., (Ed.) 2002.

Fugro Acquisition and Processing technical report, 2002, Jamestown and Angas-Bremer Airborne Surveys. Airborne magnetic, gamma-ray and elevation surveys, (Prepared by S. Murphy and L. Stenning). Bureau of Rural Sciences. FAS JOB # 1545.

Geoscience 2002: Expanding Horizons. Abstracts of the 16th Australasian Geological Convention, Adelaide Convention Centre Adelaide, South Australia. July 1-4 2002 No.67: p. 412.

Fritsch, E and Fitzpatrick, R.W., (1994). Interpretation of Soil Features Produced by Ancient and Modern Processes in Degraded Landscapes. I. A New Method for Construction Conceptual Soil-Water Models. *Australian Journal of Soil Research. 32:889-907.*

Gallant J. C and Dowling, T. I, 2003. A multi-resolution index of valley bottom flatness for mapping depositional areas, Water Resources Research, Vol 39, No 12.

Gessler, P.E., I.D. Moore, N.J. McKenzie, and P.J. Ryan. 1995. Soil-landscape modeling and spatial prediction of soil attributes. International Journal of Geographical Information Systems 9:421-432.

Gunn, R.H and Richardson, D.P., (1979). The nature and possible origins of soluble salts in deeply weathered Landscapes of eastern Australia. *Australian Journal of Soil Research. 17:197-215.*

Henschke, C., Hatton, T., Ciganovic, P., Tonkin, D., Ecker, S., (1997). Dryland Salinity Risk Assessment using HARDSD in the Bremer Barker Catchment. Unpubl. Paper.

Henschke, C.J 2002. Karrawirra and Cameron catchments – Groundwater monitoring network. Report to Eastern Hills and Murray Plains Catchment Group. Technical report. PIRSA Rural solutions, Nuriootpa SA.

Henschke, C.J, McCarthy, D.J. and Dooley, T., (1992). Hydrogeological investigations and management of dryland salinity in the Mt Eagles catchment Keyneton. (PISA unpublished internal report).

Henschke, C.J., (1997). Dryland Salinity Management in the Mount Lofty Ranges. Unpublished Technical report.

King, L.C., (1976). Plantation remnants upon high lands. *Zelt. Geomorphlogie 20, 133-148.*

Laffan, S.W. 1996. Rapid Appraisal of Groundwater discharge using fuzzy logic and topography. Proc. 3rd Intl Conf./Wshop on integrating GIS and Env. Modelling, Jan 21-25, 1996, Santa Fe

Lange, R.T., 1976, Vegetation, In Natural History of the Adelaide Region (ed. Twidale C.R.T, Tyler. M.J and Webb, B.P), Royal society of South Australia.

Lewis, M.F. (1991). Lineaments and salinity in Western Australia – carriers or barriers? Proc. International Hydrology and Water Resources Symposium, Perth, 2-4 Oct. 1991.

MacInnes, S., and Raymond, M., 2001, STEMINV Documentation - Smooth-Model TEM Inversion, version, Zonge Engineering and Research Organisation, Inc.

Maschmedt, D.J., (1993). Soil Landscapes of the Mount Lofty Ranges. Primary Industries SA (unpublished internal report).

McKenzie, N.J., P.J. Ryan, and J.J. de Gruijter. 1999. Spatial prediction of soil properties using environmental correlation. Geoderma (Pedometrics '97) 89:67-94.

McKenzie, R.C., George, R.J., Woods, S.A., Cannon, M.E and Bennett, D.L. 1997. Use of the electromagnetic-induction meter (EM38) as a tool in mapping salinisation, Hydrologeology Journal, v 5, no 1, pp37-50.

Milnes, A.R., Bourman, R.P. and Fitzpatrick, R.W., (1987). Petrology and mineralogy of 'laterites' in southern and eastern Australia and South Africa. *Chemical Geology, 60:237-250.*

Milnes, A.R., Bourman, R.P. and Northcote, K.H., (1985). Field relationships of ferricretes and weathered zones in southern South Australia: a contribution to 'laterite' studies in Australia. *Australian Journal of Soil Research.23:441-465.*

Mitasova, H., J. Hofierka, M. Zlocha, and L.R. Iverson. 1996. Modelling topographic potential for erosion and deposition using GIS. International Journal of Geographical Information Systems 10:629-641.

Moore, I.D., Lewis, A., and Ladson, A.R., 1991 – Digital terrain modelling: a review of hydrological, geomorphological and biological applications: Hydrologic processes, V. 5, no. 1, p. 3-30.

Narayan, K.A., Vink, R. and Henschke, C.J., (1996). Groundwater modelling to predict the impact of management scenarios for two dryland salinity catchments, South Australia. CSIRO Divisional Report 96/3.

Northcote, K.H., 1976. Soils, In Natural History of the Adelaide Region (ed. Twidale C.R.T, Tyler. M.J and Webb, B.P), Royal society of South Australia.

Oh, T., Telfer, A.L and Sliuzas, A., 2000. Mount Lofty Ranges Groundwater Review, Department for Environment, Heritage and Aboriginal Affairs, Report No 1, Adelaide.

PIRSA Land Information 2001. Soils of South Australia's Agricultural Lands, (CD ROM). Primary Industries and Resources South Australia.

Pugh, S., (1994). Dryland salinisation, Southern Mount Lofty Ranges. Progress Report 1: Drilling Program. Department of Mines and Energy Report Book 92/41.

Roberts D W, T I Dowling and J Walker 1997 *FLAG: A fuzzy landscape analysis GIS method for dryland salinity assessment*. CSIRO, Land and Water Technical Report 8/97, Canberra.

Rowlett, A.I., (1997). Preliminary Report of Paleodrainage in the St Vincent Basin and Mt Lofty Ranges. Department of Mines and Energy Resources South Australia. Report Book 97/25.

Salama, R.B., Hatton, T.J. and Dawes, W.R., (1996). Procedures and approaches to landscape classification, groundwater level mapping and flownet modelling. CSIRO Division of Water Resources Technical Memorandum 96.27.

Soil and land Information 2002, Spatial Data, Soil Landscapes of South Australia Agricultural Areas in GIS format (CD ROM) SaLi Group Department of Water Land and Biodiversity Conservation, Adelaide.

Soloman, A.J. and Henschke, C.J., (1997). Dryland Salinity Management – Guidelines for property management planning. PISA Bulletin (in prep).

Sprigg, R. C., 1942. The geology of the Eden-Moana Fault Block. Trans. R. Soc.S. Aust,66, 185-214.

Smitt, C. 2004. Identifying sources of salt and mobilisation processes in the Eastern Mt Lofty Ranges, SA, (the Murray-darling Basin Groundwater Workshop 'Balancing the Basin', Bendigo, Victoria 17th-19th February (Abstracts).

Stephens, C.G., Herriot, R.I, Downes, R.G, Langford Smith, T. and Acock, A.M., (1945). A Soil, Landuse and Erosion Survey of part of County Victoria South Australia. Council for Scientific and Industrial Research Bulletin No 188 p40.

Thompson, J.Mc., Cox, J.W. and Reynolds, M.B., (1994). Physical characteristics of soils associated with piezometer installations in land degradation studies in the Keynes catchment Keyneton, SA.. CSIRO Division of Soils, Technical Report 44/1994.

Thomson, B. P. 1969. *Adelaide. South Australian Geological Atlas Series Sheet SI 54-9. Zone 5 and 6, 1:250000*. Geological Survey of South Australia, Adelaide.

Tokarev V., Sandiford M. & Gostin V.A. 1999 Landscape evolution in the Mt Lofty Ranges: implications for regolith development in G. Taylor and C. Pain (eds) Regolith '98, New Approaches to an Old Continent, CRC LEME, 3rd Aust. Regolith Conference, Kalgoorlie, WA, Proceedings p 127-134.

Twidale, C.R and Bourne, J.A., (1975). Geomorphological evolution of part of the eastern Mt Lofty Ranges, South Australia. *Royal Society of South Australia, Transactions 99, 197-209.*

Twidale, C.R. 1976. Geomorphological evolution. *In*: Twidale, C.R., Tyler, M. J. & Webb, B. P. eds. *Natural History of the Adelaide Region*, 43-59. Royal Society of South Australia, Adelaide.

Ward, W. T. 1966. Geology, geomorphology and soil of the southwestern part of Country Adelaide, South Australia. *C.S.I.R.O. Australia. Soil Publications* 23.

Wilford, J. R., 1992 - Regolith mapping using integrated Landsat TM imagery and high resolution gamma-ray spectrometric imagery – Cape York Peninsula. Bureau of Mineral Resources, Australia, Record 1992/78.

Wilford, J. R., 1995 – Airborne gamma-ray spectrometry as a toll for assessing relative landscape activity and weathering development of regolith, including soils, AGSO Research Newsletter, No 22, pp12-14.

Wilford, J., Dent, D., Dowling, T. and Braaten, R, 2001. Rapid mapping of soils and salt stores - Using airborne radiometrics and digital elevation models. Geoscience Australia Research Newsletter, May 2001, No 34

Williamson, D.R., (1990). Effect of Dryland salinity on selected water resources in South Australia. CSIRO Division of Water Resources. Technical Report to Engineering and Water Supply Dept. South Australia.

Wilson, J.P., and J. Gallant, (eds.) 2000. Terrain analysis: principles and applications. Wiley & Sons, New York.

Woolnough, W. G. 1927. The duricrust of Australia.*J. Proc. R. Soc. N.S.W*. 61, 24-53.

APPENDIX 1.

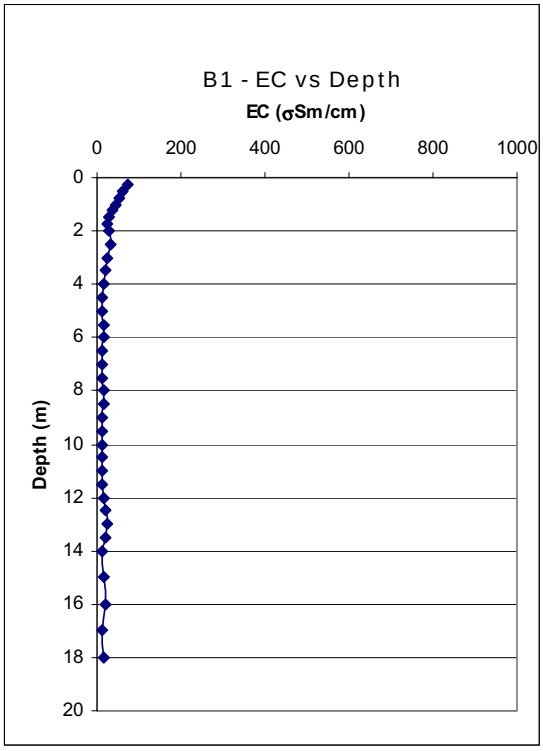
B1 - EC vs Depth
EC (σSm/cm)
0
200
400
600
800
1000
Depth (m)
0
2
4
6
8
10
12
14
16
18
20

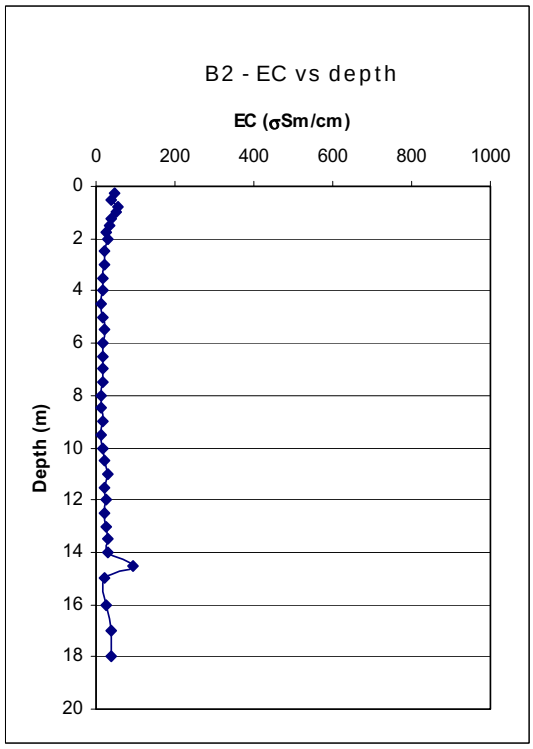
B2 - EC vs depth
EC (σSm/cm)
0
200
400
600
800
1000
Depth (m)
0
2
4
6
8
10
12
14
16
18
20

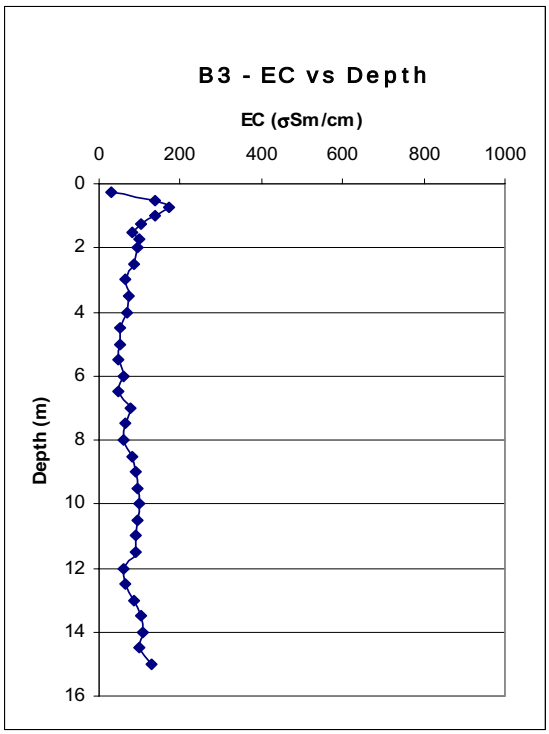
B3 - EC vs Depth
EC (σSm/cm)
0
200
400
600
800
1000
Depth (m)
0
2
4
6
8
10
12
14
16

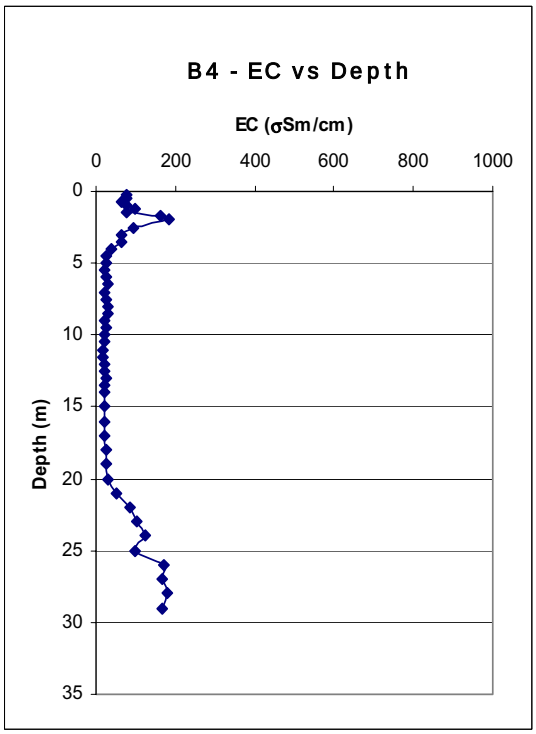
B4 - EC vs Depth
EC (σSm/cm)
0
200
400
600
800
1000
Depth (m)
0
5
10
15
20
25
30
35

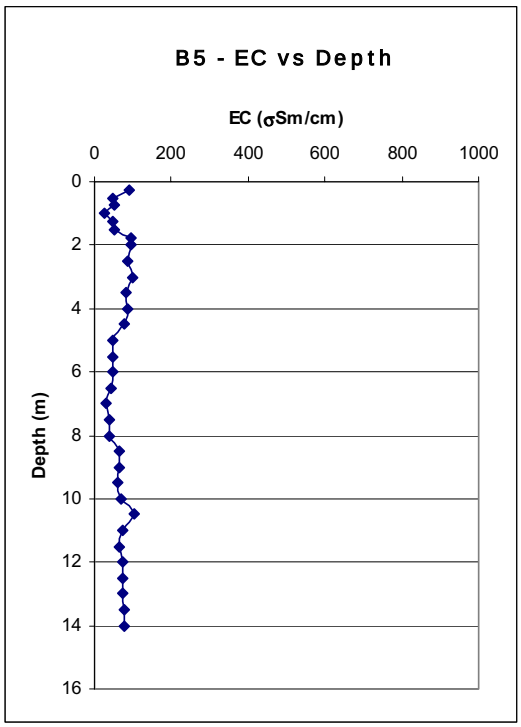
B5 - EC vs Depth
EC (σSm/cm)
0
200
400
600
800
1000
Depth (m)
0
2
4
6
8
10
12
14
16

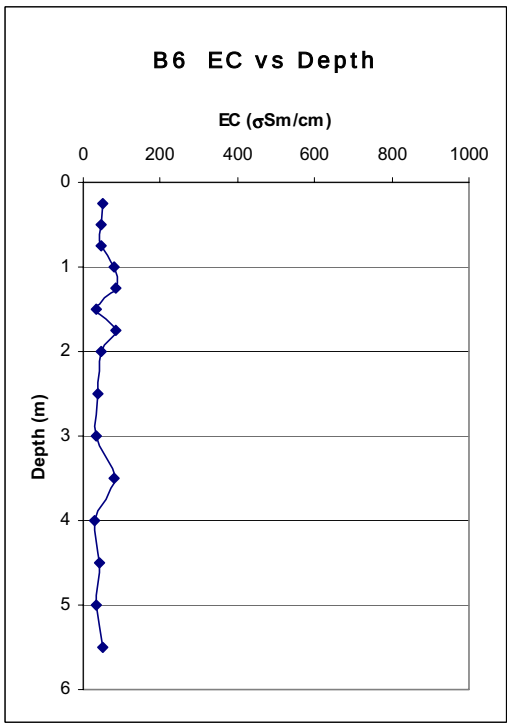
B6 EC vs Depth
EC (σSm/cm)
0
200
400
600
800
1000
Depth (m)
0
1
2
3
4
5
6

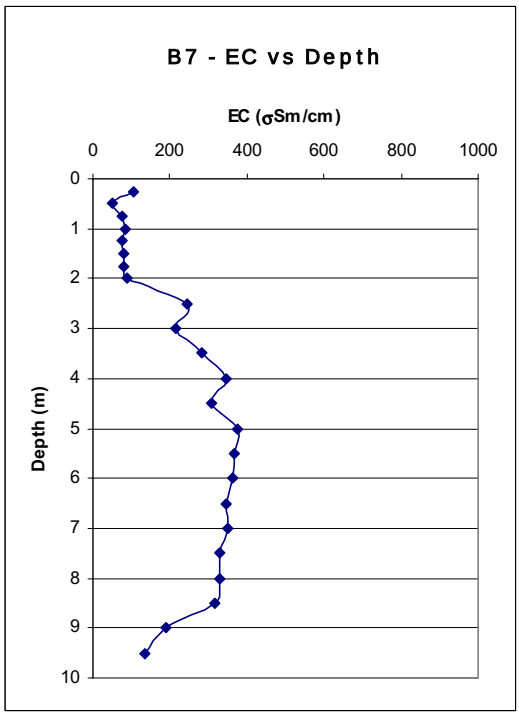
B7 - EC vs Depth
EC (σSm/cm)
0
200
400
600
800
1000
Depth (m)
0
1
2
3
4
5
6
7
8
9
10

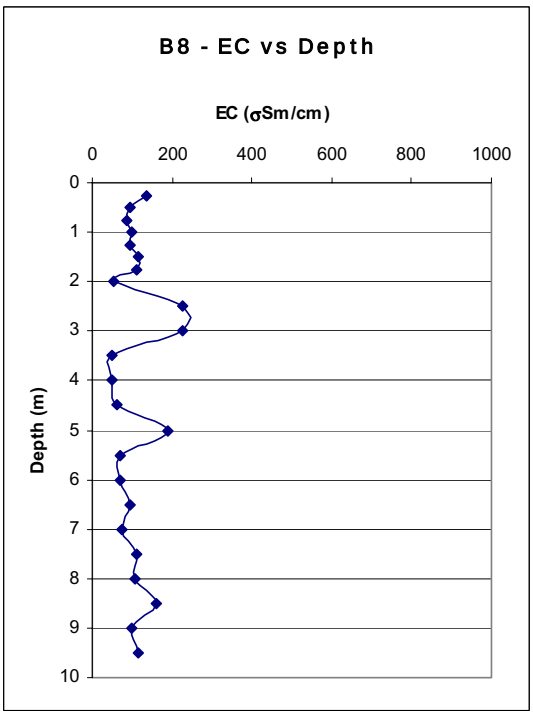
B8 - EC vs Depth
EC (σSm/cm)
0
200
400
600
800
1000
Depth (m)
0
1
2
3
4
5
6
7
8
9
10

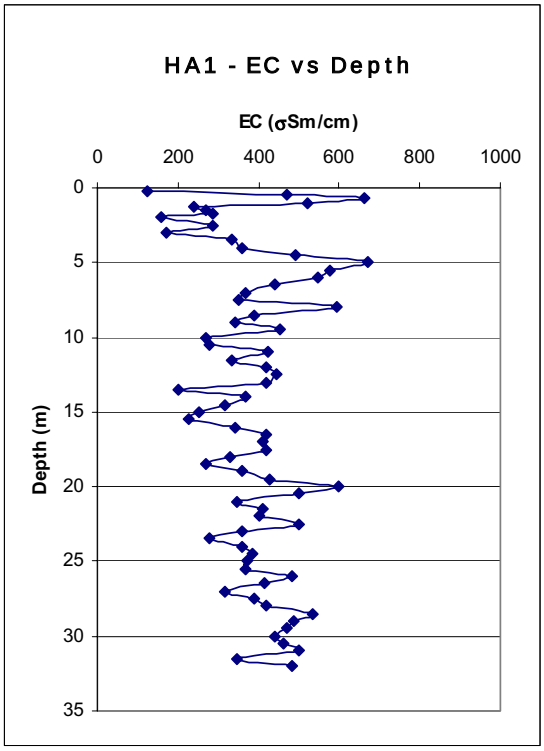
HA1 - EC vs Depth
EC (σSm/cm)
0
200
400
600
800
1000
Depth (m)
0
5
10
15
20
25
30
35

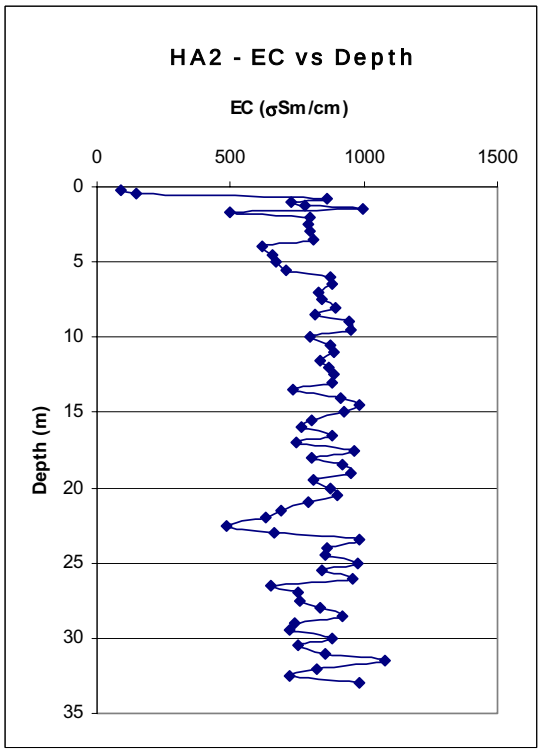
HA2 - EC vs Depth
EC (σSm/cm)
0
500
1000
1500
Depth (m)
0
5
10
15
20
25
30
35

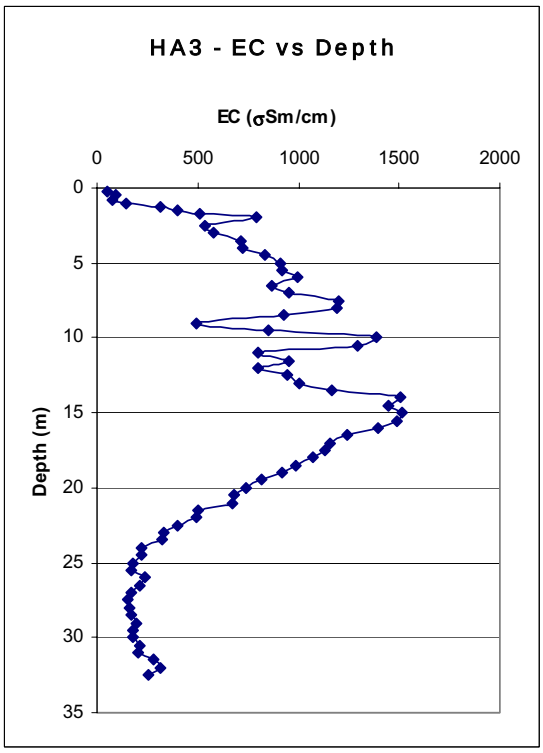
HA3 - EC vs Depth
EC (σSm/cm)
0
500
1000
1500
2000
Depth (m)
0
5
10
15
20
25
30
35

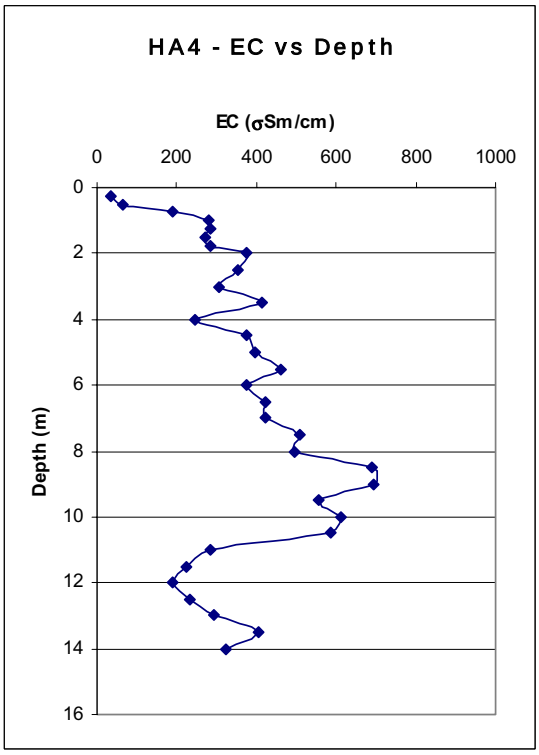
HA4 - EC vs Depth
EC (σSm/cm)
0
200
400
600
800
1000
Depth (m)
0
2
4
6
8
10
12
14
16

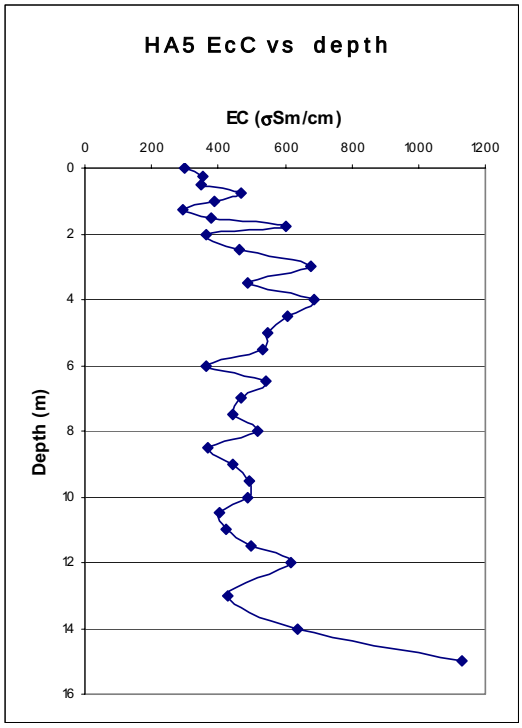
HA5 EcC vs depth
EC (σSm/cm)
0
200
400
600
800
1000
1200
Depth (m)
0
2
4
6
8
10
12
14
16

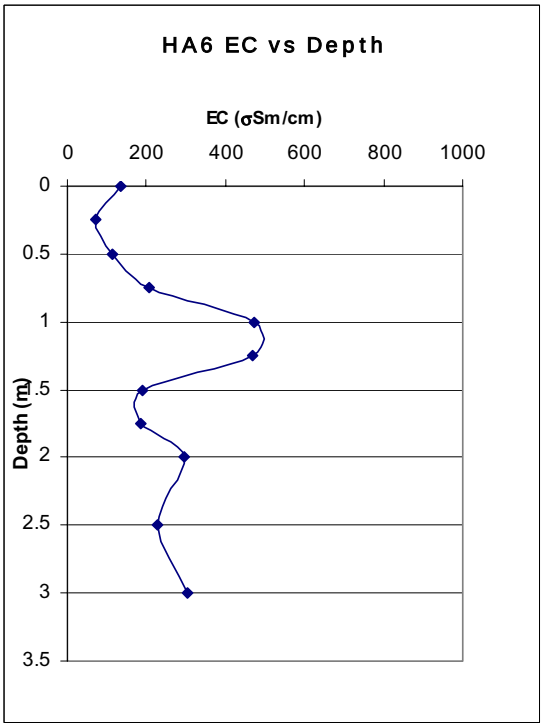
HA6 EC vs Depth
EC (σSm/cm)
0
200
400
600
800
1000
Depth (m)
0
0.5
1
1.5
2
2.5
3
3.5

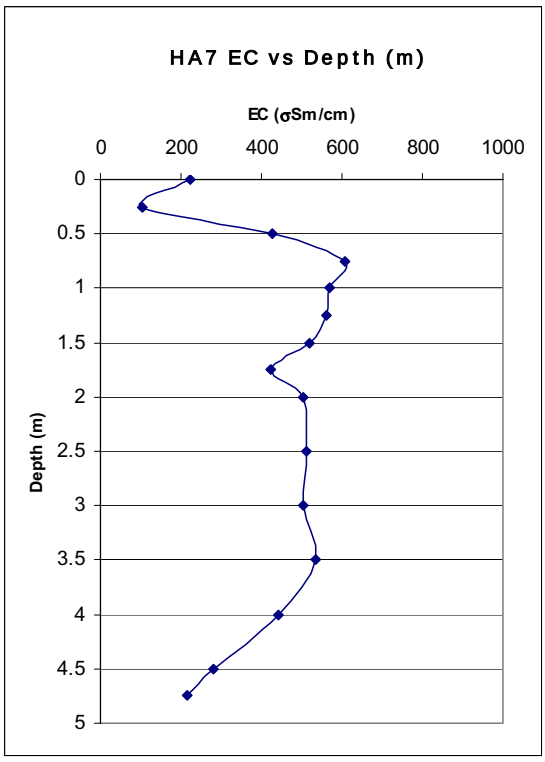
HA7 EC vs Depth (m)
EC (σSm/cm)
0
200
400
600
800
1000
Depth (m)
0
0.5
1
1.5
2
2.5
3
3.5
4
4.5
5

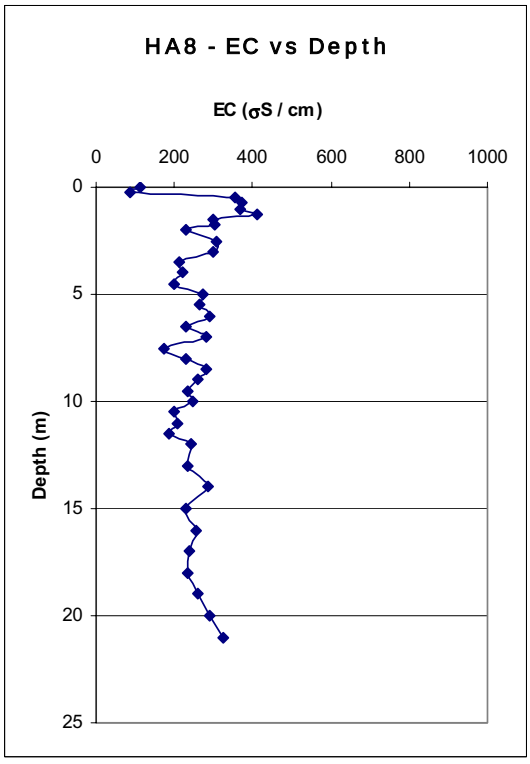
HA8 - EC vs Depth
EC (σS / cm)
0
200
400
600
800
1000
Depth (m)
0
5
10
15
20
25

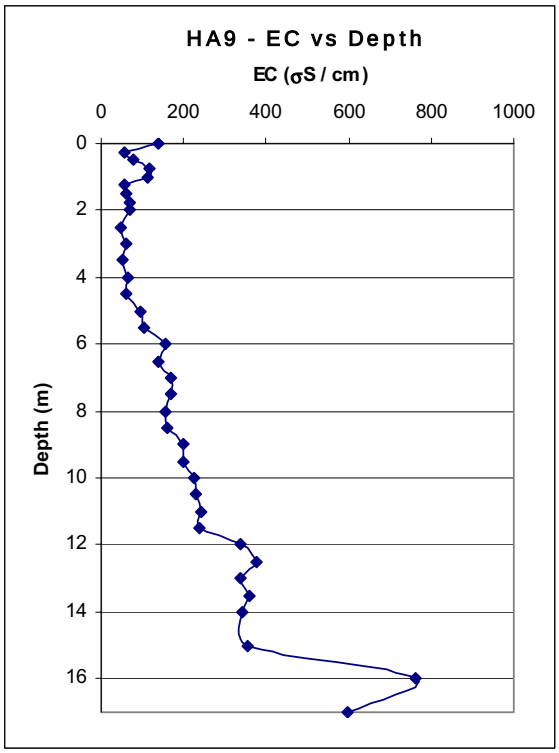
HA9 - EC vs Depth
EC (σS / cm)
0
200
400
600
800
1000
Depth (m)
0
2
4
6
8
10
12
14
16

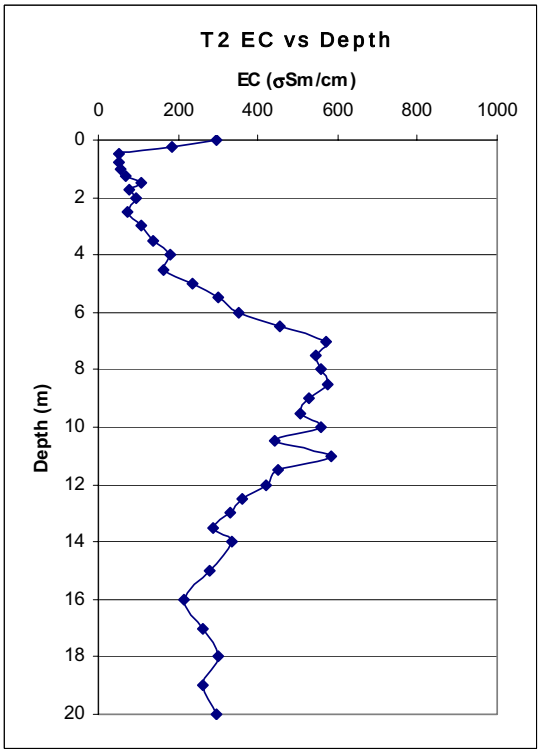
T2 EC vs Depth
EC (σSm/cm)
0
200
400
600
800
1000
Depth (m)
0
2
4
6
8
10
12
14
16
18
20

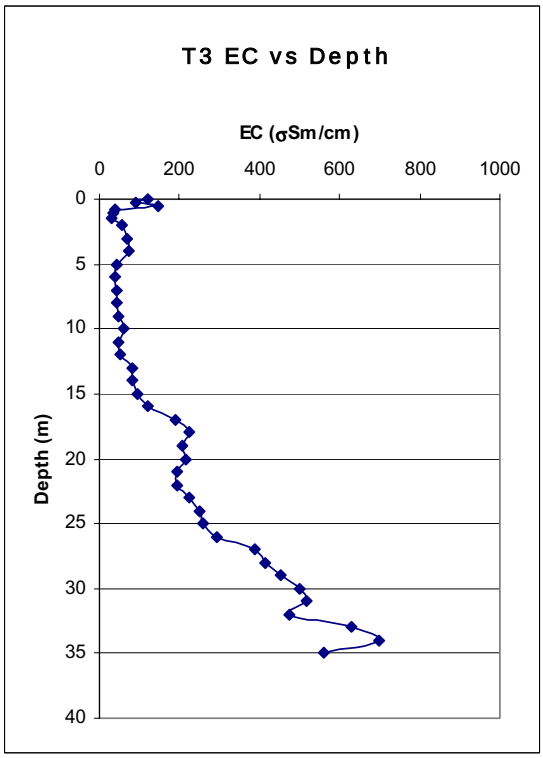
T3 EC vs Depth
EC (σSm/cm)
0
200
400
600
800
1000
Depth (m)
0
5
10
15
20
25
30
35
40

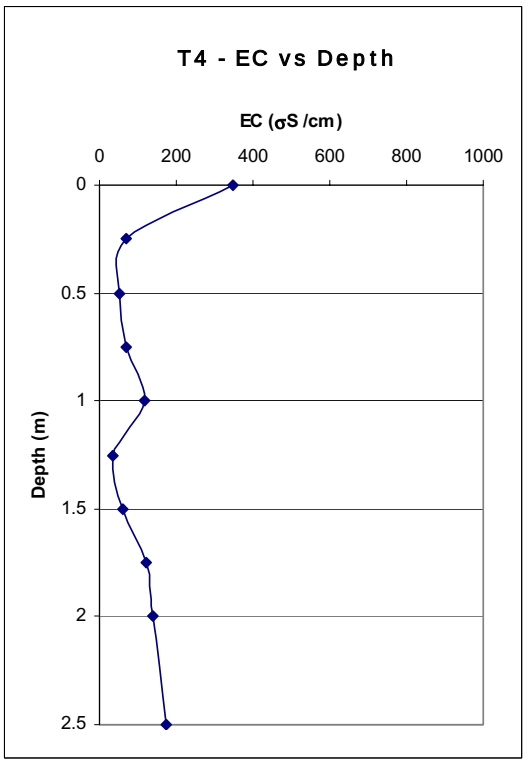
T4 - EC vs Depth
EC (σS /cm)
0
200
400
600
800
1000
Depth (m)
0
0.5
1
1.5
2
2.5

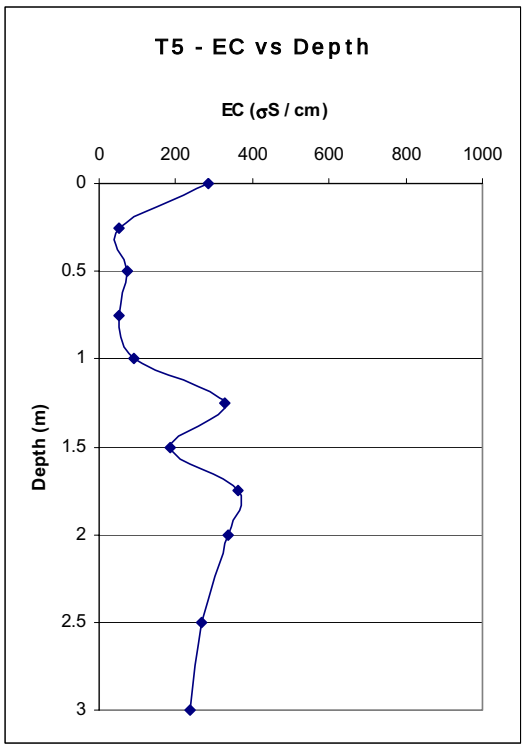
T5 - EC vs Depth
EC (σS / cm)
0
200
400
600
800
1000
Depth (m)
0
0.5
1
1.5
2
2.5
3

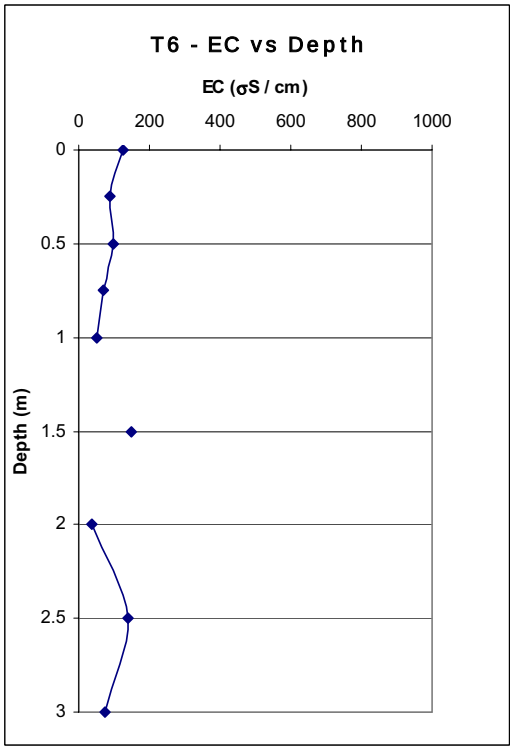
T6 - EC vs Depth
EC (σS / cm)
0
200
400
600
800
1000
Depth (m)
0
0.5
1
1.5
2
2.5
3

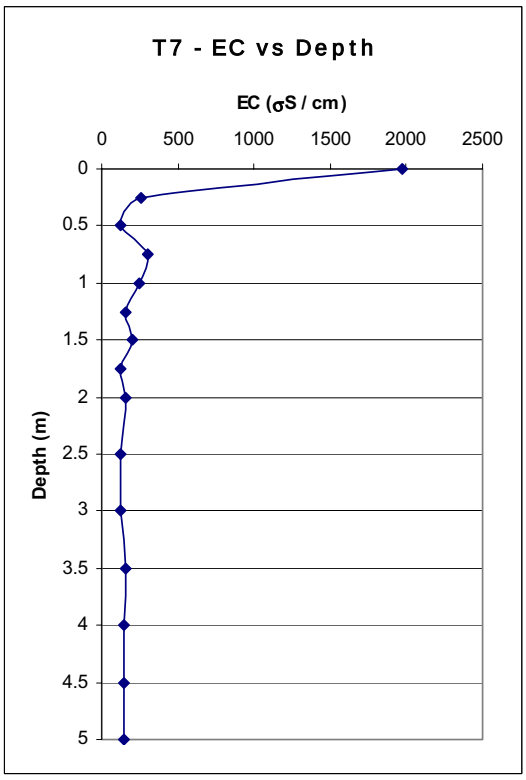
T7 - EC vs Depth
EC (σS / cm)
0
500
1000
1500
2000
2500
Depth (m)
0
0.5
1
1.5
2
2.5
3
3.5
4
4.5
5

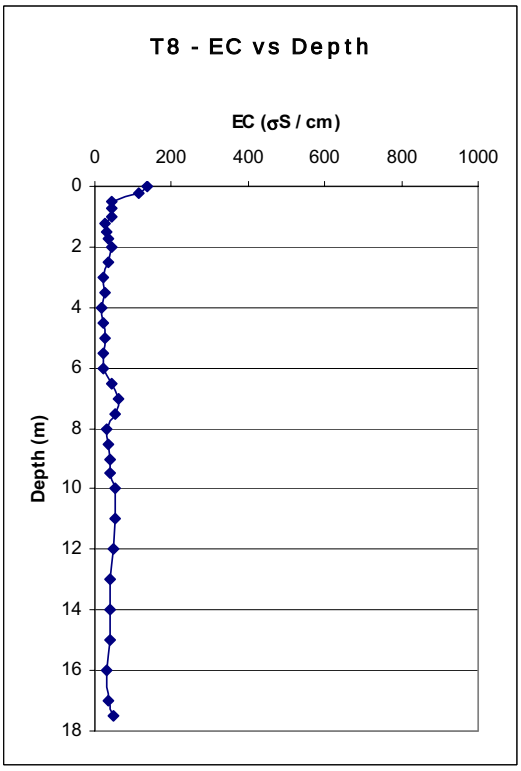
T8 - EC vs Depth
EC (σS / cm)
0
200
400
600
800
1000
Depth (m)
0
2
4
6
8
10
12
14
16
18

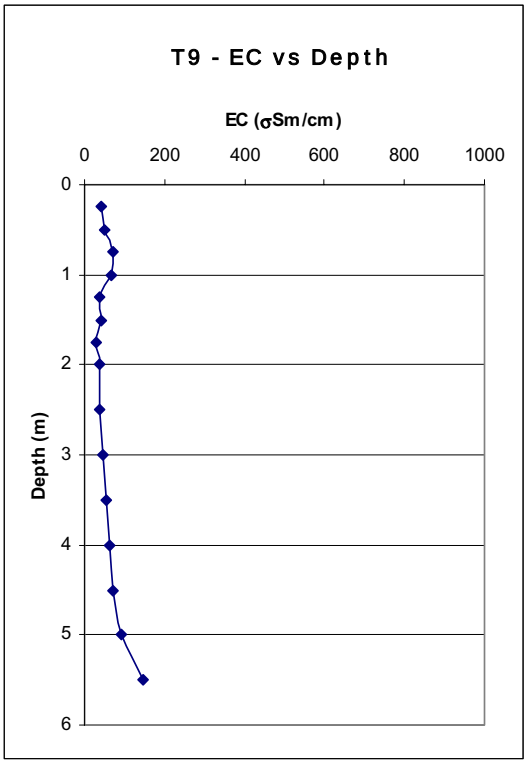
T9 - EC vs Depth
EC (σSm/cm)
0
200
400
600
800
1000
Depth (m)
0
1
2
3
4
5
6

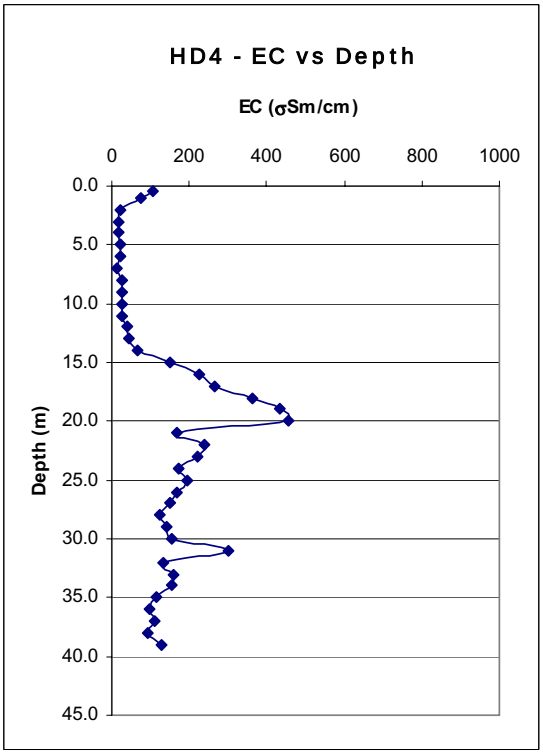
HD4 - EC vs Depth
EC (σSm/cm)
0
200
400
600
800
1000
Depth (m)
0.0
5.0
10.0
15.0
20.0
25.0
30.0
35.0
40.0
45.0

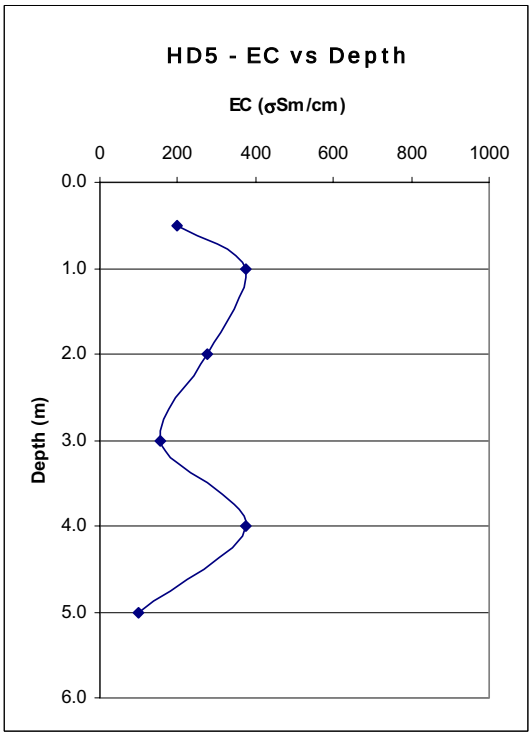
HD5 - EC vs Depth
EC (σSm/cm)
0
200
400
600
800
1000
Depth (m)
0.0
1.0
2.0
3.0
4.0
5.0
6.0

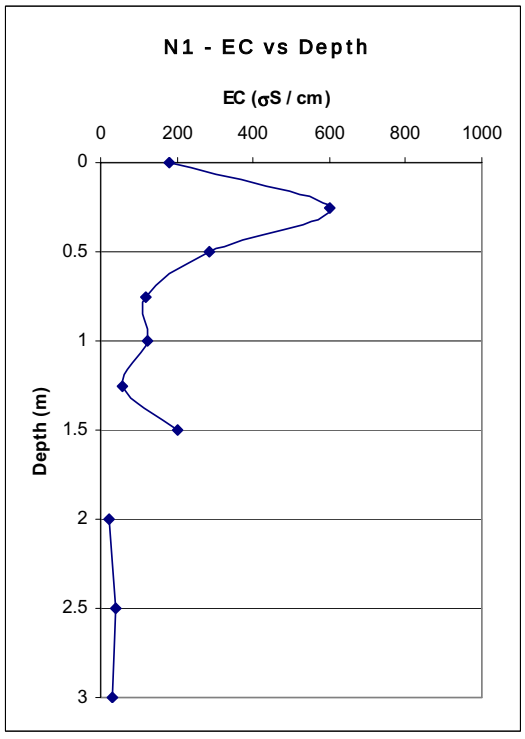
N1 - EC vs Depth
EC (σS / cm)
0
200
400
600
800
1000
Depth (m)
0
0.5
1
1.5
2
2.5
3